Mechanisms of action of novel antiepileptic drugs in chronic epileptic hippocampus

Dissertation

Dominik Holtkamp

Mechanisms of action of novel antiepileptic drugs in chronic epileptic hippocampus

Dissertation

zur
Erlangung des Doktorgrades (Dr. rer. nat.)
der
Mathematisch-Naturwissenschaftlichen Fakultät
der
Rheinischen Friedrich-Wilhelms-Universität Bonn

vorgelegt von

Dominik Holtkamp
aus
Georgsmarienhütte

Bonn 2018

Angefertigt mit Genehmigung der Mathematisch-Naturwissenschaftlichen Fakultät
der Rheinischen Friedrich-Wilhelms-Universität Bonn

1. Gutachter: Prof. Dr. Heinz Beck
2. Gutachter: Prof. Dr. Christa E. Müller

Tag der Promotion: 10.04.2019
Erscheinungsjahr: 2019

Abstract

Globally, at least 50 million people suffer from epilepsy and almost one third of these do not respond to treatment with one or even multiple antiepileptic drugs (AEDs). One of the most prominent approaches trying to explain this phenomenon termed pharmacoresistance is the target-hypothesis. It implies that epilepsy-related or seizure-induced alterations in the properties of the molecular targets of AEDs occur and ultimately result in reduced drug sensitivity.

Voltage-gated sodium channels constitute one of the key targets for many AEDs (so-called sodium channel blockers), as they are crucial for neuronal excitation and for signal transduction in the brain. For the anticonvulsant carbamazepine but also other older sodium channel blockers a strong reduction of efficacy in use-dependent blocking of sodium channels and thereby reduction of repetitive neuronal firing was shown in epileptic tissue of animal models of epilepsy as well as epilepsy patients. While older sodium channel blockers including carbamazepine interfere with the fast inactivation of sodium channels, the novel AEDs lacosamide and eslicarbazepine acetate (via its active metabolite eslicarbazepine) were shown to modulate slow inactivation of sodium channels, in contrast. Due to this unique mechanism of action both compounds were proposed to be candidate drugs to overcome pharmacoresistance.

Using the patch-clamp technique, this thesis aimed at investigating the mechanism of action and the efficacy of both substances on granule cells of the dentate gyrus, which plays an important role in limiting the spread of epileptic seizures and thereby preventing temporal lobe seizures from generalizing. Since previous studies were mostly performed on physiologically different cultured cell lines, here, multiple aspects of the still not completely understood slow inactivation of sodium channels in dentate granule cells were in the focus of investigations. Furthermore, in order to identify potential reductions in efficacy or changes in the mechanism of action of lacosamide and eslicarbazepine, comparisons between healthy and epileptic tissue were made using the pilocarpine model of epilepsy. Identical experiments were also conducted in human epileptic brain tissue that was provided after surgical removal of the epileptic foci of treatment resistant epilepsy patients.

We could show that both substances exert potent efficacy on the slow sodium channel inactivation, particularly on the voltage dependence of slow inactivation (implied by a strong hyperpolarizing shift of the inactivation curve) also in dentate granule cells. Much less pronounced effects on sodium channel fast inactivation processes were demonstrated for eslicarbazepine in an earlier study and for lacosamide within this thesis. These effects appear to be negligible when compared to the prominent shifts of the voltage dependence of slow inactivation, however. Interestingly,

all of the reported effects were not limited to healthy dentate granule cells but could also be replicated in rat and human epileptic granule cells in unaltered magnitude.

As described for lacosamide within this work and for eslicarbazepine in an earlier study, the observed effects on the slow inactivation of sodium channels translate into inhibition of action potential firing of dentate granule cells in response to prolonged depolarization – again without differences between epileptic and nonepileptic cells. Subsequent analyses of the action potential firing behavior during application of lacosamide revealed that the effects on slow inactivation processes translate into systematic changes in the action potential waveform that further increase with the duration of depolarization.

To sum up, lacosamide as well as eslicarbazepine show relatively small effects on fast inactivation processes while strongly modulating the slow inactivation of sodium channels and its voltage dependence. This is reflected by a reduction of the granule cell firing behavior. For all of the effects described, no differences between granule cells of epileptic and nonepileptic origin were observed. On the basis of these results it can be concluded that both of the investigated substances have the potential to overcome the resistance mechanism described for carbamazepine and other sodium channel blockers, at least in the light of the target-hypothesis.

Zusammenfassung

Knapp ein Drittel der weltweit mindestens 50 Millionen Menschen, die an Epilepsie leiden, spricht nicht auf die Behandlung mit einem oder sogar Kombinationsbehandlung mit mehreren Antiepileptika an. Die Zielstrukturen-Hypothese ist eine der prominentesten Hypothesen, die versucht dieses Phänomen, das als Pharmakoresistenz bezeichnet wird, zu erklären. Sie besagt, dass im Verlauf der Epilepsie oder infolge von epileptischen Anfällen eine Veränderung der Eigenschaften molekularer Zielstrukturen, an denen die Antiepileptika ihre Wirkung entfalten, stattfindet. Dies führt schlussendlich zu einer Reduktion der Medikamentensensitivität.

Spannungsabhängige Natriumkanäle stellen eine sehr wichtige Zielstruktur für viele Antiepileptika (sog. Natriumkanalblocker) dar, da sie für die Erregung von Nervenzellen und für die Signalweiterleitung im Gehirn kritisch sind. Für das Antiepileptikum Carbamazepin aber auch andere ältere Natriumkanalblocker konnte in verschiedenen Tiermodellen der Epilepsie aber auch in Hirngewebe von Epilepsiepatienten eine stark verminderte Effektivität bei der Blockade von Natriumkanälen und der daraus resultierenden Reduktion von repetitivem Feuerverhalten von Nervenzellen gezeigt werden. Im Gegensatz zu allen anderen Natriumkanalblockern modulieren die relativ neuen Antiepileptika Lacosamid sowie Eslicarbazepinacetat (über seinen aktiven Wirkstoff Eslicarbazepin) nicht die schnelle sondern die langsame Inaktivierung von Natriumkanälen. Aufgrund dieser besonderen Wirkweise wurde von beiden Substanzen erwartet, dass sie Pharmakoresistenzmechanismen potenziell überwinden können.

Die Wirkweise und Effektivität beider Substanzen wurde im Rahmen dieser Arbeit unter Verwendung der Patch-Clamp Technik an Körnerzellen des Gyrus Dentatus, dem eine wichtige Funktion in der Verhinderung der Ausbreitung epileptischer Anfälle mit Ursprung im Temporallappen des Gehirns zugesprochen wird, untersucht. Da frühere Studien weitestgehend an physiologisch andersartigen Zellkulturlinien durchgeführt wurden, wurden im Rahmen dieser Arbeit verschiedene Parameter der noch nicht vollständig verstandenen langsamen Inaktivierung von Natriumkanälen in Körnerzellen des Gyrus Dentatus untersucht. Darüber hinaus wurde die Wirkweise und die Effektivität von Lacosamid und Eslicarbazepin zwischen Kontrollgewebe und epileptischem Gewebe im Tiermodell verglichen, um mögliche Reduktionen der Effektivität oder Veränderungen im Wirkmechanismus zu erkennen. Identische Untersuchungen wurden ebenfalls in epileptischem humanem Hirngewebe, das infolge der operativen Entfernung des Epilepsieherdes behandlungsresistenter Patienten bereitgestellt wurde, durchgeführt.

Dabei konnte gezeigt werden dass beide Substanzen auch in Körnerzellen deut-

liche Effekte auf die langsame Inaktivierung von Natriumkanälen und hier besonders auf deren Spannungsabhängigkeit zeigen, zu erkennen an einer deutlichen Verschiebung der Inaktivierungskurve in Richtung hyperpolarisierter Membranpotentiale. Deutlich kleinere Effekte auf die schnelle Inaktivierung von Natriumkanälen wurden für Eslicarbazepin bereits im Vorfeld dieser Arbeit beschrieben und für Lacosamid im Rahmen dieser Arbeit aufgezeigt. Diese Effekte fallen jedoch im Vergleich zu den starken Effekten auf die Spannungsabhängigkeit der langsamen Inaktivierung vernachlässigbar klein aus. Interessanterweise sind sämtliche beschriebenen Effekte nicht nur in Kontrollgewebe beobachtet worden, sonden konnten in Körnerzellen epileptischer Ratten und Epilepsiepatienten ebenso in unveränderter Größe nachgewiesen werden.

Diese Effekte auf die langsame Inaktivierung von Natriumkanälen spiegeln sich in einer Reduktion des Feuerns repetitiver Aktionspotentiale der Körnerzellen infolge längerer Depolarisation wieder, wie für Lacosamid im Rahmen dieser Arbeit und für Eslicarbazepin in einer früheren Studie ebenfalls in epileptischem und Kontrollgewebe unverändert beobachtet werden konnte. Weitere Analysen des Feuerverhaltens während der Applikation von Lacosamid legen nahe, dass sich die Effekte auf die langsame Inaktivierung in einer systematischen Änderung der Aktionspotentialeigenschaften niederschlagen, welche mit der Dauer der Depolarisation zunimmt.

Zusammenfassend lässt sich sagen, dass sowohl Lacosamid als auch Eslicarbazepin vergleichsweise kleine Effekte auf schnelle Inaktivierungsprozesse bei vorwiegender Modulation der langsamen Inaktivierung von Natriumkanälen und hier besonders deren Spannungsabhängigkeit zeigen, was sich in einer Reduktion im Feuerverhalten der Körnerzellen wiederspiegelt. Für sämtliche der untersuchten Effekte konnten keine Unterschiede zwischen Zellen epileptischem und nichtepileptischem Ursprungs beobachtet werden. Anhand dieser Ergebnisse lässt sich festhalten, dass beide Substanzen, zumindest im Lichte der Zielstrukturen-Hypothese, das Potenzial haben, den für Carbamazepin und weitere Natriumkanalblocker beschriebenen Resistenzmechanismus zu überwinden.

Contents

1 Introduction

1.1 Epilepsy

Neuronal disorders affect millions of people all over the world. Epilepsy is one of the most common neurological disorders, only being surpassed by migraine, stroke and Alzheimer's disease (Hirtz et al., 2007). At least 50 million people worldwide suffer from epilepsy (World Health Organization, 2017). Estimations based on meta-analyses, however, indicate that this number might be substantially higher, with both prevalence as well as incidence of epilepsy in developing countries being about twice as high as in developed countries (Ngugi et al., 2010, 2011).

Epilepsy is a complex neurological disorder characterized by the occurrence of epileptic seizures or even the possibility of future seizures after a first seizing event (Fisher et al., 2014). Seizures are transiently occurring signs or symptoms caused by abnormal excessive or synchronous neuronal activity within the brain (Fisher et al., 2005). They may differ in their location of onset, spread, severity and frequency and can be classified as seizures with focal, generalized or unknown onset (Fisher et al., 2017). Focal seizures originate within specific areas of a single hemisphere and can spread locally within neuronal networks of one hemisphere of the brain as well as extend bilaterally. This kind of seizure may impair consciousness or awareness. Generalized seizures, in contrast, affect both hemispheres already at onset and impair consciousness. Seizures can be accompanied by motor or nonmotor onset-characteristics (Fisher et al., 2017). Seizure frequency can vary from less than one per year to several per day (Gasparini et al., 2016).

The first and most common step in the treatment of epilepsy is therapy with anticonvulsants, also called antiepileptic drugs (AEDs) (chapter 1.5). Currently available treatment is symptomatic and not curative (Caccamo et al., 2016; Pitkänen and Lukasiuk, 2011) and results in long-term seizure freedom in only around two thirds of patients (Annegers et al., 1979; Kwan and Brodie, 2000; Sillanpää et al., 1998). Patients which continue to have seizures despite being treated with two appropriately chosen and tolerated AEDs are considered pharmacoresistant (Kwan et al., 2010). In an attempt to achieve seizure freedom, alternative and usually more invasive approaches like resection of the brain areas involved in seizure generation are performed in these patients (Kwan et al., 2011; Schuele and Lüders, 2008; Surges and Elger, 2013).

Similar to the large variability in seizures, epilepsy itself can be highly variable in terms of etiology, comorbidities and severity in each affected individual and can be considered a spectrum of disorders rather than a single disorder (Jensen, 2011;

Scheffer et al., 2017).

1.1.1 Temporal lobe epilepsy

According to older classifications, many epilepsies were categorized – based on the localization of seizure origin instead of their cause – into temporal, frontal, parietal, and occipital lobe epilepsies (Roger et al., 1989). Temporal lobe epilepsy (TLE) is the most common type of focal epilepsy and frequently associated with pharmacoresistance (Hauser and Kurland, 1975; Semah et al., 1998). For the majority of TLE patients the epileptic seizures originate in the limbic structures of the temporal lobe such as the amygdala or the hippocampal formation, referred to as mesial temporal lobe epilepsy (mTLE). A smaller number of patients suffer from lateral temporal lobe epilepsy (lTLE) where seizures emerge in neocortical areas of the temporal lobe (Dupont et al., 1999).

The most commonly observed change in brains of mTLE patients is a neuropathological phenomenon called hippocampal sclerosis, characterized by neuronal loss in specific areas of the hippocampal formation (Blümcke et al., 2013; Curia et al., 2014, chapter 1.4). Hippocampal sclerosis can also be found in numerous animal models of epilepsy, both naturally occuring and induced (Curia et al., 2014; Kuwabara et al., 2010; Polli et al., 2014; Schmied et al., 2008; Wagner et al., 2014; see chapter 1.3).

1.2 The hippocampus

The hippocampal formation, frequently referred to as 'the hippocampus', is part of the limbic system and located in the temoral lobe of the mammalian brain (Amaral and Lavenex, 2007; Squire et al., 2004). It is involved in many functions (Morris, 2007) but most prominently associated with spatial cognition (Hartley et al., 2014; O'Keefe and Dostrovsky, 1971) and declarative memory (Squire, 1992; Squire et al., 2004). The dorsal and ventral portions of the rodent hippocampus or the posterior and anterior hippocampus in primates, respectively, have been associated with distinct functions, input and output connectivity to other brain areas, as well as molecular domains (Fanselow and Dong, 2010). The hippocampal formation consists of the three-layered dentate gyrus (DG), hippocampus proper (also referred to as Ammon's horn (CA, from latin cornu ammonis)), and subiculum (van Strien et al., 2009) and in a less strict sense also comprises the entorhinal and subicular cortices (Amaral and Lavenex, 2007). The DG and CA regions present interlocked cell layers (see figure 1) which contain the excitatory principal neurons of the hippocampal formation: The hippocampus proper is composed of areas CA3, CA1 and

the intercalated, relatiely narrow CA2 region which harbor pyramidal cells (Amaral and Lavenex, 2007) and the DG contains multiple rows of densely packed granule cells (Amaral et al., 2007, see chapter 1.2.1).

The entorhinal cortex (EC) connects the neocortex with the hippocampal formation and represents its main input and output structure (Amaral and Lavenex, 2007; Witter et al., 2017). Information is propagated through the hippocampal circuitry in many different ways: EC layer II neurons project to the granule cells of the DG through the perforant pathway, which in turn project to pyramidal neurons of area CA3 of the hippocampus proper via mossy fibers. These CA3 pyramidal neurons then project on to the smaller CA1 pyramidal neurons of the ipsi- and contralateral hemisphere through Schaffer collaterals and commissural fibers, respectively (Amaral and Lavenex, 2007; Hartley et al., 2014). The classic understanding of this pathway comprises only three synapses (EC $\rightarrow$ DG, DG $\rightarrow$ CA3, CA3 $\rightarrow$ CA1) and was therefore named trisynaptic pathway. Due to the finding of projections from CA1 to the subiculum and on to the EC the classic trisynaptic loop can be seen as a part of a more complex polysynaptic pathway (Amaral and Lavenex, 2007; van Strien et al., 2009).

In addition to the polysynaptic pathway, multiple subfields of the hippocampal formation are also interconnected by less prominent projections, e.g. areas CA3, CA1 and the subiculum receive direct monosynaptic inputs from EC layer II and III via the perforant pathway and the temporoammonic pathway, respectively (Amaral and Lavenex, 2007; Hartley et al., 2014). In recent years, alternative connectivity with involvement of the narrow CA2 area in direct as well as polysynaptic pathways have been described (Chevaleyre and Siegelbaum, 2010; Kohara et al., 2014). With ongoing research and further advances in techniques and methods the current view on hippocampal circuitry might evolve even further.

1.2.1 Function and organization of the dentate gyrus

Similar to the hippocampal formation, the DG itself is involved in multiple functions that again differ between dorsal and ventral portions (Kesner, 2017). The DG seems to be particularly important for pattern separation, i.e. transforming similar input patterns into more dissimilar output patterns to disambiguate quite similar contexts (Leutgeb et al., 2007). Furthermore, the DG is considered as a gate or filter, limiting excitatory input from the entorhinal cortex to the hippocampus (Heinemann et al., 1991; Hsu, 2007; Stringer and Lothman, 1992). Since epileptiform activity was shown to pass the DG and spread to the rest of the hippocampal formation and from there to other areas of the brain more easily under epileptic conditions, the

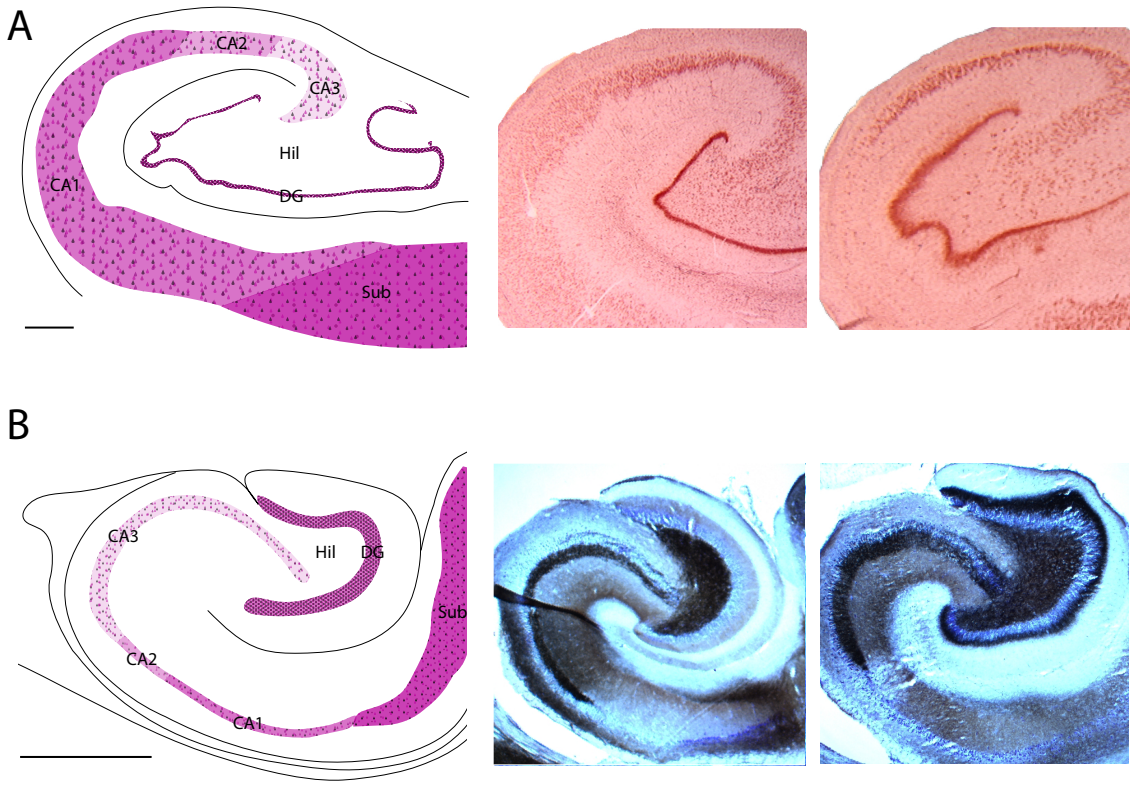

Figure 1: Overview of human and rat hippocampal formations. Schematic illustrations of the structure of hippocampal principal cell layers of a human (**A**) and a rat hippocampal formation (**B**) as seen on cross-sections. Hil = hilus, Sub = subiculum, scale bars = 1000 μm for drawings as well as photographs. The DG plays a key role in limiting the input to downstream regions during normal but also pathologic activity. Photographic insets in (**A**) demonstrate hippocampal sclerosis type 1 with well recognisable neuronal loss in areas CA1 and the hilus but not areas CA2, CA3 and the subiculum in epileptic (right photograph) compared to nonepileptic (left photograph) human specimen. Hematoxylin and eosin stainings of human hippocampal slices. Insets in (**B**) illustrate mossy fiber sprouting in brain slices of pilocarpine-treated (right photograph) but not sham-injected rats (left photograph). The zinc-containing mossy fibers are visualized in black by Timm's staining method and are counterstained with toluidine blue. Schematics redrawn after Blümcke et al., 2013 and Paxinos and Watson, 2009; photographic insets kindly provided by Albert Becker and Margit Reitze.

DG is of particular importance and interest in TLE (Behr et al., 1998; Collins et al., 1983).

The DG comprises three layers that form a curved structure and bend around or cap the CA3 region: The the molecular layer, the granule cell layer, and the polymorphic layer, also called hilus (Amaral et al., 2007; figure 1). The molecular layer is located most distal to the CA3, adjacent to the hippocampal fissure and mostly free of cell somata. It contains a low number of interneurons and other neurons (Han et al., 1993; Sancho-Bielsa et al., 2012; Soriano and Frotscher, 1989; Williams et al., 2007) as well as the dendrites of the dentate granule cells and fibers projecting to and through the DG, mostly the perforant path axons (Amaral et al., 2007; Scharfman, 2016).

The granule cell layer constitutes the middle layer of the DG and comprises predominantly granule cells, the principal cells of the DG, along with low numbers of axo-axonic cells and pyramidal basket cells (Amaral and Lavenex, 2007; Scharfman, 2016). Those perisomatic-targeting cells are inhibitory interneurons located at the border to the hilus and involved in feedforward inhibition as well as feedback inhibition (Acsády et al., 1998; Scharfman, 2016; Zipp et al., 1989). Notably, the DG is one of the few areas of the brain where adult neurogenesis occurs (Altman and Das, 1965; Eriksson et al., 1998) in addition the olfactory bulb and the striatum (Bergmann et al., 2012; Ernst et al., 2014). Dentate granule cells are continuously renewed throughout life (Bayer, 1982; Cameron and Mckay, 2001; Spalding et al., 2013) by stem cells located at the border of the granule cell layer and the hilus, the so-called subgranular zone (Palmer et al., 1997).

The hilus represents the deepest of the three layers and comprises many different cell types. In addition to the mossy fibers spanning the hilus and other fusiform neurons, mossy cells are the most common neurons found in the hilar region (Amaral, 1978; Han et al., 1993; Scharfman, 2016). The glutamatergic mossy cells can either excite GCs directly or inhibit them via interneurons. Mossy cells that give almost simultaneous input to granule cells as the perforant path are involved in translamellar potentiation which is believed to be important for pattern separation (Hsu, 2007) whereas mossy cells targeting interneurons potentially contribute to feedback inhibition (Scharfman, 2016).

1.2.2 Granule cells of the dentate gyrus

The DG consists of around 1.2 million granule cells (GCs) in the adult rat brain and about 15 million in adult human brains (both unilaterally; Bayer, 1982; West et al., 1991; West and Gundersen, 1990). Single GCs of rodents and primates

appear relatively similar in size and morphology. Rat GCs have small roundish to ovoid somata with an average size of 10×18 μm (Claiborne et al., 1990). Similar but more variable dimensions were reported for primate GCs includng humans GCs (de Ruiter and Uylings, 1987; Scheibel et al., 1974; Seress and Frotscher, 1990). Even after a trituration process, acutely isolated CGs can still be identified by their somatic morphology in the absence of most of the axonal and dendritic processes (Beck et al., 1997a; Mody et al., 1989).

The GC apical dendrites extend into the molecular layer in a cone shaped manner where they synapse with lateral and medial perforant path axons, hilar interneurons as well as other intra- and extrahippocampal neurons (Amaral and Lavenex, 2007; Scharfman, 2016). In the rat, GCs situated in the suprapyramidal blade (located between areas CA3 and CA1) or infrapyramidal blade (located on the opposite side) of the DG display mostly differences in the architecture and spread of the dendrites (Claiborne et al., 1990). Primate GCs however are more variable in terms of dendritic arborization, density of spines on the dendrites and even soma size (Seress and Frotscher, 1990). The most prominent difference between rodent and primate GCs is the presence of basal dendrites which are virtually absent in healthy rodents but present in more than 20% of healthy human GCs (Lim et al., 1997; Ribak et al., 2000; Seress and Mrzljak, 1987).

The axons of the granule cells – the mossy fibers – project through the hilus to the CA3 where they terminate in large boutons that synapse with the the dendrites of CA3 pyramidal neurons. In the hilus the mossy fiber boutons make contact with hilar mossy cell dendrites but also collateralize and target interneuronal dendrites located within the hilus and the granule cell layer (Amaral and Lavenex, 2007; Lim et al., 1997). The mossy fibers are glutamatergic, but also contain and are able to release γ-aminobutyric acid (GABA), ATP, dynorphin, and zinc upon stimulation (Chavkin et al., 1983; Howell et al., 1984; Terrian et al., 1989; Terrian et al., 1988; Walker et al., 2002).

In comparison to other neurons, many GCs have a highly hyperpolarized resting membrane potential around -80 mV or even lower, both in vivo and in vitro (Penttonen et al., 1997; Spruston and Johnston, 1992; Staley et al., 1992) as well as a relatively high threshold for generation of action potentials around -49 mV (Staley et al., 1992). These properties as well as the strong control of feedforward and feedback inhibition possibly result in a low spontaneous activity with firing rates around 0.1 Hz in behaving animals (Jung and McNaughton, 1993; Penttonen et al., 1997). In response to current injections, GCs show adaptation of the frequency of repetitive action potentials, which in turn are characterized by afterhyperpolarizations (Penttonen et al., 1997; Staley et al., 1992). The majority of those properties were found

to be similar in GCs recorded from animal and human hippocampal slices (Isokawa et al., 1991; Williamson et al., 1993). Adult born GCs, however, differ substantially in many aspects from the mature GCs described above. They are characterized by higher input resistance, more depolarized resting membrane potentials, and generate single or rudimentary action potentials of lower amplitude (Liu et al., 1996; Pedroni et al., 2014; Staley et al., 1992). They further possess smaller somata, incomplete dendritic arborization and tend to be GABAergic (Cabezas et al., 2013; Liu et al., 1996). Over several weeks, these characteristics gradually change and match those of mature GCs at the end of their maturation process (Ambrogini et al., 2004; Espósito et al., 2005). Mature and immature GCs also differ in the expression of molecular markers, such as calcium binding proteins (Brandt et al., 2003; Brown et al., 2003; Overstreet et al., 2004). Prox1, however, is a molecular marker which is expressed in the entire GC lineage (Iwano et al., 2012; Liu et al., 2000).

GCs are not exclusively located within the granule cell layer. If located within the hilus, they are termed ectopic GCs (Gaarskjaer and Laurberg, 1983). Those cells usually display similar electrophysiological properties and connectivity as normal GCs from the principal cell layer (Scharfman et al., 2003; Scharfman et al., 2000). In contrast, Prox1-expressing cells with differences in soma shape, dendritic arborization, axon collateral targets and in electrophysiology were found in the inner molecular layer and called semilunar GCs (Gupta et al., 2012; Larimer and Strowbridge, 2010; Williams et al., 2007).

GCs express different voltage-gated ion channels in their membranes. Various subforms of voltage-gated potassium, sodium, and calcium channels can be found throughout all compartments of the granule neurons, however, they show distinct expression patterns in different subcellular localizations (Vacher et al., 2008). A subset of those channels is enriched in the axon initial segment, located in close proximity to the soma (King et al., 2014; Schmidt-Hieber and Bischofberger, 2010; Vacher et al., 2008). Since the description of an enzymatic approach to generate isolated dentate GCs (Mody et al., 1989) the properties of different voltage gated potassium, calcium and sodium currents have been described in rat (Beck et al., 1992; Ellerkmann et al., 2003; Ketelaars et al., 2001; Köhr and Mody, 1991) and human GCs (Beck et al., 1997a,b; Reckziegel et al., 1998).

1.3 Animal models of epilepsy

During the development and research of novel AEDs, numerous animal models mimicking specific features of human epilepsy are used. Models for acute or chronic induced seizures, models for epilepsies other than TLE and models of chronic epilepsy

with spontaneous recurrent seizures that mimick a subset of the pathophysiological conditions found in human TLE are widely used (Löscher, 2011). Seizures alone can be evoked by electrical stimulation (e.g. maximal electroshock seizure (MES) test) or by injection of convulsant chemicals (e.g. pentylenetetrazole, PTZ seizure test). Those acute seizure models are mainly used during screening of substances acting as potential new AEDs (Löscher, 2011). Other approaches such as repeated electrical stimulation of limbic structures of the brain (kindling) or electrical or chemical induction of a status epilepticus (SE) are used to generate animals that display chronic or spontaneous recurrent seizures and may be used for further characterisation of screened compounds or for studies of epileptogenesis or pharmacoresistance (Kandratavicius et al., 2014; Löscher, 2011). In addition to the seizures, those animal models display similar patterns of neuronal loss and mimic the most striking pathophysiological features of human TLE (Curia et al., 2008; Sutula et al., 1994, see chapter 1.4). However, even between similar animal models the temporal profile and magnitude of neuropathological alterations can differ (Covolan and Mello, 2000; Kandratavicius et al., 2014; Morrisett et al., 1987).

1.3.1 The pilocarpine model of temporal lobe epilepsy

Whereas in human TLE patients epilepsy may be caused by brain malformations, infections, diseases or be influenced by genetic factors, one of the most common ways to induce SE in laboratory rodents and thereby generate epileptic animals that suffer from spontaneous recurrent seizures is the administration of the chemoconvulsant pilocarpine (Cavalheiro et al., 1991; Turski et al., 1983).

Injection of the muscarinic acetylcholine receptor agonist pilocarpine, either systemically or even directly into the brain, causes an imbalance between neuronal inhibition and excitation that results in increasingly stronger seizure activity which builds up into a SE (Priel and Albuquerque, 2002; Racine, 1972; Turski et al., 1983). To avoid unwanted peripheral cholinergic stimulation (piloerection, salivation, tremor, chromodacryorrhea and diarrhea) after pilocarpine-injection and restrict the effects to the brain, blood-brain barrier impermeable cholinergic antagonists (e.g. methyl-scopolamine) are frequently injected before application of pilocarpine (Clifford et al., 1987). This so-called acute period (SE) is followed by an epoch with reduced or predominantly nonconvulsive seizure activity (Goffin et al., 2007; Mazzuferi et al., 2012; Pitsch et al., 2017). During this often termed latent or silent period, rodents are believed to develop and show a similar pathophysiological changes as seen in human TLE (see chapter 1.4) thus this animal model is often used to mimic TLE and investigate its mechanisms and treatment (Curia et al.,

2008). Finally, during the chronic period higher numbers of behaviorally detectable spontaneous recurrent seizures – as observed in TLE patients – emerge.

One feature of the pilocarpine model that distinguishes it from many other animal models is the development of comparatively strong extrahippocampal or extratemporal damage and loss of neurons e.g. in cortical areas which can also be found in epilepsy patients (Covolan and Mello, 2000; Marsh et al., 1997; Sanabria et al., 2002). In the pilocarpine model of epilepsy, just like in other animal models, there are groups of animals that respond well to AEDs, as well as groups of animals that do respond in a variable manner or not at all to certain AEDs (Glien et al., 2002; Löscher and Rundfeldt, 1991). Similarly, a high inter-individual and even intra-individual variability is also an issue in human epilepsy and requires individually monitored and optimized AED schedules (Patsalos et al., 2008).

1.4 Changes in the epileptic hippocampus, dentate gyrus and granule cells

In many cases of TLE insults to the brain, often in early childhood, were reported and considered a possible starting point of a latent or silent period of epileptogenesis that finally leads to epilepsy (Mathern et al., 2002a). These initial precipitating injuries can range from head trauma and tumors over infectious or hypoxic conditions of the brain to febrile seizures or status epilepticus (Curia et al., 2014; Hauser et al., 1996; Mathern et al., 2002a).

In the epileptic brain, numerous changes are observed following epileptogenesis or SE and some alterations follow even single seizures (Parent et al., 1997; Wehner and Lüders, 2008). It is important to mention, however, that epileptogenesis can also occur without obvoius lesions, neuronal loss and network reorganization (Margerison and Corsellis, 1966; Zhang et al., 2002). The most obvious changes found in epileptic patients and animal models are volumetric reductions of hippocampal as well as extrahippocampal structures and thereby increased ventricle sizes (Cook et al., 1992; Marsh et al., 1997; Perez et al., 1985; Persinger et al., 1998; Polli et al., 2014; Sanabria et al., 2002). Hippocampal sclerosis is the most commonly observed pathologic condition and characterized by gliosis and severe loss of neurons in single or multiple subfields of the hippocampal formation, mainly in areas CA1 and the hilus (Blümcke et al., 2013; Margerison and Corsellis, 1966; see figure 1A). Cell loss was reported for mossy cells and different inhibitory interneurons of the hilar region and the surviving cells show aberrant morphology and synaptic connections (de Lanerolle et al., 1989; Maglóczky et al., 2000; Sloviter et al., 2003). Dentate GCs are also subject to multiple changes. Neurogenesis of GCs is altered following

induced seizures and during epilepsy (Crespel et al., 2005; Mathern et al., 2002b; Parent et al., 1997). An increasing number of the newly born granule cells integrate aberrantly outside the GC layer and are found in the hilus and the molecular layer (Crespel et al., 2005; Parent et al., 1997; Scharfman et al., 2000). This broadening of the cell layer is termed granule cell dispersion and may be associated with loss of GCs or not (Houser, 1990). Compared to healthy brains, basal dendrites are induced in 5% of epileptic rodent GCs and in more than 40% of cells in TLE patients (see chapter 1.2.2; Ribak et al., 2000; Scheibel et al., 1974; von Campe et al., 1997) accompanied by swelling or shrinkage of dendrites and a general loss or reduction of dendritic spines (Scheibel et al., 1974). Degenerating nerve terminals as well as sprouting of mossy fibers, i. e. a reorganization of the GC axons that aberrantly terminate on other GCs within the principal cell layer and the molecular layer are frequent findings in epileptic tissue (Houser et al., 1990; Parent et al., 1999; Scheibel et al., 1974; Tauck and Nadler, 1985; see figure 1B).

In summary, loss of inhibitory interneurons and mossy cells together with increased and aberrant recurrent excitatory connections and neurogenesis cause changes in the excitation-inhibition balance and may result in reverbatory networks that are able to initiate unprovoked seizures on their own (Jinde et al., 2013; Kobayashi and Buckmaster, 2003; Ribak et al., 2000; Spampanato and Dudek, 2017). At least some of the alterations described so far may act as compensatory mechanisms in an attempt to restore excitation and inhibition to levels found in healthy brains.

1.4.1 Pharmacoresistance

In addition to the cellular and structural pathological alterations that make the hippocampus hyperexcitable, there are further changes that occur during epileptogenesis. Numerous hypotheses were prepared trying to explain why AEDs lose their efficacy in pharmacoresistant epilepsy patients or model animals. Whereas many approaches to characterize the occurrence of pharmacoresistance imply alterations in the severity of the resistance with time, it has been further suggested that patients might be aleady pharmacoresistant from the beginning of the disease (Berg et al., 2006; Kwan and Brodie, 2000; Löscher and Schmidt, 2006).

Genetic factors such as mutations in ion channels can not only cause cause epilepsy, they have also been shown to affect AED efficacy and required drug dosages (Lerche et al., 2013; Tang et al., 2017). The gene variant hypothesis of pharmacoresistance considers genetic alterations in genes encoding ion channels as well as AED-metabolizing enzymes as possible causes of drug resistance. In this way, the medication itself may also contribute to the development of tolerance as a form of

pharmacoresistance. Repeated application of AEDs over prolonged periods of time may lead to an increase in the metabolism of the drug or to drug-induced changes in receptor densities or sensitivity (Löscher and Schmidt, 2006).

In epilepsy and especially in pharmacoresistant epilepsy the active transport or clearance of antiepileptic and other drugs from the brain via multidrug transporters located in the endothelial cells of the blood–brain barrier (BBB) was shown to be altered (Rizzi et al., 2002; Volk and Löscher, 2005). The BBB becomes more permeable following SE as well as during seizures in the chronic phase of human and experimental epilepsy which in turn results in increased expression of drug efflux transporters as a compensatory mechanism (van Vliet et al., 2006; van Vliet et al., 2010). In animal models of and patients with pharmacoresistant epilepsy, P-glycoprotein (PGP) and multidrug-resistance associated proteins (MRPs) as well as further proteins related to drug resistance in diseases other than epilepsy were found to be overexpressed (Dixit et al., 2017; Remy and Beck, 2006; Zhang et al., 2012). The extent to which AEDs and other substrates are transported out of the brain can vary between different tissues in which these proteins are expressed and even more between homologous transporters of different species, however (Baltes et al., 2007). As this upregulation of drug efflux transporters causes decreased AED brain but not plasma levels the so-called transporter hypothesis is considered as one of the possible mechanisms of pharmacoresistance (Remy and Beck, 2006; Zhang et al., 2012). Similarly, the pharmacokinetic hypothesis claims that overexpression of drug transporters is not only limited to endothelial cells of the BBB but extends to astrocytes, neurons and even peripheral organs such as the liver which would result in overall low AED concentrations (Lazarowski et al., 2007; Tang et al., 2017).

Another prominent approach trying to explain why AEDs lose their efficacy in pharmacoresistant epilepsy is the target hypothesis (Remy and Beck, 2006). Altered expression levels of voltage-gated sodium, potassium and calcium channel subunits along with alternative splicing of sodium channel mRNA were found following SE in different animal models of epilepsy or in human epilepsy syndromes (Lerche et al., 2013; Remy and Beck, 2006). Similar to voltage-gated ion channels, the expression levels and subunit composition of neurotransmitter receptors were either found or hypothesized to be altered in TLE patients and epilepsy models (Brooks-Kayal et al., 1999, 1998; Mathern et al., 1997, 1998; Notenboom et al., 2005). Furthermore, seizure-induced posttranslational modifications can induce translocation or internalization of both voltage-gated ion channels as well as neurotransmitter-receptors and thereby alter their surface-expression (Rakhade and Jensen, 2009). As many of those channels act as targets for (novel) AEDs (Bialer et al., 2017; Doeser et al., 2014a; Rogawski et al., 2016) those differences in channel structure, expression

and localization may lead to impaired AED-target binding and thereby to reduced efficacy in pharmacoresistant patients and animal models (Remy and Beck, 2006).

1.5 Antiepileptic drugs

Antiepileptic drugs (AEDs) mean to suppress the occurrence of seizures and are therefore also referred to as antiseizure drugs or anticonvulsants, however, many AEDs are also used in neurological disorders other than epilepsy (Landmark, 2008; Rogawski et al., 2016). Some AEDs show additional neuroprotective properties (Caccamo et al., 2016; Landmark, 2008; Licko et al., 2013) and only recently developed drugs seem to address the long demanded requirements of having disease modifying or antiepileptogenic properties (Doeser et al., 2014a). Different AEDs mediate their effects on different groups of targets which include voltage-gated ion channels but also neurotransmitter receptors and other synaptic proteins involved in neurotransmitter release and trafficking thereby altering and ideally restoring excitation or inhibition towards more balanced levels as found in nonepileptic, healthy brains or reducing the intrinsic excitability of neurons (Landmark, 2008; Rogawski et al., 2016). At least seven of the more than twenty currently available AEDs block voltage-gated sodium channels (VGSCs) as their main mechanism of action and further AEDs with multiple modes of action affect VGSCs along other or yet unidentified main targets (Brodie, 2017).

1.5.1 Voltage-gated sodium channels as antiepileptic drug targets

VGSCs are bell-shaped transmembrane proteins that form a cation-conducting pore in the cell membrane of neurons and other excitable cells and are crucial for the initiation and propagation of action potentials and the intrinsic excitability of neurons (Hille, 1971, 1972; Sato et al., 2001). The Na^+-conducting pore of VGSCs is formed by a ~260 kDa α subunit which can be associated with regulatory 30–40 kDa β subunits (see figure 2). Small differences in VGSC α isoforms result in different properties regarding their activation and inactivation as well as their sensitivity towards toxins and drugs (Catterall et al., 2005; Vilin and Ruben, 2001). Whereas expression of α subunits alone is sufficient to conduct ions, the presence of one or two $\beta 1$ to $\beta 4$ subunits in the VGSC complex can further modify gating properties as well as drug and toxin sensitivity and efficacy (Catterall et al., 2005; Gilchrist et al., 2013; Grieco et al., 2005; Lenkowski et al., 2003; Uebachs et al., 2010; Zhang et al., 2013b). Nine isoforms of VGSC α subunits termed $Na_v1.1$–$Na_v1.9$ have been identified, with $Na_v1.1$, $Na_v1.2$, $Na_v1.3$, and $Na_v1.6$ being the major isoforms expressed in the mammalian CNS (Goldin, 2001). While $Na_v1.1$ seems to be preferentially

expressed on somata of hippocampal principal neurons, $Na_v1.2$ is located rather in processes and terminals of neurons than on their somata. High densities of $Na_v1.6$ but also other brain soidum channels can be found clustered at the axon initial segment. $Na_v1.3$ is mainly expressed in the developing brain (Vacher et al., 2008).

The sodium channel α subunit is a polypeptide folding into four homologous domains (termed I–IV) each of which comprises six α-helical transmembrane segments (S1–S6; figure 2). Each of these domains comprises a voltage-sensing domain (VSD, composed of S1–S4) and a pore-forming domain (PD, S5, S6 and their linking P-loop). The membrane reentrant P-loops connecting segments S5 and S6 contribute one amino acid per domain to the selectivity filter determining the selectivity for Na^+ ions (Catterall, 2017). In response to membrane depolarization, the positively charged amino acid residues of the voltage-sensors (S4 segments) move outward and confer an opening of the channel pore via conformational changes in the VSD and PD thereby permitting Na^+ ions to cross the membrane (Catterall and Swanson, 2015). Sustained depolarization results in fast inactivation of VGSCs after few milliseconds (Hodgkin and Huxley, 1952). This is mediated by coupling movement of one of the voltage sensors to the intracellular linker connecting domains III and IV which acts as a blocking particle folding towards the intracellular mouth of the channel and thereby prevents ion conduction (Kühn and Greeff, 1999; Vassilev et al., 1988). After repolarization, sodium channels recover from fast inactivation, slightly slower but also within milliseconds (Hodgkin and Huxley, 1952). Following prolonged depolarization or trains of action potential firing, VGSCs can enter a distinct, slow inactivated state – either from the fast inactivated state but also directly from open or closed channel conformations (Ellerkmann et al., 2001; Ruff, 1996). Both, entry into and recovery from slow inactivation emerge on a substantially slower time scale (ranging from seconds to minutes) than entry and recovery of fast inactivation (Ellerkmann et al., 2001; Vilin and Ruben, 2001). The mechanism of slow sodium channel inactivation is still not completely understood. However, structural changes in the outer pore forming loops that would cause a collapse of the ion permeation pathway are likely involved in slow inactivation alongside with movements of the voltage sensors and the intracellular blocking particle (Boiteux et al., 2014a; Tikhonov and Zhorov, 2007; Vilin and Ruben, 2001; Xiong et al., 2006). Whereas fast inactivation controls the availability of VGSCs during single action potentials and their refractory time, slow inactivation affects membrane excitability and properties of multiple action potentials or bursts over tens of seconds to minutes for example during seizure activity (Vilin and Ruben, 2001).

The Na^+ current mediated by the fast or transient activation and inactivation described above is termed transient sodium current (I_{NaT}). A small fraction (around

1%) of VGSCs however can stay open without inactivating or can reopen at later time points of depolarization resulting in a persistent, non-inactivating Na^+ current (I_{NaP}) that regulates neuronal excitability around and below firing threshold (Alzheimer et al., 1993; Patlak and Ortiz, 1986). Both of these currents are found in hippocampal principal cells (Doeser et al., 2014a; Uebachs et al., 2010). A third type of Na^+ current mediated by VGSCs – however not present in hippocampal principal neurons – is the so-called resurgent current that occurs upon repolarization (Grieco et al., 2005; Raman and Bean, 1997). Both, differences in the properties of I_{NaT} and I_{NaP} were reported in epileptic conditions (Ellerkmann et al., 2003; Mantegazza et al., 2010).

Sodium channels harbor a wide variety of binding sites for toxins and other drugs (Catterall, 2017; Stevens et al., 2011; Waszkielewicz et al., 2013). Despite differences in their precise mode of action, most sodium channel blocking AEDs were found to bind to the same binding site (neurotoxin binding site 2) in studies replacing batrachotoxin (BTX) or other toxins from this site (Kuo, 1998; Waszkielewicz et al., 2013). In addition, the common AED binding site seems to partially overlap with the local anaesthetic binding site (Tikhonov and Zhorov, 2017; Yang et al., 2010). Interestingly, binding of BTX (and other site 2 neurotoxins) confers completely opposite effects on VGSCs than sodium channel blocking AEDs do although binding to the same primary binding site (Huang et al., 1982; Rogawski et al., 2016; Stevens et al., 2011; Tikhonov and Zhorov, 2005, 2017). Neurotoxin binding site 2 is located in the central cavity of the aequous pore and the S6 segments of all four domains as well as parts of the pore-forming loops seem to contribute to this binding site (Tsang et al., 2005; Wang and Wang, 2003). In addition to this high affinity binding site different drugs seem to have multiple low affinity binding sites on VGSCs that bind drugs more weakly while accessing their primary binding site in the lumen of the channel pore (Boiteux et al., 2014b; Martin and Corry, 2014; Yang et al., 2010). Many sodium channel blocking drugs act in a voltage-dependent and activity-dependent manner which is explained by preferential binding to VGSCs in their inactivated states (Catterall and Swanson, 2015). After the conformational changes leading to opening of the channel pore drugs are believed to access and bind their receptor site in the central cavity more easily than in the resting state (Hille, 1977; Lipkind and Fozzard, 2010).

Due to differences in structure and mechanism of action, i.e. interaction with different amino acid residues and functional parts of VGSCs, AEDs can show differential effects on multiple properties of VGSCs (Eijkelkamp et al., 2012). Since I_{NaT} and I_{NaP} can be mediated by the same channel, it is not surprising that AEDs can affect both types of currents (Alzheimer et al., 1993; Eijkelkamp et al.,

2012). Effects on I_{NaP} typically involve reductions of the maximal conductance and can be accompanied by small hyperpolarizing shifts of the voltage dependence of activation (Doeser et al., 2014b; Stafstrom, 2007; Taverna et al., 1998; Uebachs et al., 2012, 2010). I_{NaP} under normal conditions and especially increased I_{NaP} in epileptic conditions contribute to subthreshold excitability and thus can facilitate repetitive firing, however, a reduction of the I_{NaP} amplitude by AEDs may counterbalance this increased neuronal excitability (Mantegazza et al., 2010; Stafstrom, 2007). On I_{NaT}, however, AEDs can exert a broader spectrum of effects including effects on fast and slow inactivated channels. The effects on fast inactivation include a slowing of the recovery from VGSC inactivation, as well as shifts in the activation and inactivation properties (Remy et al., 2003a,b; Vreugdenhil and Wadman, 1999). Activity-dependent reduction of repetitive action potential firing and slowing of the recovery from fast inactivation as an underlying mechanism were proposed as a major mechanism of action of older AEDs (Kuo et al., 1997). Hyperpolarizing shifts of the voltage dependence of the steady-state inactivation as well as depolarizing shifts in the voltage dependence of activation result in reduced channel availability and consequently current amplitudes. Notably, those drug-induced shifts occur exactly in the opposite direction to those shifts that have been described following epileptogenesis (Ellerkmann et al., 2003; Ketelaars et al., 2001; Vreugdenhil et al., 1998). Newer anticonvulsants interact with VGSCs in their slow inactivated state without or with minor effects on fast inactivation processes (Doeser et al., 2014a; Errington et al., 2008; Hebeisen et al., 2015). These effects include enhancement of entry into slow inactivated states characterized by hyperpolarizing shifts of the voltage dependence of slow inactivation, however, without affecting the recovery time course. Interactions with slow inactivated channels were proposed to be beneficial since they would result in stronger reductions of repetitive firing during prolonged depolarizations e.g. during seizures and much less prominent effects during normal neuronal activity (Beyreuther et al., 2007).

1.5.2 Carbamazepine

Being in use since the 1960s for treatment of epilepsy and other diseases, carbamazepine (CBZ) is among the oldest and most commonly used AEDs (Androsova et al., 2017; Morselli and Frigerio, 1975). CBZ affects a variety of targets including multiple neurotransmitter receptors and ion channels, however the most prominent of its antiepileptic effects are mediated via VGSCs (Ragsdale and Avoli, 1998; Soares-da-Silva et al., 2015). CBZ binds these channels preferentially in the fast inactivated state and mediates its antiepileptic effects in a voltage-dependent and

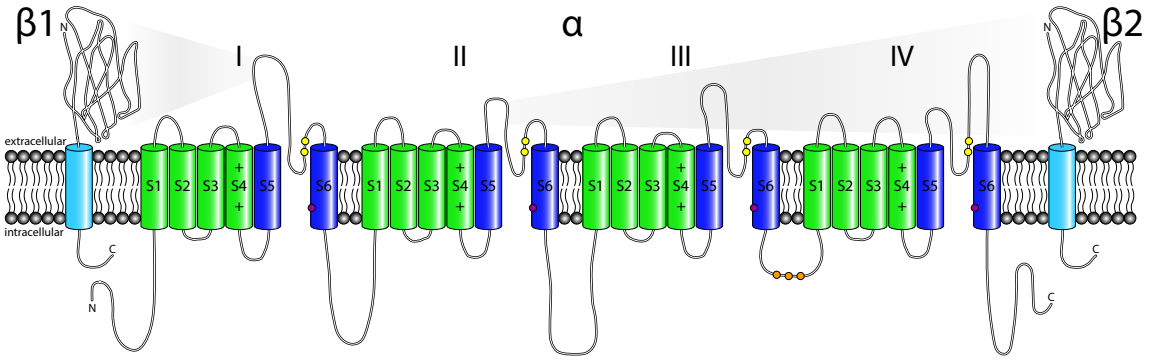

Figure 2: Schematic diagram of a VGSC complex. Structure of a pseudo-tetrameric pore-forming α subunit (green/blue) and two modulatory β subunits (cyan). Each homologous domain of the α subunit is composed of a VSD (green) and a PD (blue). The membrane reentrant pore-forming loops of each PD harbor two amino acid residues determining the ion selectivity of the channel (indicated in yellow). The portion of the intracellular blocking particle important for fast inactivation by binding to its receptor-sites at the inner mouth of the channel pore is highlighted in orange. Pore facing residues located in all four S6 segments are part of neurotoxin bindig site 2 (shown in purple) parts of which are also involved in high affinity binding of AEDs and other drugs. Redrawn after Stevens et al., 2011, Catterall and Swanson, 2015, and Das et al., 2016.

activity-dependent (use-dependent) manner by shifting the steady-state inactivation curve to hyperpolarized potentials, thereby reducing maximal I_{NaT} amplitudes but also by slowing the recovery of fast inactivation (Kuo et al., 1997; Lipkind and Fozzard, 2010; Ragsdale and Avoli, 1998).

Although being commonly used, a number of drawbacks were reported for CBZ including induction of its own metabolism and interference with many other drugs (including AEDs) as well as neurotoxicity due to its active metabolite CBZ epoxide (Gillham et al., 1988; Morselli and Frigerio, 1975). Potential proepileptic tendencies of CBZ were also reported (Booker et al., 2015; So et al., 1994). The main problem, especially in the context of this work, however, is the prominent role of CBZ (but also other older AEDs) in pharmacoresistance to AEDs (Remy et al., 2003a,b; Schaub et al., 2007). Studies conducted in different animal models of epilepsy but also in chronic epileptic tissue of epilepsy patients found a marked reduction or even a loss of CBZ efficacy (Jandová et al., 2006; Löscher and Rundfeldt, 1991; Reckziegel et al., 1999; Remy et al., 2003a; Uebachs et al., 2010; Vreugdenhil and Wadman, 1999). According to the target hypothesis of pharmacoresistance, changes in the properties of VGSCs as a target for AEDs may result in reduced efficacy of slowing the recovery of fast inactivation which translates into reduced blockade of repetitive

action potential firing and increased seizure activity (Ellerkmann et al., 2003; Remy and Beck, 2006; see chapter 1.4.1).

1.6 Aim and outline of this thesis

Pharmacoresistance to AEDs is a problem affecting around one third of epilepsy patients. Loss of efficacy of use-dependent blocking of the older AED carbamazepine (CBZ) but also reduced blocking effects of other older AEDs were repeatedly reported in tissue resected from chronic epilepsy patients but also in multiple animal models of epilepsy and consequently and led to the establishment of the target hypothesis of pharmacoresistance.

This thesis addresses the question whether the same or similar phenomena that result in a reduced efficacy of older anticonvulsants also apply to recently approved AEDs. Two novel compounds, namely eslicarbazepine (S-Lic) and lacosamide (LCM) were investigated with respect of their detailed mechanism of action on dentate gyrus granule cells (DGCs). Previous studies investigated the mechanism of action of both compounds in cultured neuroblastoma cells and only one other study researched whether fast inactivation processes and repetitive action potential firing in epileptic versus control tissue are differently affected by S-Lic. Publication one continues investigating the mechanisms of action of S-Lic in DGCs using the same approach that was used to reveal loss of efficacy of CBZ, however on the yet fairly uncharted mechanism of slow inactivation processes under epileptic conditions:

1. Holtkamp, D., Opitz, T., Hebeisen, S., Soares-da-Silva, P., and Beck, H. (2018). Effects of eslicarbazepine on slow inactivation processes of sodium channels in dentate gyrus granule cells. *Epilepsia* 59, 1492–1506.

Publication two adresses the effects of LCM on fast and slow inactivation processes as well as action potential firing, again in brain tissue obtained from nonepileptc and epileptic rats as well as chronic epilepsy patients:

2. Holtkamp, D., Opitz, T., Niespodziany, I., Wolff, C., and Beck, H. (2017). Activity of the anticonvulsant lacosamide in experimental and human epilepsy via selective effects on slow Na^+ channel inactivation. *Epilepsia* 58, 27–41.

2 Effects of eslicarbazepine on slow inactivation processes of sodium channels in dentate gyrus granule cells

2.1 Introduction

Novel AEDs are developed with the aim of increasing tolerability or anticonvulsant potency over existing drugs (Benes et al., 1999; Hainzl et al., 2001). Carbamazepine (CBZ; first generation) as well as its derivatives oxcarbazepine (OXC; second generation) and eslicarbazepine acetate (ESL; third generation) represent structurally related members of the dibenzazepine family of AEDs. Both, OXC and ESL act as prodrugs for their pharmacologically active metabolites – the R- and S-enantiomers of licarbazepine (R-Lic, S-Lic). Due to a higher brain penetration, longer half-life and slightly increased anticonvulsant potency, S-Lic was considered favorable over R-Lic (Alves et al., 2008; Fortuna et al., 2013; McLean et al., 1994). While around 80% of OXC undergoes stereoselective biotransformation to S-Lic, ESL is almost completely (~95%) converted to S-Lic (Almeida et al., 2008; Flesch et al., 1992; Perucca et al., 2011). In patients treated with ESL, therapeutic mean plasma levels between 10 and 90 μM were reported for S-Lic (Elger et al., 2009; Perucca et al., 2011). Plasma to whole brain ratios ranging from ~0.2 to 0.7 were calculated, however, the actual S-Lic concentration in brain tissue was predicted to be considerably higher since its preference to accumulate in the organic phase of the brain (Soares-da-Silva et al., 2015).

Although ESL was initially approved for adjunctive treatment and more recently as monotherapy for the treatment of focal seizures, its precise mechanism of action was not fully determined at the time of approval (Shirley and Dhillon, 2016). Compared to its precursor-drugs, the metabolites of ESL show strongly reduced interactions with other AEDs and drug-metabolizing enzymes and seem to cause less neurological impairment (Araújo et al., 2004; Benes et al., 1999; Falcão et al., 2012; Landmark et al., 2016; Morte et al., 2013). Instead, antiepileptogenic potency was reported (Doeser et al., 2014a). S-Lic acts on a less broad target spectrum than CBZ including blockade of T-type calcium channels along with its most prominent effects on VGSCs (Soares-da-Silva et al., 2015). While conflicting data on the modulation of VGSC fast inactivation by S-Lic are available, strong reductions of repetitive action potential firing were observed in epileptic as well as control tissue in unaltered magnitude (Doeser et al., 2014a; Hebeisen et al., 2015). Only recently, potent efficacy in modulation of slow inactivation processes was reported for S-Lic

in cultured N1E-115 mouse neuroblastoma cells (Hebeisen et al., 2015).

The following publication investigates the so far undetermined effects of S-Lic on slow sodium channel inactivation processes in rat and human epileptic principal neurons of the DG and sensorimotor cortex and compares those findings to nonepileptic control cells.

2.2 Publication

Accepted: 6 June 2018

DOI: 10.1111/epi.14504

FULL-LENGTH ORIGINAL RESEARCH

Epilepsia®

Effects of eslicarbazepine on slow inactivation processes of sodium channels in dentate gyrus granule cells

Dominik Holtkamp[1] | Thoralf Opitz[1] | Simon Hebeisen[2] | Patrício Soares-da-Silva[3,4] | Heinz Beck[1]

[1]Institute of Experimental Epileptology and Cognition Research, University of Bonn, Bonn, Germany

[2]B'SYS, Witterswil, Switzerland

[3]Bial - Portela & C[a], S.A., São Mamede do Coronado, Portugal

[4]MedInUP - Center for Drug Discovery and Innovative Medicines, Faculty of Medicine, University of Porto, Porto, Portugal

Correspondence
Heinz Beck, Institute of Experimental Epileptology and Cognition Research, University of Bonn, Bonn, Germany.
Email: Heinz.beck@ukb.uni-bonn.de
and
Patrício Soares-da-Silva, MedInUP - Center for Drug Discovery and Innovative Medicines, Faculty of Medicine, University of Porto, Porto, Portugal.
Email: psoares.silva@bial.com

Funding information
Deutsche Forschungsgemeinschaft, Grant/Award Number: SFB 1089; BIAL – Portela & Ca. S.A.; BONFOR; EpiTarget

Summary

Objective: Pharmacoresistance is a problem affecting ~30% of chronic epilepsy patients. An understanding of the mechanisms of pharmacoresistance requires a precise understanding of how antiepileptic drugs interact with their targets in control and epileptic tissue. Although the effects of (S)-licarbazepine (S-Lic) on sodium channel fast inactivation are well understood and have revealed maintained activity in epileptic tissue, it is not known how slow inactivation processes are affected by S-Lic in epilepsy.

Methods: We have used voltage clamp recordings in isolated dentate granule cells (DGCs) and cortical pyramidal neurons of control versus chronically epileptic rats (pilocarpine model of epilepsy) and in DGCs isolated from hippocampal specimens from temporal lobe epilepsy patients to examine S-Lic effects on sodium channel slow inactivation.

Results: S-Lic effects on entry into and recovery from slow inactivation were negligible, even at high concentrations of S-Lic (300 μmol/L). Much more pronounced S-Lic effects were observed on the voltage dependence of slow inactivation, with significant effects at 100 μmol/L S-Lic in DGCs from control and epileptic rats or temporal lobe epilepsy patients. For none of these effects of S-Lic could we observe significant differences either between sham-control and epileptic rats, or between human DGCs and the two animal groups. S-Lic was similarly effective in cortical pyramidal neurons from sham-control and epileptic rats. Finally, we show in expression systems that S-Lic effects on slow inactivation voltage dependence are only observed in $Na_v1.2$ and $Na_v1.6$ subunits, but not in $Na_v1.1$ and $Na_v1.3$ subunits.

Significance: From these data, we conclude that a major mechanism of action of S-Lic is an effect on slow inactivation, primarily through effects on slow inactivation voltage dependence of $Na_v1.2$ and $Na_v1.6$ channels. Second, we demonstrate that this main effect of S-Lic is maintained in both experimental and human epilepsy and applies to principal neurons of different brain areas.

KEYWORDS
anticonvulsant drugs, epilepsy, eslicarbazepine, pharmacoresistance

1 | INTRODUCTION

In chronic epilepsy, there is an urgent need for novel antiepileptic drugs (AEDs). Currently, seizures in ~30% of epilepsy patients are insufficiently controlled by drug therapy; this number can be much higher in subtypes of focal epilepsy. An understanding of the mechanisms of pharmacoresistance is therefore mandatory and requires a precise understanding of how AEDs interact with their targets in control and epileptic tissue.

We had previously shown that transient Na^+ channels in chronically epileptic tissue exhibit a key change that renders them less susceptible to the anticonvulsant drug carbamazepine (CBZ); use-dependent block of transient Na^+ channels is lost in both human and experimental epilepsy, suggesting that this is a key mechanism underlying pharmacoresistance to CBZ on the cellular level.[1,2] We have shown that eslicarbazepine (also [S]-licarbazepine [S-Lic]) overcomes this potential cellular resistance mechanism to conventional AEDs.[3] S-Lic is the active metabolite of eslicarbazepine acetate, a third-generation member of the dibenzazepine family of AEDs. After oral administration, eslicarbazepine acetate is hydrolyzed to S-Lic, which constitutes its major active metabolite.[4]

These studies, however, have examined only fast activation, inactivation, and recovery from inactivation. These processes take place on a millisecond time scale, as is appropriate for mediating rapid events such as action potentials. However, sodium channels invariably show slow inactivation processes that can modulate the availability of Na^+ channels on a time scale of seconds to minutes. Slow inactivation processes can powerfully modulate the availability of Na^+ channels in a membrane potential–dependent manner. In particular, slow inactivation and recovery will be invoked strongly during prolonged depolarization shifts or high-frequency activity. Thus, agents that modulate slow inactivation might potently interfere with ictogenesis under conditions of increased excitability.

We have therefore systematically investigated effects of S-Lic on slow inactivation of sodium channels. We have examined sodium channels in isolated dentate granule cells (DGCs) and sensorimotor cortex pyramidal neurons of control versus chronically epileptic rats (pilocarpine model of epilepsy) as well as in DGCs isolated from surgical specimens obtained during epilepsy surgery.

Key Points

- S-Lic potently reduces sodium current amplitudes
- S-Lic strongly affects slow inactivation at clinically relevant concentrations
- The main effect of S-Lic on slow inactivation is via a hyperpolarizing shift of the voltage dependence of slow inactivation
- S-Lic activity on voltage dependence of slow inactivation is maintained in experimental and human epilepsy
- S-Lic efficacy extends to cortical principal neurons
- Effects are mediated by $Na_v1.2$ and $Na_v1.6$ channels, whereas $Na_v1.1$ and $Na_v1.3$ are not affected
- S-Lic has multiple modes of action, including fast inactivation and slow inactivation as well as antiepileptogenic activity

2 | MATERIALS AND METHODS

2.1 | Pilocarpine animal model of epilepsy

Epileptic rats were generated as described previously.[3,5] Briefly, male Wistar rats (~200 g) obtained from Charles River (Wilmington, MA, USA) were housed under a 12-hour light/dark cycle and received food and water ad libitum. Status epilepticus (SE) was induced by single intraperitoneal injections of the muscarinic agonist pilocarpine (340 mg/kg; Sigma, Saint Louis, MO, USA) 30 minutes after the administration of methyl-scopolamine via the same route (1 mg/kg, Sigma), which aimed at reducing peripheral muscarinic effects. Around 50% (range = 20%-80%) of rats developed and survived SE. SE was attenuated and eventually terminated by a subcutaneous injection of diazepam (20 mg/kg; Ratiopharm, Ulm, Germany). Sedated animals were allowed to recover in individual cages and were video monitored for the development of chronic seizures starting approximately 2 weeks after SE. More than 75% (range = 50%-100%) of rats experienced video-documented and therefore behaviorally detectable seizures and were used as epileptic animals during this study. Animals that did not develop seizures following SE were not used in this study. Sham-injected control animals were treated equally but were injected with saline instead of pilocarpine. All experimental procedures were conducted in accordance with the guidelines of appropriate animal care committees.

2.2 | Surgical specimens from temporal lobe epilepsy patients

Hippocampal tissue was obtained from 11 pharmacoresistant epilepsy patients (average age = 42.09 ± 3.37 years) who underwent surgery to achieve improved seizure control (for details, see Table S1). Hippocampus sclerosis was reported in nine of 11 patients. Three of these patients

suffered from additional pathologic features (ganglioglioma and malformations of cortical development), and in the last two patients less pronounced pathological correlates were apparent. Informed consent was obtained for use of the specimens. Studies on human tissue were approved by the institutional research ethics committee.

2.3 | Animal preparation—hippocampal slices

Experiments were performed 54.9 ± 2.4 days (control group) to 61.6 ± 6.9 days post-SE (pilocarpine group). Animals were anesthetized with ketamine (100 mg/kg) and xylazine (15 mg/kg) and subsequently perfused through the heart with ice-cold, carbogenated (95% O_2, 5% CO_2; Linde, Munich, Germany) sucrose-based artificial cerebrospinal fluid (ACSF) comprising (in mmol/L) NaCl 60, sucrose 100, $NaHCO_3$ 26, KCl 2.5, NaH_2PO_4 1.25, $MgCl_2$ 5, $CaCl_2$ 1, and glucose 20, pH = 7.4, osmolality = 305 mOsm. The brain was rapidly removed and prepared for slicing.

2.4 | Preparation of rat and human hippocampal slices and dissociated dentate granule neurons

Horizontal hippocampal slices (rat, 300 µm; human, 400 µm) were prepared with a vibrating microslicer (VT1200S; Leica, Wetzlar, Germany) in carbogenated sucrose ACSF. Rat brains were sectioned in the same sucrose-based ACSF as was used during perfusion and subsequently transferred to a storage chamber filled with sucrose-based ACSF, prewarmed to 35°C in a water bath, where they remained for ~20 minutes. The corresponding solution used for slicing of human tissue contained (in mmol/L) NaCl 87, sucrose 75, $NaHCO_3$ 25, KCl 2.5, NaH_2PO_4 1.25, $MgCl_2$ 7, $CaCl_2$ 0.5, and glucose 25. Immediately after their preparation, human hippocampal slices were stored in ACSF composed of (in mmol/L) NaCl 124, KCl 3, $MgCl_2$ 2, $CaCl_2$ 2, $NaHCO_3$ 26, NaH_2PO_4 1.25, and glucose 10. Finally, rat as well as human slices were transferred into a chamber filled with carbogenated ACSF containing the following (in mmol/L): NaCl 125, KCl 3.5, $MgCl_2$ 2, $CaCl_2$ 2, $NaHCO_3$ 26, NaH_2PO_4 1.25, and glucose 15, pH = 7.4, osmolality = 307 mOsm. Slices remained there at room temperature until they were used for preparation of dissociated cells, for a minimal equilibration period of 30 minutes, however.

Acutely isolated DGCs were obtained by first digesting one slice at a time for 12 minutes in trituration solution composed of (in mmol/L) Na methanesulfonate 145, KCl 3, $CaCl_2$ 0.5, $MgCl_2$ 1, 4-(2-hydroxyethyl)-1-piperazineethanesulfonic acid (HEPES) 10, glucose 15, pH = 7.4 adjusted with NaOH, osmolality = 315 mOsm, which also contained pronase (protease type XIV, 2 mg/mL, Sigma), saturated with oxygen (Linde) and warmed to 36°C. This step was followed by an equilibration period of 10 minutes at room temperature (21-24°C) and a washing step in enzyme-free trituration solution. The dentate gyrus was dissected, and the neurons were isolated with fire-polished Pasteur pipettes of decreasing aperture in a Nunc dish (3.5 cm; Thermo Scientific, Waltham, MA, USA). Cells were allowed to settle for 10 minutes before patch clamp experiments commenced.

2.5 | Animal preparation—sensorimotor cortex

Animals were sacrificed 34.2 ± 2.4 days (pilocarpine group) to 39.9 ± 4.4 days post-SE (control group). Following ketamine/xylazine anesthesia, rats were perfused through the heart with ice-cold and carbogenated ACSF comprising (in mmol/L) NaCl 130, $NaHCO_3$ 26, KCl 3, NaH_2PO_4 1.25, $MgCl_2$ 2, $CaCl_2$ 2, and glucose 10, pH = 7.4. The frontal portion of the brain was rapidly removed and prepared for slicing.

2.6 | Preparation of sensorimotor cortex slices and dissociated pyramidal neurons

On a vibrating microslicer, a single 500-µm-thick coronal slice comprising primary sensory and motor cortices was cut approximately 1.8 mm anterior to the bregma. Slicing in the same ice-cold carbogenated ACSF that was also used during perfusion was followed by a 1-hour recovery period in the same solution warmed to 32°C. Subsequently, half of a slice was incubated at 28°C for 90 minutes in oxygenated bicarbonate-free ACSF that contained 25 mmol/L HEPES instead and was freshly supplemented with 0.01 mmol/L cysteine and 19 U/mL papain on every experimental day. After a washing step in enzyme-free solution, 1-to 2-mm-wide gray matter chunks were prepared and either stored in enzyme-free solution or triturated in a Ca^{2+}-free solution that contained 10 mmol/L ethyleneglycol-bis(2-aminoethylether)-*N*,*N*,*N*′,*N*′-tetraacetic acid instead, as well as 2 mmol/L freshly added kynurenic acid as described previously.[6]

2.7 | Whole cell voltage clamp experiments of isolated neurons

The trituration solution was exchanged slowly, and cell debris was washed away with recording solution containing (in mmol/L) Na methanesulfonate 40, tetraethylammonium-Cl 90, $CaCl_2$ 1.6, $MgCl_2$ 2, HEPES 10, $CdCl_2$ 0.2, 4-aminopyridine 5, glucose 15, pH = 7.4 adjusted with HCl;

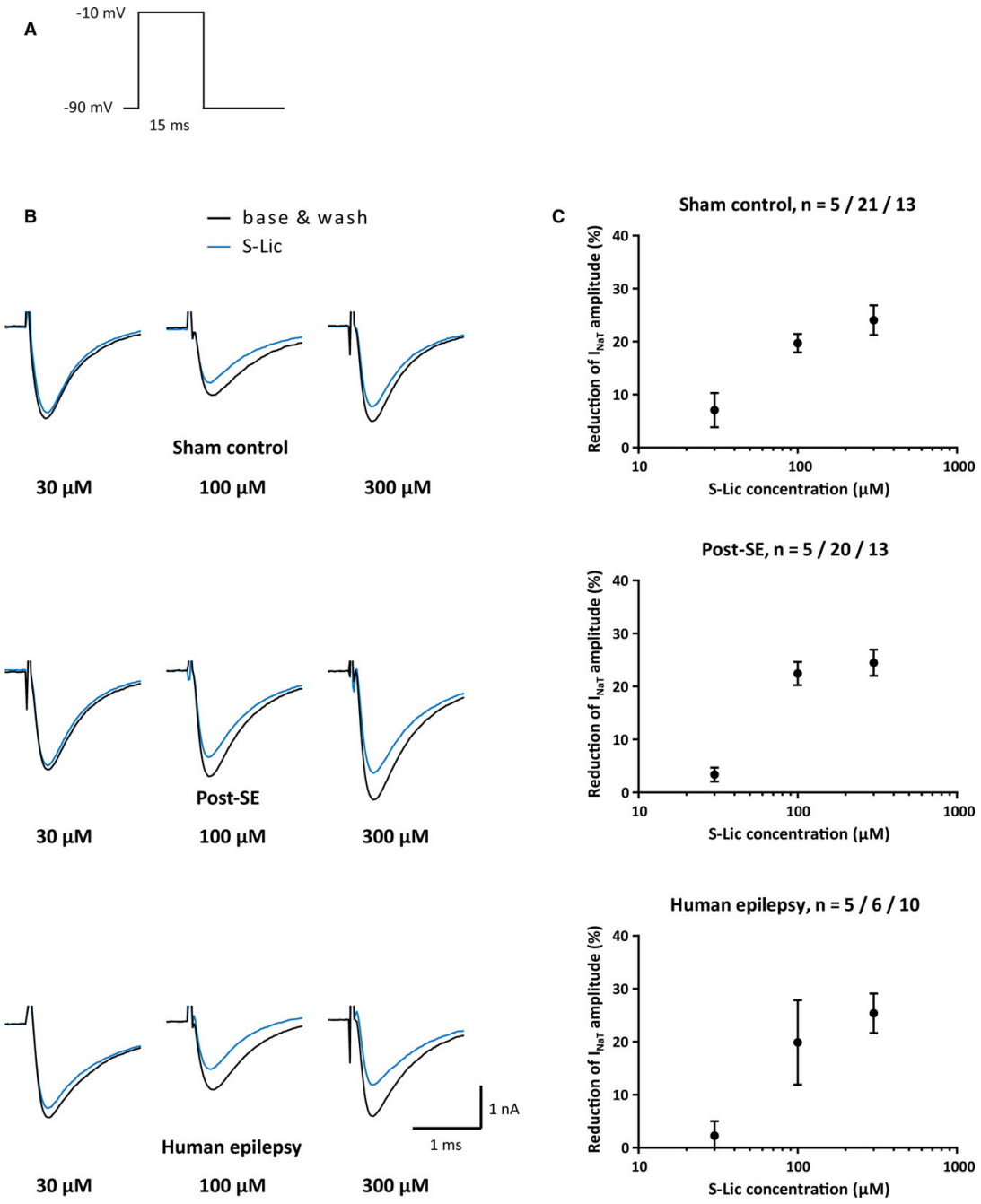

FIGURE 1 Reduction in maximal transient Na^+ current (I_{NaT}) at resting membrane potential. A, I_{NaT} was elicited in rat or human dentate granule cells by short test pulses (15-millisecond duration, every 5 seconds) from −90 mV to −10 mV during washin or washout of either 30, 100, or 300 µmol/L (S)-licarbazepine (S-Lic). B, Current traces are representative traces of currents with S-Lic (blue lines) and those recorded in drug-free solution (black lines, average of control and washout condition). C, On average, I_{NaT} was reduced by 7.09 ± 3.26%, 3.40 ± 1.32%, and 2.27 ± 2.75% in response to 30 µmol/L S-Lic, further reduced by 19.72 ± 1.75%, 22.44 ± 2.22%, and 19.87 ± 7.97% following perfusion of 100 µmol/L S-Lic, and even further reduced by 24.05 ± 2.79%, 23.71 ± 2.49%, and 25.37 ± 3.75% in the presence of 300 µmol/L S-Lic, in granule cells isolated from sham-injected rats, epileptic rats, and human epilepsy patients, respectively. SE, status epilepticus

osmolality = 310 mOsm adjusted with glucose. The recording pipettes were pulled from borosilicate glass capillaries (0.86 mm inner diameter, 1.5 mm outer diameter, with filament; Science Products, Hofheim, Germany) using a micropipette puller (Model P-97; Sutter Instruments, Novato, CA, USA) and were filled with intracellular solution that contained (in mmol/L) CsF 110, HEPES-Na 10, ethyleneglycoltetraacetic acid 11, $MgCl_2$ 2, tetraethylammonium-Cl 20, Na_2-GTP 0.5, ATP-Na_2 5, pH = 7.25 adjusted with CsOH, osmolality = 300 mOsmol. Patch pipettes displayed open tip resistances ranging from 4 to 7 MΩ in the bath solution. With the Nunc dish mounted on an inverted microscope (Axiovert 100; Zeiss, Gottingen, Germany), isolated granule cells were identified by their morphology as described previously.[7,8] Putative cortical pyramidal neurons were selected by their roundish-triangular morphology independent of soma size, which could vary from slightly larger to several-fold the size of DGCs. After formation of tight seal-resistances > 1 GΩ, the plasma membranes were ruptured, and transient Na^+ currents (I_{NaT}s), were recorded at room temperature under constant superfusion with oxygenated recording solution using a patch clamp amplifier (Axopatch 200B; Molecular Devices, Sunnyvale, CA, USA). Currents were filtered at 10 kHz, sampled at 50 kHz using a Digidata 1440A, and stored on a personal computer running Clampex 10.2 (Molecular Devices). Series resistance of recorded rat pyramidal neurons, and rat and human granule cells was 7.18 ± 0.53 MΩ, 7.95 ± 0.21 MΩ, and 6.89 ± 0.38 MΩ, respectively, and could be compensated between 75% and 85% resulting in maximal residual voltage errors of 3.41 ± 0.39 mV and 4.48 ± 0.19 mV for rat and 3.94 ± 0.52 mV for human recordings. Leak current was generally below 300 pA, input resistance between 300 and 800 MΩ, and series resistance ranged from 5 to 10 MΩ. Cells deviating significantly from these values were discarded. Neurons experiencing jumps in leak current resulting in sudden alterations of the peak amplitude and neurons with a rapid rundown of current amplitude resulting in currents too small for meaningful analyses were also discarded. Measured as well as command potentials were corrected for a calculated liquid junction potential of 10.0 mV.

2.8 | Expression systems

Stably transfected cell lines expressing human $Na_v1.1$ αβ1 or $Na_v1.2$ αβ1 sodium channels (both in HEK-293 cells; Scottish Biomedical, Glasgow, UK) or stably transfected cell lines expressing human $Na_v1.3$ α or $Na_v1.6$ α sodium channels (both in CHO-K1 cells; B'SYS, Witterswil, Switzerland) were grown in Dulbecco modified Eagle medium (Sigma-Aldrich, Saint Louis, MO, USA; containing 2 μg/mL blasticidin and 600 μg/mL geneticin [$Na_v1.1$ and $Na_v1.2$]) or HAM F12 medium (Sigma-Aldrich; containing 500 μg/mL geneticin [$Na_v1.3$] or 100 μg/mL hygromycin [$Na_v1.6$]) supplemented with 0.15 mg/mL L-glutamine, 10% fetal bovine serum (Sigma-Aldrich), and 1% penicillin/streptomycin under standard laboratory conditions (37°C, 5% CO_2, 95% relative humidity) and passaged at a confluence of 50%-80%.

For electrophysiological recordings 4-48 hours after the last passaging, cells were transferred to 35-mm culture dishes (Nunc) at a confluence suitable for recording from single cells. The cell culture medium was exchanged with recording solution containing (in mmol/L) Na methanesulfonate 30, NaCl 34.25, KCl 1, tetraethylammonium-Cl 67.5, $CaCl_2$ 1.65, $MgCl_2$ 1.75, $CdCl_2$ 0.15, HEPES 10, 4-aminopyridine 3.75, glucose 13.75, pH = 7.4 adjusted with HCl. Patch pipettes were pulled from borosilicate glass capillaries (0.86 mm inner diameter, 1.5 mm outer diameter, with filament; Warner Instruments, Hamden, CT, USA) on a vertical micropipette puller (P-10; Narishige, Tokyo, Japan) and filled with intracellular solution of identical composition as used for isolated cells. Open tip resistances ranged between 2 and 7 MΩ, series resistance was 7.52 ± 0.30 MΩ, and resistance was compensated by at least 50%. Recordings were obtained using an EPC-9/10 patch clamp amplifier (HEKA, Lambrecht, Germany) and PatchMaster software (HEKA) under the same conditions as stated above for isolated neurons.

FIGURE 2 Increased entry into slow inactivation. A, Entry of Na^+ channels into slow inactivation was induced by depolarizing dentate granule cells (DGCs) with a conditioning pulse for 1, 10, or 30 seconds from −90 mV holding potential to −10 mV. To allow recovery from fast inactivation, cells were repolarized for 1 second, and subsequently the fraction of channels available was determined by a 15-millisecond test pulse. The reduction compared to the current amplitude initiated by the conditioning pulse is due to slow inactivation. B, Representative recordings of Na^+ currents elicited by different conditioning pulses (black traces) or the test pulse 1 second after the end of the depolarizations (red traces). Examples from a granule cell of a sham-injected rat, a pilocarpine-treated rat, and an epilepsy patient. C, Lower transient Na+ current amplitudes as seen in B indicate increased slow inactivation of Na^+ channels in response to longer conditioning pulse durations. In both sham-injected and pilocarpine-treated rats, blocking effects increased slightly after washin of 300 μmol/L (S)-licarbazepine (S-Lic). D, Additional blocking effects were also seen in human DGCs. E, All three experimental groups do not differ in observed S-Lic effect sizes at any conditioning pulse duration. *$P < 0.05$, **$P < 0.01$, and ***$P < 0.001$. ACSF, artificial cerebrospinal fluid; SE, status epilepticus

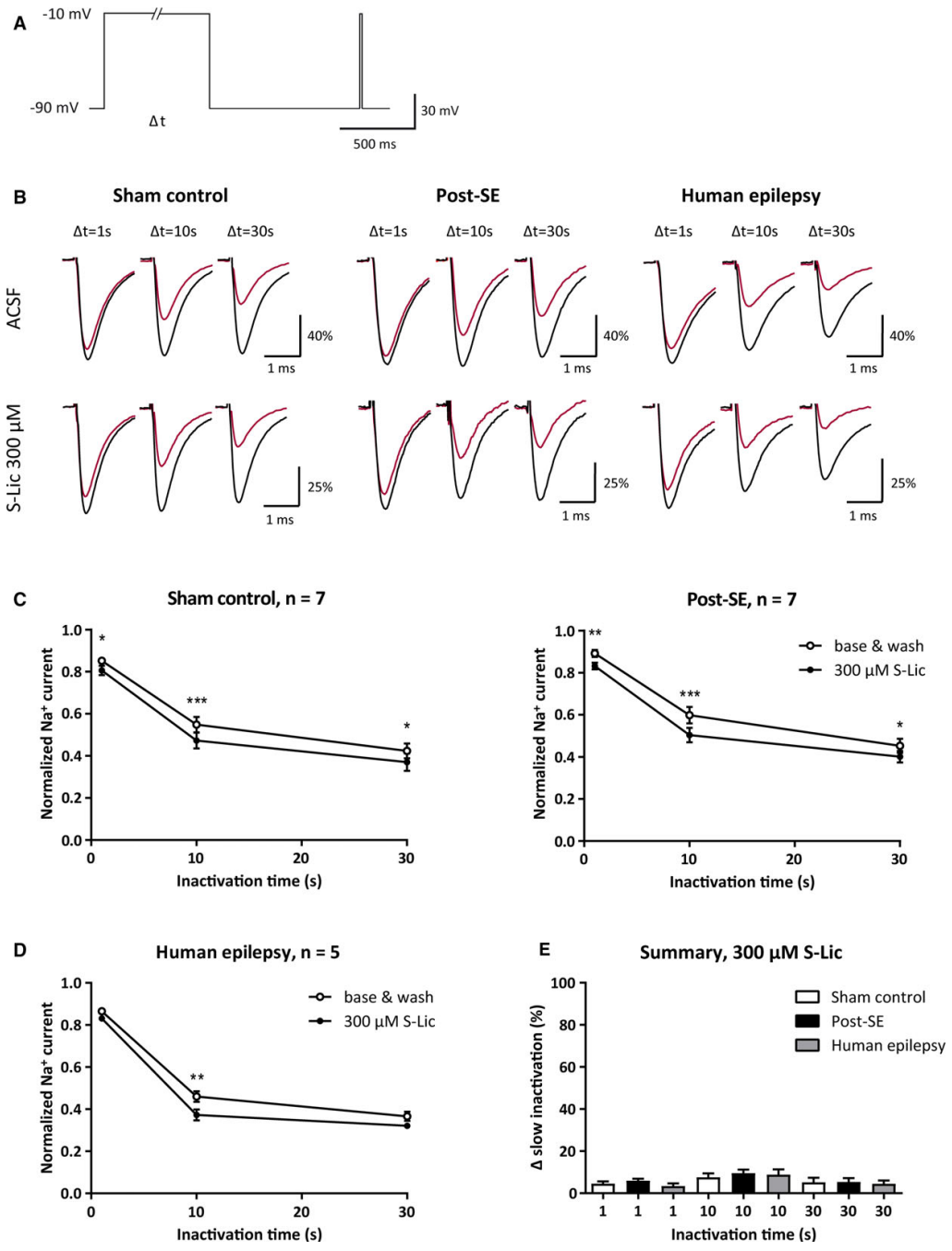

2.9 | Drugs

Stock solutions of S-Lic (obtained from Bial, São Mamede do Coronado, Portugal) were prepared freshly once per experimental day in dimethylsulfoxide (Merck, Darmstadt, Germany; Sigma) and added to the recording solution at 1:1000 (isolated cells). For cultured cells, the stock solution was diluted in recording solution and the final dimethylsulfoxide concentration was adjusted to 0.4% in all groups. The drug-free recording solution always contained equal amounts

of dimethylsulfoxide. Throughout the Results and Discussion, the drug-free recording solution will be abbreviated as "base & wash" or "ACSF," although being of different composition than ACSF stated above, whereas an identical solution containing S-Lic will be termed "S-Lic" with or without the respective concentration. In expression systems, only one test concentration or ACSF was tested per cell.

2.10 | Data analysis—isolated neurons

For the drug-dependent reduction of the peak I_{NaT} amplitude, currents recorded in drug-free recording solution (average of the first current of the washin phase and the last current of the washout phase of S-Lic) were compared to currents recorded in bath solution containing additional S-Lic (average of the last current of the drug washin and the current recorded at the beginning of the washout phase).

The change in I_{NaT} amplitudes was analyzed by comparing normalized currents elicited (by test pulses) during inactivation to the initial current amplitude (elicited by the conditioning pulse or a test pulse preceding the conditioning pulse) of each recording. Also, baseline values before washin of S-Lic and values after washout of the drug were averaged and compared to the values of the S-Lic recordings to correct for rundown effects over the duration of the experiments. Datasets for the voltage dependence of slow inactivation were additionally normalized to the current recorded after hyperpolarizing the granule cell, as this was generally the largest of all recorded currents.

The time course of the recovery of slow inactivation was fitted to the following biexponential function using a Levenberg-Marquardt algorithm:

$$I(t) = A_0 + A_{slow1} * e^{-t/\tau slow1} + A_{slow2} * e^{-t/\tau slow2}$$

with τ_{slow1} and τ_{slow2} being the slow and ultraslow time constant of recovery, A_{slow1} and A_{slow2} as their relative amplitude contributions, and $I(t)$ as the normalized current amplitude at time point t offset by A_0.

2.11 | Data analysis—cultured cells

In cultured cells, only one test concentration was tested per cell. The ratio of normalized (I_{norm}) amplitudes obtained after and before the conditioning pulse was plotted against the conditioning pulse voltage for each tested concentration and fitted with a sigmoidal equation:

$$I_{norm} = I_{min} + (I_{max} - I_{min})/1 + 10^{((V_{50}-X)*H)}$$

with I_{max} being the maximal normalized current fixed to 1 and I_{min} the remaining fraction of not slowly inactivated channels, X being the command potential, V_{50} the potential at half maximal inactivation, and H the Hill coefficient.

2.12 | Statistical analysis

All statistical tests were performed at a significance level α of 0.05. For statistical comparison of τ values, paired t tests were used. Individual voltage dependence experiments were analyzed by analysis of variance (ANOVA) with proper posttests mentioned in each individual experiment. If assumptions for an ANOVA were not met, appropriate nonparametric tests were used, which are also indicated for each individual statistical comparison. Normality was tested using a Shapiro-Wilk test. Results and other given values are presented as mean ± standard error of the mean. For posttest results omitted in the main text body see Table S3. Fitting and statistics were made in Prism 7 (GraphPad Software, La Jolla, CA, USA).

3 | RESULTS

3.1 | S-Lic reduces I_{NaT} amplitudes at resting membrane potential

We first determined the effects of S-Lic on sodium currents elicited from (hyperpolarized) potentials close to the resting membrane potential of DGCs, at which channels are fully recovered from fast inactivation. I_{NaT} was evoked by depolarizing DGCs from −90 mV to −10 mV before, during, and after perfusion of different concentrations (30, 100, 300 µmol/L) of S-Lic (Figure 1A). Concentration-dependent effects of S-Lic on I_{NaT} could be observed in granule cells isolated from sham-injected rats, epileptic rats, and human epilepsy patients (Figure 1B, black vs blue traces, summary with numbers given in Figure 1C). These data suggest that S-Lic exerts strong effects on sodium channels aside from the known effects on fast inactivation.

3.2 | S-Lic effects on entry into and recovery from slow inactivation

We next tested the idea that the entry into slow inactivation, or the recovery from slow inactivated states, is affected by S-Lic. Entry of Na^+ channels into slow inactivation was induced by depolarizing rat and human DGCs for 1, 10, or 30 seconds from −90 mV holding potential to −10 mV. A 15-millisecond test pulse 1 second after the end of the conditioning pulse was used to determine the reduction of the I_{NaT} amplitude by slow inactivation processes, as described previously (Figure 2A). In DGCs of sham-injected and epileptic rats as well as human patients, increasing the duration of the conditioning prepulses from 1 to 30 seconds caused a strong reduction in I_{NaT} due to increased entry into slow inactivation (Figure 2B, red traces vs black traces). In both rat groups, the fraction of channels entering slow inactivation was

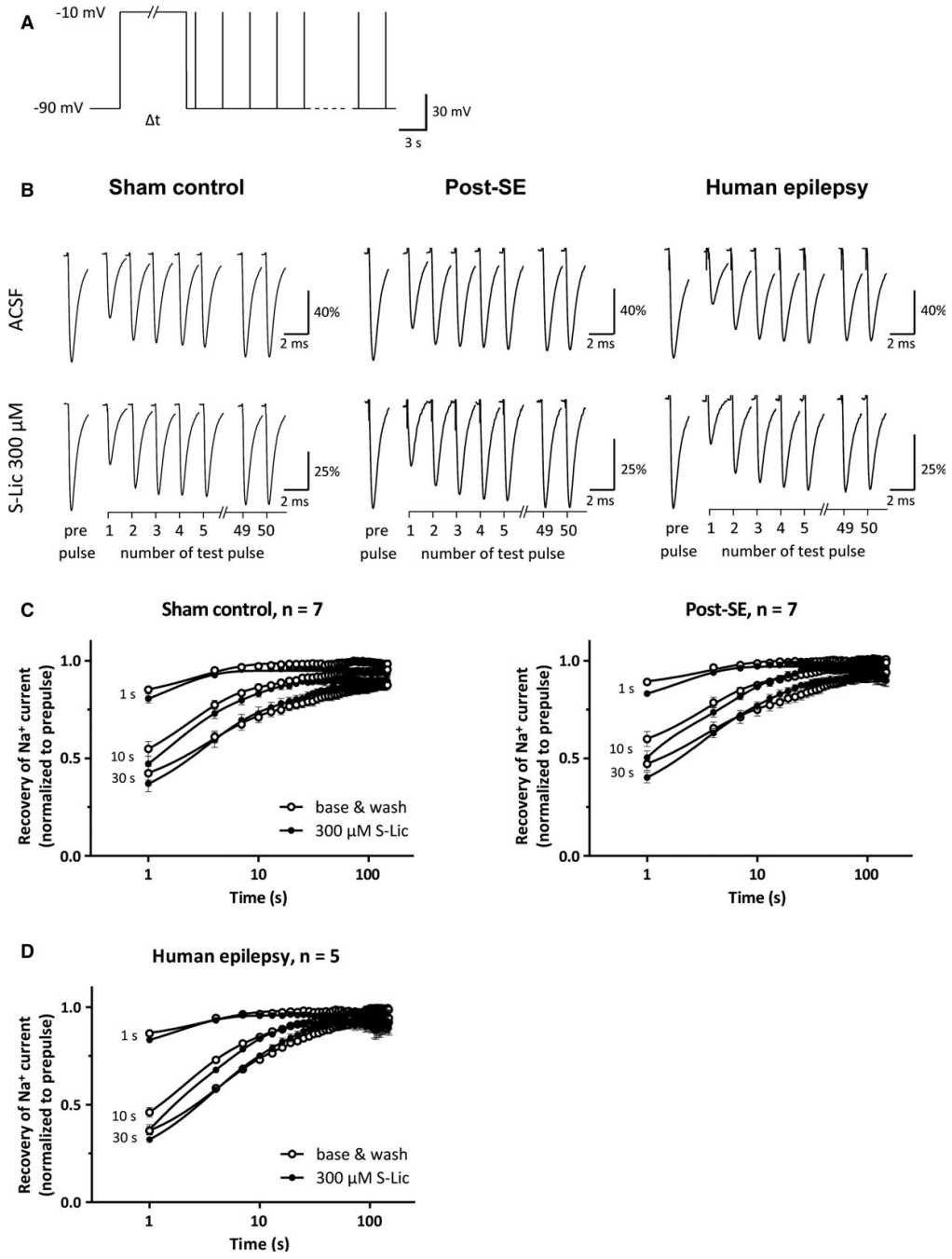

FIGURE 3 Unaltered recovery from slow inactivation. A, The time course of recovery from Na^+ channel slow inactivation was studied by applying 50 additional test pulses every 3 seconds following the conditioning pulse used to induce slow inactivation. B, Individual currents recorded in response to the conditioning pulse and test pulses to track recovery from slow inactivation over time for dentate granule cells (DGCs) isolated from normal rats, epileptic rats, and human epilepsy patients. C, Average recovery time course for both groups of rat granule cells in drug-free recording solution and under 300 µmol/L (S)-licarbazepine (S-Lic). D, Equivalent experimental results for human DGCs. ACSF, artificial cerebrospinal fluid; SE, status epilepticus

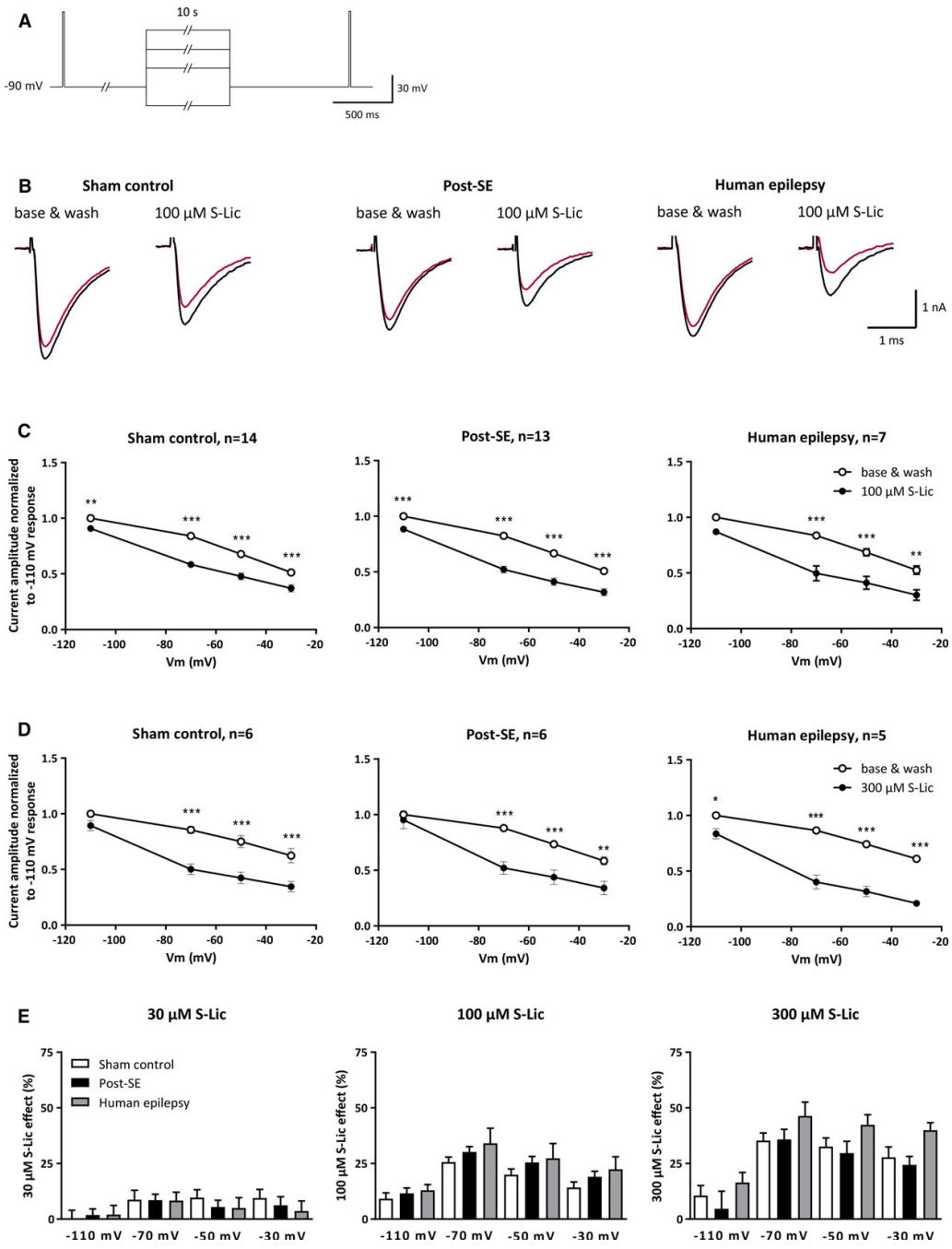

enhanced in response to 300 µmol/L S-Lic (Figure 2C, two-way ANOVA, sham control: $F_{1,\ 18} = 38.69$, $P < 0.001$; post-SE: $F_{1,\ 18} = 52.82$, $P < 0.001$, with $^{*}P < 0.05$, $^{**}P < 0.01$, and $^{***}P < 0.001$ in Bonferroni multiple comparisons test for S-Lic efficacy). Similar results were obtained from human epileptic DGCs (Figure 2D, two-way ANOVA, human epilepsy: $F_{1,\ 12} = 25.15$, $P < 0.001$, posttest as for rat groups). These effects were rather small and did not differ between all three experimental groups (Figure 2E, Kruskal-Wallis test

FIGURE 4 Potent hyperpolarizing shifts of the voltage dependence of slow inactivation. A, Voltage step protocol used to study the voltage dependence of Na^+ channel slow inactivation. A short test pulse to −10 mV was followed by variable conditioning pulse potentials ranging from −110 to −30 mV. Another test pulse was applied after recovery from fast inactivation at holding potential (−90 mV) 1 second after the end of the conditioning pulse. B, Representative examples of recorded Na^+ currents elicited by the test pulse before (black lines) and after a 10-second conditioning pulse to −70 mV (red lines). Note overall reduced current amplitudes and increased slow inactivation in the presence of 100 μmol/L (S)-licarbazepine (S-Lic). C, D, Summary of individual test pulse amplitudes normalized to the averaged baseline and washout test pulse amplitude following the −110-mV conditioning pulse. Averaged baseline and washout amplitudes (white symbols) were compared to those recorded under S-Lic (black symbols; C, 100 μmol/L; D, 300 μmol/L), resulting in significant amplitude reductions caused by a prominent hyperpolarizing shift of the voltage dependence. E, Effects of 30, 100, and 300 μmol/L S-Lic on the voltage dependence of slow inactivation for all three experimental groups were compared for each conditioning pulse voltage. None of the tested S-Lic concentrations resulted in significant differences at any tested conditioning pulse voltage, irrespective of comparing only healthy and epileptic rats (white vs black bars, Mann-Whitney test, not significant) or both rat groups and human epilepsy patients (white, black, and gray bars, Kruskal-Wallis test with Dunn multiple comparisons test, not significant). $^*P < 0.05$, $^{**}P < 0.01$, and $^{***}P < 0.001$. SE, status epilepticus

with Dunn multiple comparisons test, not significant). Lower concentrations of S-Lic (100 μmol/L, Figure S1) similarly increased the entry into slow inactivation (Figure S1B, C, and D, experiments done as in Figure 2). Again, the effect sizes were indistinguishable between both rat groups (Figure S1D, Mann-Whitney test, not significant). Collectively, these data show significant, but small, effects on entry into slow inactivation, with magnitudes below 10% of the maximal current amplitude.

We then studied the time course of recovery from Na^+ channel slow inactivation using established protocols. Briefly, slow inactivation was induced with a prolonged voltage step of 1, 10, or 30 seconds. Subsequently, the recovery from inactivation was monitored using brief test pulses applied every 3 seconds (Figure 3A). This protocol allows determination of the time course of recovery as a gradual increase in the I_{NaT} measured during the brief test pulses (Figure 3B, examples depicted for sham-control rats, epileptic rats, and human epilepsy patients in the absence and presence of 300 μmol/L S-Lic). The average recovery time course for both groups of rat granule cells and for human granule cells is depicted in Figure 3C and 3D, respectively. Similar recordings with 100 μmol/L S-Lic are depicted in Figure S2. As already apparent from these recordings and recovery time courses, the time constants derived after fitting the recovery of individual granule neurons were also largely unaffected by 100 or 300 μmol/L S-Lic (Figure S3, paired *t* test for comparison of recovery time constants, Wilcoxon matched-pairs test for comparison of fractions of slow and ultraslow recovery). Thus, both entry and recovery from inactivation are largely unaffected even by high concentrations of S-Lic (300 μmol/L).

3.3 | S-Lic strongly shifts the voltage dependence of slow inactivation to hyperpolarized potentials

To determine additional mechanisms that could account for the reduction in I_{NaT} via effects on slow inactivation, we studied whether S-Lic affects the voltage dependence of slow inactivation. To this end, we used a conditioning voltage protocol consisting of 10-second steps to various voltages between −110 mV and −30 mV to induce slow inactivation. Voltage-dependent inactivation was then assessed by determining the fraction of I_{NaT} inactivated by the conditioning pulse (Figure 4A, I_{NaT} assessed by brief test pulses before and after the conditioning pulse). Representative recordings are shown in Figure 4B for I_{NaT} preceding a conditioning pulse (black lines) and I_{NaT} evoked after the conditioning pulse (10 seconds, −70 mV, red lines).

In the presence of 100 μmol/L S-Lic, significant reductions in I_{NaT} amplitudes were found for all conditioning pulse voltages in rat as well as human granule cells (Figure 4C, two-way ANOVA, sham control: $F_{1,\ 52} = 189.1$, $P < 0.001$; pilocarpine-treated: $F_{1,\ 48} = 301.2$, $P < 0.001$; human epilepsy: $F_{1,\ 24} = 73.24$, $P < 0.001$; followed by Bonferroni multiple comparisons test for S-Lic efficacy with $^{**}P < 0.01$ and $^{***}P < 0.001$). We performed equivalent experiments applying 30 μmol/L and 300 μmol/L S-Lic (summarized in Figure 4E). Whereas 30 μmol/L S-Lic resulted in nonsignificant shifts, the effects seen for 300 μmol/L S-Lic were slightly more prominent than those observed for 100 μmol/L S-Lic. (Figure 4D, two-way ANOVA, sham control: $F_{1,\ 20} = 162.7$, $P < 0.001$; pilocarpine-treated: $F_{1,\ 20} = 71.43$, $P < 0.001$; human epilepsy: $F_{1,\ 16} = 229.5$, $P < 0.001$; followed by Bonferroni multiple comparisons test for S-Lic efficacy with $^*P < 0.05$, $^{**}P < 0.01$, and $^{***}P < 0.001$). For all tested drug concentrations, the efficacy of S-Lic on DGCs was unaltered between nonepileptic and epileptic rats (Figure 4E, white and black bars, Mann-Whitney test, not significant) as well as between rats and human epilepsy patients (Kruskal-Wallis test with Dunn multiple comparisons test, not significant). These data indicate that strong effects of S-Lic are observed on the voltage dependence of slow inactivation that seem to saturate at concentrations > 100 μmol/L.

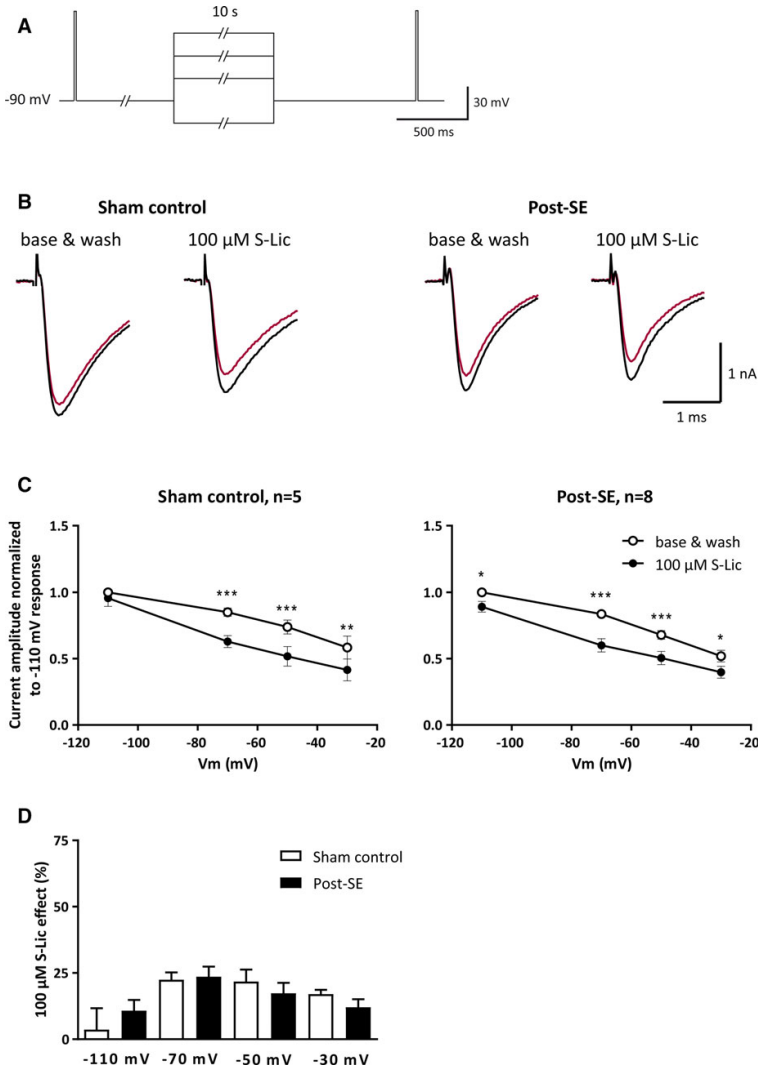

FIGURE 5 Similar efficacy in cortical pyramidal neurons. A, Same voltage step protocol as used to study the voltage dependence of Na^+ channel slow inactivation in dentate granule cells. B, Example transient Na^+ current recordings before (black lines) and after a 10-second conditioning pulse to −70 mV (red lines) under averaged predrug and postdrug application and under 100 µmol/L (S)-licarbazepine (S-Lic). C, Averaged current amplitudes from baseline and drug washout conditions (white symbols) and in the presence of 100 µmol/L S-Lic (black symbols) normalized to the test pulse recorded 1 second after the nondrug −110-mV conditioning pulse. Significantly reduced current amplitudes were revealed by two-way analysis of variance (sham control: $F_{1,\ 16} = 73.83$, $P < 0.001$; pilocarpine-treated: $F_{1,\ 28} = 74.12$, $P < 0.001$; Bonferroni multiple comparisons test for S-Lic efficacy with $^*P < 0.05$, $^{**}P < 0.01$, and $^{***}P < 0.001$). D, No significant differences in effect sizes between epileptic and nonepileptic pyramidal neurons at any tested voltage

They also demonstrate that these effects are maintained in chronic experimental and human epilepsy.

3.4 | S-Lic shows similar efficacy in epileptic and healthy cortical pyramidal neurons

We were curious whether the efficacy of S-Lic in chronic epileptic tissue is limited to hippocampal neurons or extends to extrahippocampal brain areas. Therefore, we studied the effects of S-Lic on voltage dependence of slow inactivation in isolated neocortical pyramidal neurons in nonepileptic and epileptic rats (Figure 5A). Similar to the results in DGCs, 100 µmol/L S-Lic reduced the maximal average I_{NaT} amplitude by 16.2 ± 3.9% and 19.7 ± 4.4% in sham control and pilocarpine-treated rats, respectively (examples in Figure 5B, calculated as for DGCs in

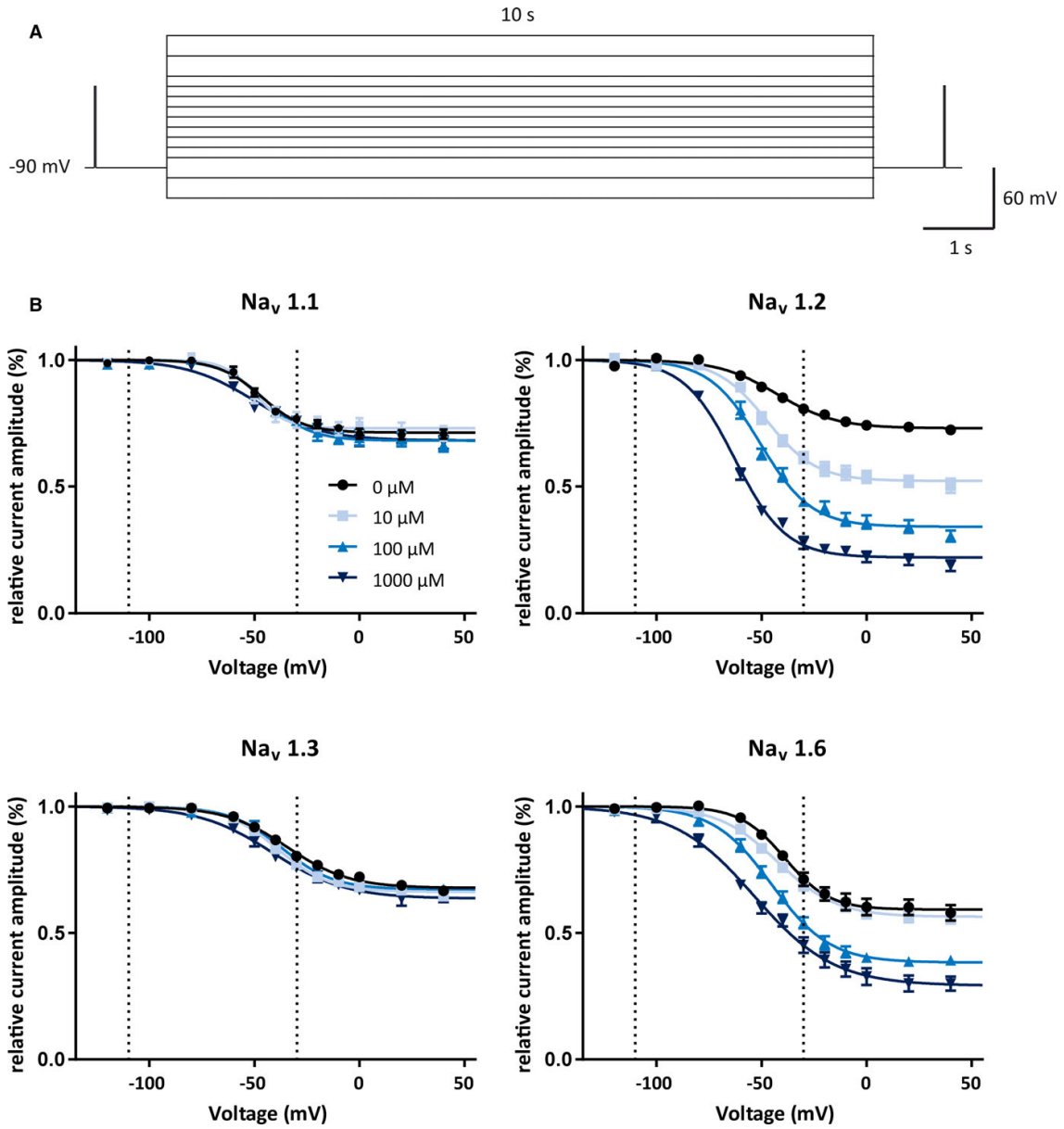

FIGURE 6 Sodium channel isoform-specific effects of (S)-licarbazepine. A, Voltage step protocol used to examine voltage dependence of slow inactivation in expression systems expressing either $Na_v1.1$, $Na_v1.2$, $Na_v1.3$, or $Na_v1.6$ channels. A 20-millisecond test pulse to −10 mV was applied 1 second before and 1 second after a 10-second conditioning pulse ranging from −120 to +40 mV in either 20- or 10-mV increments. B, Dose-dependent hyperpolarizing shifts of the voltage-dependence curves and increases in the fraction of slow inactivated channels were observed for $Na_v1.2$ and $Na_v1.6$ but not $Na_v1.1$ and $Na_v1.3$ channels. Dashed lines indicate the more confined voltage range tested in isolated neurons

Figure 1). Voltage-dependent S-Lic effects were also observed in pyramidal neurons, again with the strongest effects at intermediate voltages close to the resting membrane potential (Figure 5C and 5D). The drug effect sizes were also indistinguishable between pyramidal neurons isolated from healthy and epileptic brains (Figure 5D, Mann-Whitney test, not significant). From these data, we conclude that S-Lic exerts antiepileptic potency in DGCs as well as cortical pyramidal neurons to a similar extent, both in epileptic and nonepileptic tissue.

3.5 | S-Lic effects are predominantly mediated via $Na_v1.2$ and $Na_v1.6$ sodium channel isoforms

Finally, we investigated the effects of different concentrations of S-Lic on relevant brain sodium channel isoforms expressed in either CHO or HEK cells. In these experiments, we were able to assess a more extensive range of voltage, due to the high stability of recordings in expression systems (Figure 6A). In cells expressing $Na_v1.1$ or $Na_v1.3$ channels, no or very limited effects on the voltage dependence of slow inactivation were observed up to concentrations of 1000 μmol/L S-Lic (Figure 6B, left panels). In contrast, in cells expressing $Na_v1.2$ or $Na_v1.6$, a strong hyperpolarizing shift of the voltage-dependence curves and an additional increase in the fraction of slow inactivated channels could be observed in the presence of S-Lic (Figure 6B, right panels). These effects were strongly dose-dependent and increased with higher concentrations of S-Lic. Interestingly and in contrast to all other tested sodium channel isoforms, obvious yet insignificant S-Lic effects on $Na_v1.2$ channels were already apparent at very low S-Lic concentrations of 10 μmol/L (Table S2; ANOVA followed by Dunnett posttest for V_{50} and Kruskal-Wallis test followed by Dunn posttest for I_{min}).

4 | DISCUSSION

The main result of this study is that S-Lic exhibits strong effects of sodium channel slow inactivation, mainly via effects on the voltage dependence of slow inactivation in native human and rat neurons. These effects are confined to $Na_v1.2$ and $Na_v1.6$ subunits and are not observed in $Na_v1.1$ and $Na_v1.3$ subunits. Moreover, the efficacy of S-Lic in modulating slow inactivation voltage dependence is maintained in chronic human and experimental epilepsy and extends to principal cells of at least the two investigated brain areas.

The strong effects on slow inactivation seen for S-Lic have been observed previously in expression systems.[9] Similar effects are shared by some other AEDs. Lacosamide also exerts effects on slow inactivation in different types of neurons.[5,10,11] Moreover, as seen for S-Lic, lacosamide also shifts the voltage dependence of slow inactivation in a hyperpolarizing direction as a major effect, whereas other effects on slow inactivation were small.[5,10] In contrast to those AEDs, the effects of CBZ on slow inactivation are virtually negligible, with well-known pronounced effects on fast inactivation processes.[9] Lacosamide does differ from S-Lic in that effects on fast inactivation voltage dependence were undetectable or small,[5,10,11] whereas S-Lic does have significant effects on fast sodium channel gating in native neurons.[3] Another study, however, did not find significant S-Lic effects on fast inactivation in expression systems.[9] These findings underscore that sodium channel blockers are not by any means equivalent. Rather, they show marked differences in how they act on different kinetic parameters of sodium channels, in this case in particular slow versus fast inactivation. The structural basis for these differences is unclear, but the question of why these compounds behave differently is intriguing. Molecular modeling approaches may be extremely useful to determine candidate mechanisms related to the interaction between AEDs and channel structures.[12]

A further difference between AEDs is additional targets aside from voltage-gated Na^+ channels. Sodium channels are not the only targets for S-Lic, with T-type calcium channels being another relevant target that may be responsible for antiepileptogenic mechanisms of action.[3] In contrast, sodium channels seem to be the major target for lacosamide, as binding studies have excluded binding of lacosamide to different types of γ-aminobutyric acid and glutamate receptors, as well as a variety of other neurotransmitter receptors, and voltage-gated potassium or calcium channels.[13,14]

A first question addressed in this study was whether the effects of S-Lic are maintained in chronic epilepsy. A previous study has shown that the active metabolite of the anticonvulsant eslicarbazepine acetate has potent use-dependent effects in experimental and human epilepsy, and has add-on effects to CBZ.[3] Is this also the case for slow inactivation? Our data show that the answer to this question is yes. We observed quantitatively maintained effects of S-Lic not only on slow inactivation in experimental epilepsy, but also on sodium channels in granule cells obtained from epilepsy surgical specimens. This is similar to the maintained activity of lacosamide on slow inactivation and use-dependent block in chronic experimental and human epilepsy that was observed in a previous study.[5] In addition, we have shown that the maintained activity also extends to cortical areas, which also display pathological changes in chronic epilepsy models.[15-17]

Given the prominent effects of S-Lic on the voltage dependence of slow inactivation in different types of native neurons, we examined which Na channel alpha subunits are responsible for this effect. The results were surprisingly clear—$Na_v1.1$ and $Na_v1.3$ slow inactivation is not affected by S-Lic even at high concentrations, whereas strong effects are seen for $Na_v1.2$ and $Na_v1.6$. The largest effects of S-Lic could be observed on $Na_v1.2$ channels with potent effects even at low concentrations of 10 μmol/L.

$Na_v1.2$ and $Na_v1.6$ channels are both expressed prominently in principal neurons. In contrast, $Na_v1.1$ is strongly expressed in fast-spiking interneurons.[18] This may argue

for a cell type–specific inhibitory action of S-Lic that spares interneurons enriched in $Na_v1.1$. Moreover, this specificity positions S-Lic as a potential anticonvulsant therapy in diseases with compromised $Na_v1.1$ function in interneurons, such as loss-of-function $Na_v1.1$ mutations or Alzheimer's disease.[19-22] Intriguingly, in Alzheimer's disease, anticonvulsants that block Na^+ channels indiscriminately are ineffective, presumably because they further impair interneuron functionality, whereas levetiracetam, which has a presynaptic mode of action, is effective.[23] This and these previous studies suggest that AED effects on slow inactivation are an important mode of action that is surprisingly isoform specific.

Two important considerations emerge from these and published data. First, it may be important to develop AEDs with multiple modes of action such as S-Lic; however, far from being indiscriminate, each of these modes of action shows a sometimes surprising specificity for ion channel isoforms. It has been argued with a similar logic that classical use-dependent Na^+ channel blockers could be meaningfully combined with other compounds with different specificity. Future studies will have to show whether combining specific modes of action shows synergistic effects, both in animal models and in humans. Second, it will be increasingly important to show that anticonvulsant mechanisms of action are maintained in chronic epilepsy, as shown for S-Lic with respect to effects on both fast and slow inactivation. Developing such compounds with multiple specific mechanisms of action that are stable even in chronic epilepsy will be important to overcome target mechanisms of pharmacoresistance.

ACKNOWLEDGMENTS

This work was supported by the Deutsche Forschungsgemeinschaft (SFB 1089, to H.B.), the EU integrated project EpiTarget, the BONFOR program of the University of Bonn Medical Center, and Bial.

DISCLOSURE OF CONFLICTS OF INTEREST

P.S.-d.-S. was an employee of Bial at the time of the study. S.H. and H.B. have served as paid consultants for Bial. The remaining authors have no conflicts of interest to report. We confirm that we have read the Journal's position on issues involved in ethical publication and affirm that this report is consistent with those guidelines.

ORCID

Patrício Soares-da-Silva http://orcid.org/0000-0002-2446-5078

REFERENCES

1. Remy S, Gabriel S, Urban BW, et al. A novel mechanism underlying drug resistance in chronic epilepsy. Ann Neurol. 2003;53:469–79.
2. Remy S, Beck H. Molecular and cellular mechanisms of pharmacoresistance in epilepsy. Brain. 2006;129:18–35.
3. Doeser A, Dickhof G, Reitze M, et al. Targeting pharmacoresistant epilepsy and epileptogenesis with a dual-purpose antiepileptic drug. Brain. 2015;138:371–87.
4. Almeida L, Potgieter JH, Maia J, et al. Pharmacokinetics of eslicarbazepine acetate in patients with moderate hepatic impairment. Eur J Clin Pharmacol. 2008;64:267–73.
5. Holtkamp D, Opitz T, Niespodziany I, et al. Activity of the anticonvulsant lacosamide in experimental and human epilepsy via selective effects on slow Na+channel inactivation. Epilepsia. 2017;58:27–41.
6. Alzheimer C, Schwindt PC, Crill WE. Modal gating of Na+ channels as a mechanism of persistent Na+ current in pyramidal neurons from rat and cat sensorimotor cortex. J Neurosci. 1993;13:660–73.
7. Mody I, Salter MW, MacDonald JF. Whole-cell voltage-clamp recordings in granule cells acutely isolated from hippocampal slices of adult or aged rats. Neurosci Lett. 1989;96:70–5.
8. Beck H, Clusmann H, Kral T, et al. Potassium currents in acutely isolated human hippocampal dentate granule cells. J Physiol. 1997;498:73–85.
9. Hebeisen S, Pires N, Loureiro AI, et al. Eslicarbazepine and the enhancement of slow inactivation of voltage-gated sodium channels: a comparison with carbamazepine, oxcarbazepine and lacosamide. Neuropharmacology. 2015;89:122–35.
10. Errington AC, Stöhr T, Heers C, et al. The investigational anticonvulsant lacosamide selectively enhances slow inactivation of voltage-gated sodium channels. Mol Pharmacol. 2008;73:157–69.
11. Niespodziany I, Leclère N, Vandenplas C, et al. Comparative study of lacosamide and classical sodium channel blocking antiepileptic drugs on sodium channel slow inactivation. J Neurosci Res. 2013;91:436–43.
12. Boiteux C, Vorobyov I, French RJ, et al. Local anesthetic and antiepileptic drug access and binding to a bacterial voltage-gated sodium channel. Proc Natl Acad Sci U S A. 2014;111:13057–62.
13. Errington AC, Coyne L, Stöhr T, et al. Seeking a mechanism of action for the novel anticonvulsant lacosamide. Neuropharmacology. 2006;50:1016–29.
14. Rogawski MA, Tofighy A, White HS, et al. Current understanding of the mechanism of action of the antiepileptic drug lacosamide. Epilepsy Res. 2015;110:189–205.
15. Covolan L, Mello LE. Temporal profile of neuronal injury following pilocarpine or kainic acid-induced status epilepticus. Epilepsy Res. 2000;39:133–52.
16. Sanabria ERG, Da Silva AV, Spreafico R, et al. Damage, reorganization, and abnormal neocortical hyperexcitability in the pilocarpine model of temporal lobe epilepsy. Epilepsia. 2002;43:96–106.
17. Young NA, Szabó CÁ, Phelix CF, et al. Epileptic baboons have lower numbers of neurons in specific areas of cortex. Proc Natl Acad Sci U S A. 2013;110:19107–12.
18. Ogiwara I, Miyamoto H, Morita N, et al. Nav1.1 localizes to axons of parvalbumin-positive inhibitory interneurons: a circuit

basis for epileptic seizures in mice carrying an Scn1a gene mutation. J Neurosci. 2007;27:5903–14.
19. Yu FH, Mantegazza M, Westenbroek RE, et al. Reduced sodium current in GABAergic interneurons in a mouse model of severe myoclonic epilepsy in infancy. Nat Neurosci. 2006;9:1142–9.
20. Hedrich UBS, Liautard C, Kirschenbaum D, et al. Impaired action potential initiation in GABAergic interneurons causes hyperexcitable networks in an epileptic mouse model carrying a human Na(V)1.1 mutation. J Neurosci. 2014;34:14874–89.
21. Tai C, Abe Y, Westenbroek RE, et al. Impaired excitability of somatostatin- and parvalbumin-expressing cortical interneurons in a mouse model of Dravet syndrome. Proc Natl Acad Sci U S A. 2014;111:E3139–48.
22. Verret L, Mann EO, Hang GB, et al. Inhibitory interneuron deficit links altered network activity and cognitive dysfunction in Alzheimer model. Cell. 2012;149:708–21.
23. Sanchez PE, Zhu L, Verret L, et al. Levetiracetam suppresses neuronal network dysfunction and reverses synaptic and cognitive deficits in an Alzheimer's disease model. Proc Natl Acad Sci U S A. 2012;109:E2895–903.

SUPPORTING INFORMATION

Additional supporting information may be found online in the Supporting Information section at the end of the article.

How to cite this article: Holtkamp D, Opitz T, Hebeisen S, Soares-da-Silva P, Beck H. Effects of eslicarbazepine on slow inactivation processes of sodium channels in dentate gyrus granule cells. *Epilepsia*. 2018;59:1492–1506. https://doi.org/10.1111/epi.14504

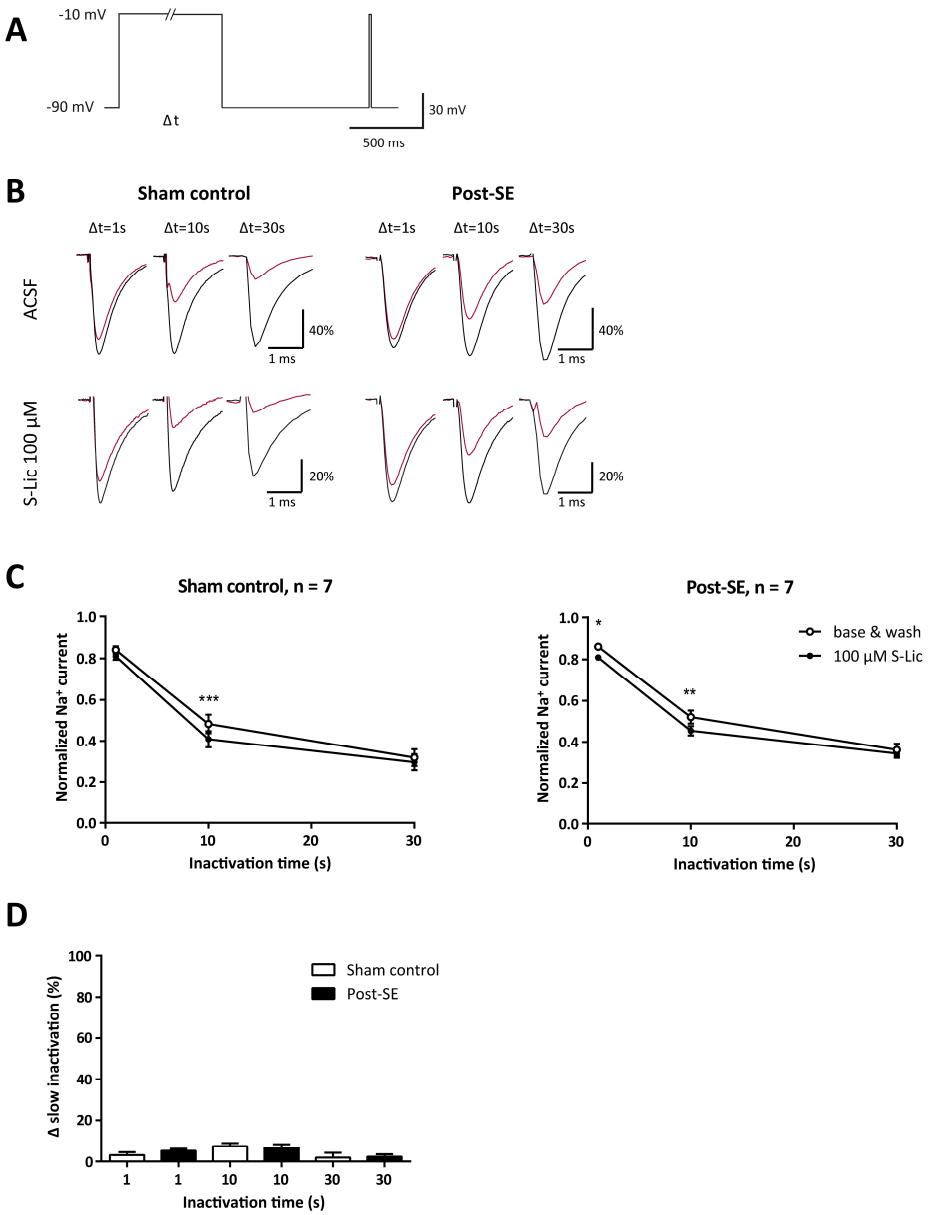

Supplementary Fig. 1: Lower concentrations of S-Lic also increase entry into slow inactivation. (**A**) Washing in recording solution that contained 100 µM instead of 300 µM S-Lic, the same voltage step protocol as explained in Fig. 2 was used. (**B**) Representative recordings of Na^+ currents following 1, 10 and 30 second depolarizing conditioning pulses in normal rats and epileptic rats (color scheme as in Fig. 2). (**C**) Following S-Lic application, lower Na^+ currents were recorded in DGCs of both rat groups (two-way ANOVA, sham control: $F_{(1, 18)}$=28.4, p<0.001; post-SE: $F_{(1, 18)}$=19.91, p<0.001, with * indicating p<0.05, ** p<0.01 and *** p<0.001 in Bonferroni's multiple comparisons test for S-Lic efficacy. (**D**) Effect sizes do not differ between both rat groups (Mann-Whitney test, n.s.).

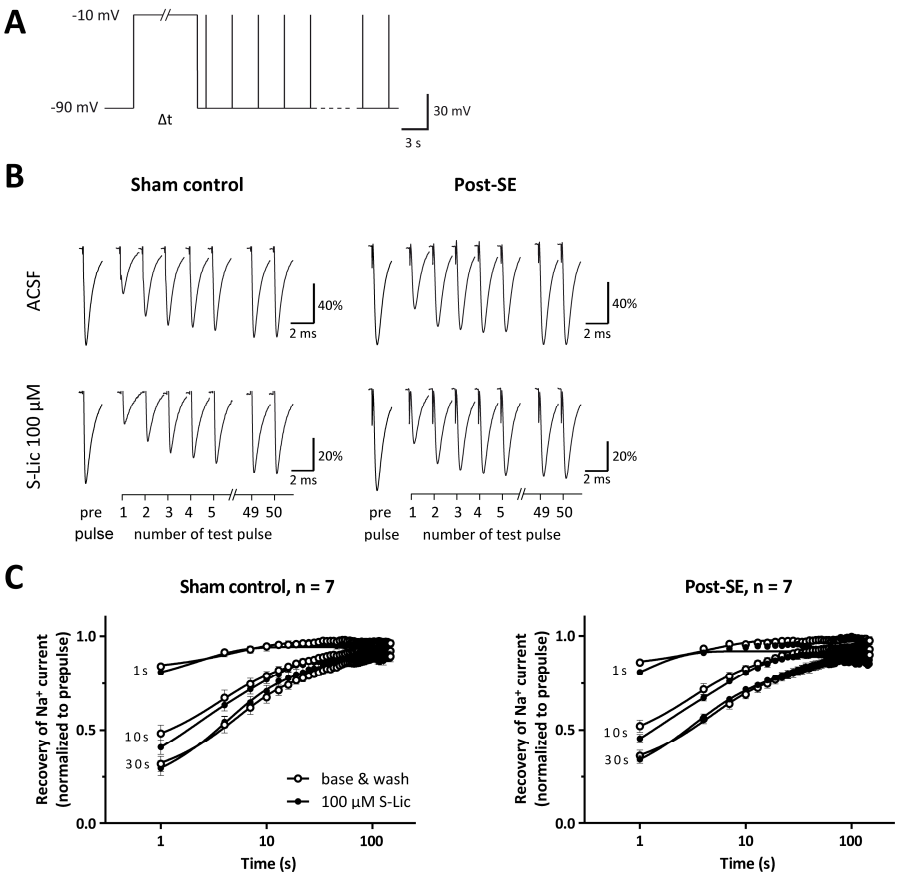

Supplementary Fig. 2: Unaltered recovery from slow inactivation following 100 µM S-Lic. (**A**) Experiments as described in Fig. 3 were replicated in presence of 100 µM instead of 300 µM S-Lic using identical protocols. (**B**) Individual currents recorded at the beginning of and after the conditioning pulse for dentate granule cells isolated from normal and epileptic rats. (**C**) Averaged time course of recovery from slow inactivation for both groups of rat granule cells in drug-free recording solution and following perfusion of 100 µM S-Lic.

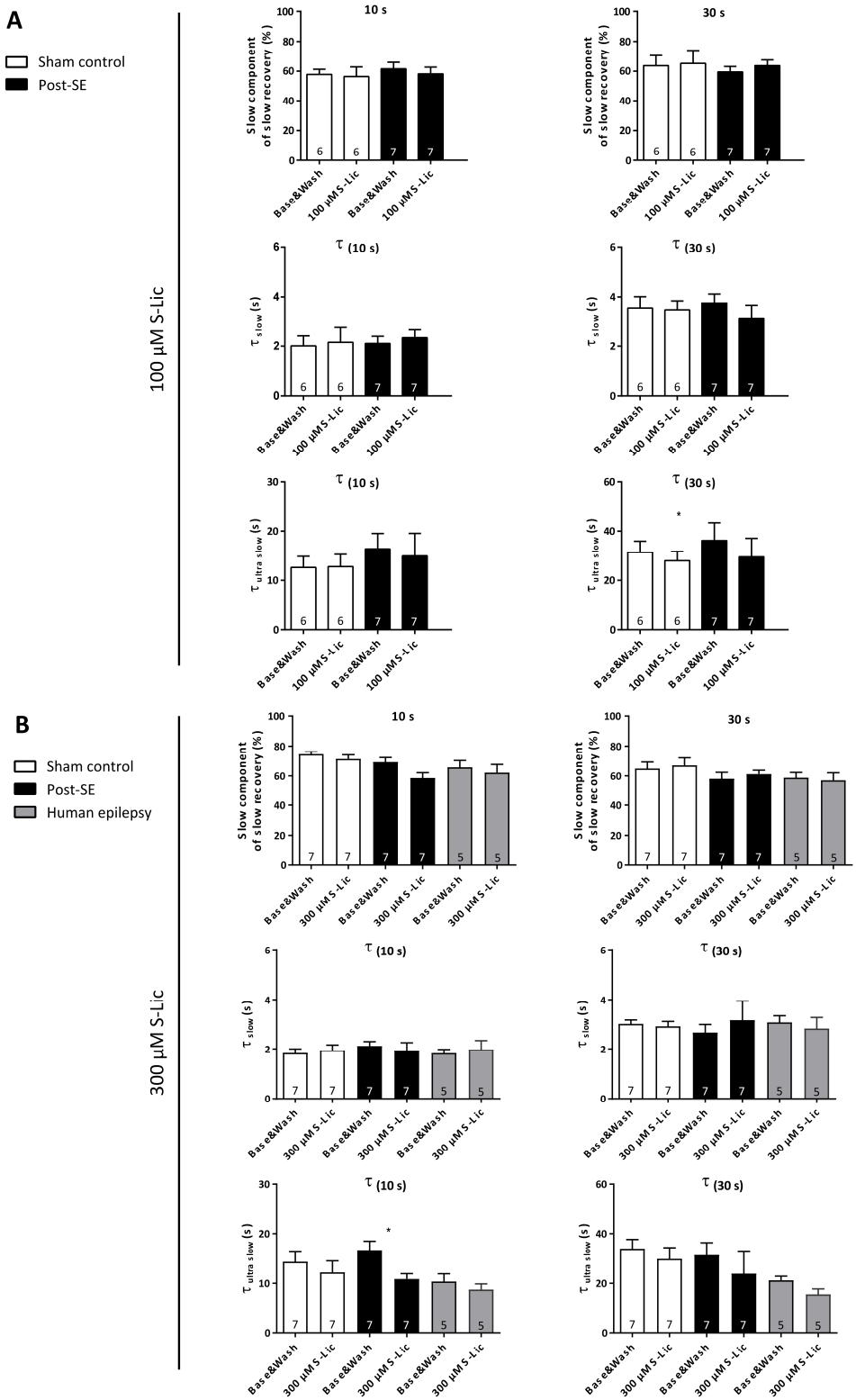

Supplementary Fig. 3: Similar recovery time constants and fractions of slow and ultra slow recovery. Summary of recovery parameters derived after fitting the recovery of individual DGCs (see methods for details). The slow and ultra-slow time constants of recovery as well as the fraction of channels recovering with given time constants are summarized in (**A**) for ACSF vs 100 µM S-Lic and in (**B**) for ACSF vs 300 µM S-Lic. Paired t-test for comparison of recovery time constants and Wilcoxon matched-pairs test for comparison of fractions of slow and ultra slow recovery.

Patient ID	Age at surgery	Gender	No cells	Type of recording	Part of Fig.	Type of surgery	Pathology	Treated with ESL / OXC *	Current medication	Past medication
P1	44	m	3	VC	1, 4, 5	temp. pole resection & AH right	AHS right	no	OXC, LEV	GBP, PGB
P2	53	f	2	VC	1, 4, 5	temp. pole resection & AH left	temp. pole loss of grey-white matter differentiation & AHS l	no	CLB, PER, PB	same
P3	54	f	2	VC	1, 4, 5	sel. AH right	AHS right	no	LEV, LTG	CBZ, PB/PRM, GBP, LCM
P4	39	f	1	VC	1-3, S3	sel. AH left	AHS left	no	ZNS	LEV
P5	14	m	1	VC	1, 4, 5	sel. AH & temp. pole resection right	temp. pole loss of grey-white matter differentiation & AHS r	no	VPA, LEV, CLB	same
P6	54	m	2	VC	1-5, S3	temp. pole resection & AH left	Ganglioglioma & AHS left	no	LEV, LTG	VPA
P7	18	m	2	VC	1, 5	sel. AH right	AHS right	yes	LTG, LEV	OXC, VPA, ST
P8	37	m	1	VC	1, 5	sel. AH right	AHS right	no	PB/PRM, LEV, ZNS	same
P9	41	m	1	VC	1, 4, 5	temp. pole resection & AH left	Reactive astrogliosis	no	CBZ, VPA, TPM	PB/PRM, LTG, LEV
P10	59	f	2	VC	1, 4, 5	sel. AH right	Volume accentuation of right amygdala, likely past limbic encephalitis	no	LEV	VPA, LTG, LCM
P11	50	f	4	VC	1-3, 5, S3	sel. AH left	AHS left	no	LCM, LTG, LEV	CBZ, LCM, LTG, TPM

Supplementary Table 1: Overview of patients with refractory TLE included in the study. Sel. AH, selective amygdalohippocampectomy; AHS, Ammon's horn sclerosis; ESL, eslicarbazepine acetate; OXC, oxcarbazepine; LEV, levetiracetam; GBP, gabapentin; PGB, pregabalin; CLB, clobazam; PER, perampanel; PB, phenobarbital; PRM, primidone; LTG, lamotrigine; CBZ, carbamazepine; LCM, lacosamide; ZNS, zonisamide; VPA, valproic acid; ST, sultiam; TPM, topiramate; * ESL and OXC share S-Lic as their major active metabolite; see patient data.

V_{50} (mV)	S-Lic concentration				Statistics (Dunnett's post-test)		
	0 µM	10 µM	100 µM	1000 µM	0 vs 10	0 vs 100	0 vs 1000
$Na_v1.1$	-47.5±1.9	-48.6±2.5	-44.7±0.9	-49.4±1.8	0.959	0.559	0.803
$Na_v1.2$	-42.2±1.4	-47.6±1.3	-51.8±2.7	-62.9±1.6	0.108	0.002 **	<0.001 ***
$Na_v1.3$	-34.4±1.9	-39.6±1.3	-37.0±2.0	-40.5±2.0	0.155	0.650	0.071
$Na_v1.6$	-39.2±1.6	-43.4±2.4	-45.3±1.9	-52.5±1.3	0.253	0.065	<0.001 ***

I_{min} (%)	S-Lic concentration				Statistics (Dunn's post-test)		
	0 µM	10 µM	100 µM	1000 µM	0 vs 10	0 vs 100	0 vs 1000
$Na_v1.1$	71.4±1.8	72.6±2.7	68.1±2.8	67.7±2.5	>0.999	>0.999	0.702
$Na_v1.2$	72.8±1.6	52.0±2.4	34.9±2.9	22.0±2.2	0.155	<0.001 ***	<0.001 ***
$Na_v1.3$	67.7±1.6	66.5±1.7	67.0±1.8	62.6±2.9	>0.999	>0.999	0.348
$Na_v1.6$	59.3±3.1	56.4±2.4	38.1±1.6	27.8±3.3	>0.999	0.004 **	<0.001 ***

Supplementary Table 2: Detailed data for the potential of half maximal inactivation (V_{50}) and the remainder fraction of sodium channels not being in slow inactivated state (I_{min}) both derived from fitting with a sigmoidal equation (n = 9-10 per condition). Potential hyperpolarizing shifts of V_{50} or decreases in the fraction of available channels between drug-free conditions and indicated concentratios of S-Lic were investigated by ANOVA followed by Dunnett's post-test or Kruskal-Wallis test followed by Dunn's post-test, respectively.

Supplementary Table 3: Post-test p-values. Omitted in main text for better readability.

Suppl. Fig. 1		**1 s**	**10 s**	**30 s**
	Sham control	0.118	<0.001	0.351
100 µM	Post-SE	0.028	0.004	0.669
	Comparison	0.097	0.62	0.62

Fig. 2		**1 s**	**10 s**	**30 s**
	Sham control	0.034	<0.001	0.012
	Post-SE	0.005	<0.001	0.024
	Human epilepsy	0.286	0.002	0.108
300 µM	Group comparison			
	Sham vs. post-SE	>0.999	>0.999	>0.999
	Post-SE vs. human	0.368	>0.999	>0.999
	Sham vs. human	>0.999	>0.999	>0.999

Fig. 4		**-110 mV**	**-70 mV**	**-50 mV**	**-30 mV**
	Sham control	>0.999	0.146	0.089	0.099
	Post-SE	>0.999	0.057	0.391	0.251
	Human epilepsy	>0.999	0.271	>0.999	>0.999
30 µM	Group comparison				
	Sham vs. post-SE	>0.999	>0.999	0.966	>0.999
	Post-SE vs. human	>0.999	>0.999	>0.999	>0.999
	Sham vs. human	>0.999	>0.999	0.774	0.601
	Sham control	0.003	<0.001	<0.001	<0.001
	Post-SE	<0.001	<0.001	<0.001	<0.001
	Human epilepsy	0.119	<0.001	<0.001	0.002
100 µM	Group comparison				
	Sham vs. post-SE	>0.999	0.627	0.476	0.592
	Post-SE vs. human	>0.999	>0.999	>0.999	>0.999
	Sham vs. human	>0.999	0.855	0.68	0.489
	Sham control	0.078	<0.001	<0.001	<0.001
	Post-SE	>0.999	<0.001	<0.001	0.001
	Human epilepsy	0.014	<0.001	<0.001	<0.001
300 µM	Group comparison				
	Sham vs. post-SE	>0.999	>0.999	>0.999	>0.999
	Post-SE vs. human	0.679	0.469	0.255	0.068
	Sham vs. human	>0.999	0.519	0.32	0.09

Fig. 5		**-110 mV**	**-70 mV**	**-50 mV**	**-30 mV**
	Sham control	>0.999	<0.001	<0.001	0.002
100 µM	Post-SE	0.028	<0.001	<0.001	0.012
	Comparison	0.461	>0.999	0.683	0.214

2.3 Summary

A highly reduced efficacy of use-dependent blocking of VGSCs by classical AEDs such as CBZ was demonstrated as a potential mechanism of pharmacoresistance (Doeser et al., 2014a; Remy et al., 2003a). A previous study reported maintained S-Lic efficacy on sodium channel fast inactivation processes and on reduction of repetitive action potential firing when comparing epileptic and nonepileptic tissue (Doeser et al., 2014a). Recordings in cultured neurons recently indicated potent S-Lic effects on the modulation of slow inactivation processes (Hebeisen et al., 2015). Therefore, the aim of the present publication was twofold. The first goal was to characterize the effects of S-Lic on sodium channel slow inactivation processes in acutely isolated neurons, using the same approach that identified the loss of CBZ efficacy in epileptic tissue in previous studies (Doeser et al., 2014a; Remy et al., 2003a). Secondly and more importantly, the question was asked whether these effects are lost, reduced or maintained in chronic epileptic tissue.

Putative principal neurons were isolated from the dentate gyrus (and for a subset of experiments from the sensorimotor cortex) and used for voltage-clamp recordings. Prolonged depolarizations induced slow inactivation of VGSCs. Application of S-Lic reduced sodium currents in a dose-dependent manner and enhanced entry into slow inactivation while the recovery from slow inactivation was unaffected. The voltage dependence of slow inactivation was investigated by applying a wider range of depolarizing or hyperpolarizing prepulses. Whereas for the lowest tested concentration of S-Lic (30 μM) no significant voltage-dependent effects were observable in DGCs, 100 μM and even more 300 μM evoked significant reductions of sodium current amplitudes caused by a prominent hyperpolarizing shift of the inactivation curves. Similar effect sizes were observed in granule cells isolated from the dentate gyrus and pyramidal neurons of the sensorimoror cortex. Most importantly, no significant differences were found when comparing S-Lic effects on cells derived from nonepileptic control tissue and epileptic rats or TLE patients. Finally, in cultured neurons expressing individual brain sodium channel isoforms, a subtype-specific blocking effect of S-Lic was demonstrated.

To conclude, this and previous studies have shown that S-Lic exerts its antiepileptic effects resulting in reduced action potential firing mainly via a hyperpolarizing shift of the voltage dependence of slow inactivation. This effect is limited to a subset of sodium channel isoforms which might result in a cell-type-specific efficacy. However, similar S-Lic efficacy was observed between principal cells of the dentate gyrus and the sensorimoror cortex and importantly also when comparing epileptic and healthy control cells.

3 Activity of the anticonvulsant lacosamide in experimental and human epilepsy via selective effects on slow Na^+ channel inactivation

3.1 Introduction

A series of screening experiments for novel compounds with antiepileptic potency led to the discovery of functionalized amino acids and subsequently revealed potent anticonvulsant activity in the lead compound lacosamide (LCM), a synthetic derivative of the endogenous amino acid D-serine (Choi et al., 1996). LCM was initially approved for adjunctive treatment and more recently as monotherapy of focal epileptic seizures (Villanueva et al., 2018). In drug interaction studies and clinical studies, a low interaction profile with other AEDs and drug metabolizing enzymes was found (Doty et al., 2007). Both, neuroprotective potency following SE but also neurotoxic effects when combined with valproate or other traditional AEDs were reported for LCM (Licko et al., 2013; Novy et al., 2011; Stephen et al., 2014).

Mean drug serum levels ranging from 20–80 μM were reported in epilepsy patients (Greenaway et al., 2011; Sattler et al., 2011). At therapeutic concentrations, LCM seems to be subject to active transport by drug efflux transporters of the BBB resulting in brain to plasma ratios between 0.5 in rats and 0.9 in epilepsy patients (Koo et al., 2011; May et al., 2015; Zhang et al., 2013a). However, intracellular accumulation of LCM was reported which might facilitate binding to intracellular portions of VGSCs (Boiteux et al., 2016; Gáll and Vancea, 2018). LCM is devoid of effects on neurotransmitter receptors and ion channels other than VGSCs (Errington et al., 2006). Controversial results considering interactions with other targets (collapsin response mediator protein 2, carbonic anhydrases or a 14-3-3 protein) were published and discussed to be unspecific or artificial (Rogawski et al., 2015). LCM was shown to enhance entry into VGSC slow inactvation and to strongly shift the slow inactivation voltage dependence in the hyperpolarizing direction by preferentially binding to the channels in their slow inactivated state (Boiteux et al., 2016; Errington et al., 2008; Hebeisen et al., 2015; Niespodziany et al., 2013; Sheets et al., 2008). These experiments, however, were mostly conducted in N1E-115 mouse neuroblastoma cells and did not compare drug effects in nonepileptic and epileptic tissue and subsequently brought this study into being.

This publication investigates the effects of LCM on fast and slow sodium channel inactivation processes as well as repetitive action potential firing in DGCs of healthy and epileptic rats as well as chronic epilepsy patients.

3.2 Publication

FULL-LENGTH ORIGINAL RESEARCH

Activity of the anticonvulsant lacosamide in experimental and human epilepsy via selective effects on slow Na^+ channel inactivation

***Dominik Holtkamp, *Thoralf Opitz, †Isabelle Niespodziany, †Christian Wolff, and *‡Heinz Beck**

Epilepsia, 58(1):27–41, 2017
doi: 10.1111/epi.13602

Dominik Holtkamp is a doctoral student at the Department of Epileptology at the University of Bonn.

Summary

Objective: In human epilepsy, pharmacoresistance to antiepileptic drug therapy is a major problem affecting ~30% of patients with epilepsy. Many classical antiepileptic drugs target voltage-gated sodium channels, and their potent activity in inhibiting high-frequency firing has been attributed to their strong use-dependent blocking action. In chronic epilepsy, a loss of use-dependent block has emerged as a potential cellular mechanism of pharmacoresistance for anticonvulsants acting on voltage-gated sodium channels. The anticonvulsant drug lacosamide (LCM) also targets sodium channels, but has been shown to preferentially affect sodium channel slow inactivation processes, in contrast to most other anticonvulsants.

Methods: We used whole-cell voltage clamp recordings in acutely isolated cells to investigate the effects of LCM on transient Na^+ currents. Furthermore, we used whole-cell current clamp recordings to assess effects on repetitive action potential firing in hippocampal slices.

Results: We show here that LCM exerts its effects primarily via shifting the slow inactivation voltage dependence to more hyperpolarized potentials in hippocampal dentate granule cells from control and epileptic rats, and from patients with epilepsy. It is important to note that this activity of LCM was maintained in chronic experimental and human epilepsy. Furthermore, we demonstrate that the efficacy of LCM in inhibiting high-frequency firing is undiminished in chronic experimental and human epilepsy.

Significance: Taken together, these results show that LCM exhibits maintained efficacy in chronic epilepsy, in contrast to conventional use-dependent sodium channel blockers such as carbamazepine. They also establish that targeting slow inactivation may be a promising strategy for overcoming target mechanisms of pharmacoresistance.

KEY WORDS: Pharmacoresistance, Epilepsy, Anticonvulsant drugs, Lacosamide.

Chronic epilepsies are a common and serious neurologic disorder that affects up to 50 million patients worldwide. About one third of these patients are refractory to currently available medical treatments. It is therefore important to understand the cellular mechanisms underlying resistance to anticonvulsant drugs in order to identify strategies to overcome drug resistance.

One key candidate mechanism for drug resistance that has emerged in recent years is an epilepsy-associated change in the anticonvulsant pharmacology of voltage-gated Na^+ channels.[1,2] Voltage-gated Na^+ channels are an important class of therapeutic targets for many anticonvulsant drugs, including both classical anticonvulsants and third-generation antiepileptic drugs (AEDs).[3–5] The mechanism of action of most classical anticonvulsants, for instance carbamazepine (CBZ) or phenytoin, has been

Accepted October 7, 2016; Early View publication November 19, 2016.
*Department of Epileptology, Laboratory for Experimental Epileptology and Cognition Research, University of Bonn, Bonn, Germany; †UCB Pharma, Braine l'Alleud, Belgium; and ‡German Center for Neurodegenerative Diseases (DZNE), Bonn, Germany
Address correspondence to Heinz Beck, Department of Epileptology, Laboratory for Experimental Epileptology and Cognition Research, University of Bonn, Sigmund-Freud Str. 25, 53105 Bonn, Germany.
E-mail: heinz.beck@ukb.uni-bonn.de or Christian Wolff, UCB Biopharma sprl, 1420 Braine l'Alleud, Belgium. E-mail: christian.wolff@ucb.com

Key Points

- LCM reduces sodium current amplitude strongly
- LCM has large effects on the voltage dependence of slow inactivation, with only small effects on other sodium current properties
- LCM activity on voltage dependence of slow inactivation and neuronal firing is maintained in experimental and human epilepsy
- Sodium channel blockers targeting slow inactivation processes may be a promising strategy for overcoming target mechanisms of pharmacoresistance

examined in great detail. It involves pronounced use-dependent blocking effects, in which the development of the block depends on opening of the Na^+ channel.[3,4,6] This is likely because the putative binding site for these and other drugs is exposed only upon channel opening.[6–8] This use-dependent block has been shown to be reduced in chronic human and experimental epilepsy in the case of CBZ,[1,2] resulting in a reduced efficacy of this anticonvulsant in inhibiting neuronal firing.[9] However, it is clear that a number of new anticonvulsants exert effects that are markedly different from those of CBZ. One such anticonvulsant is lacosamide (LCM), a third-generation AED that is approved as monotherapy or adjunctive therapy in adults with partial-onset seizures in the United States. Notably, although many anticonvulsants do not seem to affect Na^+ channel slow inactivation markedly, LCM shows a pronounced effect on slow inactivation properties.[10,11] LCM seems to exert its effects primarily via shifting the slow inactivation voltage dependence to more hyperpolarized potentials.[10,11] LCM also—as shown in previous work—blocks persistent Na^+ currents.[12] This raises the question if effects of anticonvulsants acting on slow inactivation processes are maintained in chronic human and experimental epilepsy.

We show here that the activity of LCM in modulating voltage-gated Na^+ channels is maintained in chronic experimental and human epilepsy. Furthermore, we demonstrate that the efficacy of LCM in inhibiting high-frequency firing is maintained in chronic experimental and human epilepsy.

Materials and Methods

Animal model

All animal experiments were conducted in accordance with the guidelines of the Animal Care Committee of the University of Bonn Medical Center. Male Wistar rats (180–200 g) were housed under a 12-h light/dark cycle with unrestricted access to food and water. Rats were injected with a single high dose of the muscarinic agonist pilocarpine (340 mg/kg, administered intraperitoneally), which induced behaviorally detected status epilepticus (SE) in most (~80%) animals.[13–17] Peripheral muscarinic effects were reduced by prior administration of methyl-scopolamine (1 mg/kg, administered intraperitoneally [i.p.]; 30 min before injecting pilocarpine). Diazepam (Ratiopharm: 20 mg/kg, administered subcutaneously) was administered 40 min after onset of SE. It attenuated the SE in the seizing rats and sedated all animals. Within 24 h after pilocarpine injection the rats appeared behaviorally normal and were video-monitored for the development of chronic seizures starting ~17 days after SE. Only animals that experienced multiple generalized video-documented seizures were used for the study.

Human specimens from patients with epilepsy

Surgical specimens were obtained from 16 patients with therapy-refractory temporal lobe epilepsy (Table S1, age on average 35.8 ± 2.8 years). The histopathology of most specimens showed typical features of Ammon's horn sclerosis (11 specimens). One specimen (P6) showed a developmental malformation, and one further specimen a cavernoma (P7). Most patients had complex partial and secondary generalized seizures. Studies on human material were approved by the institutional research ethics committee. Appropriate consent was obtained from human subjects for use of the material.

Animal preparation

Animals were perfused through the heart under deep anesthesia (ketamine 100 mg/kg, xylazine 15 mg/kg) 28–49 days after SE with ice-cold sucrose-based artificial CSF (ACSF) comprising (in mM): NaCl 60, sucrose 100, $NaHCO_3$ 26, KCl 2.5, NaH_2PO_4 1.25, $MgCl_2$ 5, $CaCl_2$ 1, and glucose 20, pH 7.4, osmolality 305 mOsmol. Subsequently the brain was rapidly removed. The time from pilocarpine injection to the experiment was 49.5 ± 3.9 days.

Animal and human slice and dissociated cell preparation

Transverse hippocampal slices (rat: 300 μm, human: 400 μm) were prepared with a vibrating microslicer (VT1200S; Leica) in carbogenated sucrose ACSF (95% O_2, 5% CO_2). For rat tissue, the same sucrose-based ACSF as for perfusion was used; for human tissue it had the following composition (in mM): NaCl 87, sucrose 75, $NaHCO_3$ 25, KCl 2.5, NaH_2PO_4 1.25, $MgCl_2$ 7, $CaCl_2$ 0.5, and glucose 25. Immediately after their preparation, human hippocampal slices were stored in ACSF containing (in mM) NaCl 124, KCl 3, $MgCl_2$ 2, $CaCl_2$ 2, $NaHCO_3$ 26, NaH_2PO_4 1.25, and glucose 10. Rat slices, however, were first transferred to a storage chamber filled with sucrose-based ACSF, gradually warmed to 35°C in a water bath, and maintained at this temperature for ~20 min. Finally, all slices were transferred into a chamber filled with ACSF containing the following (in mM): NaCl 125, KCl 3.5, $MgCl_2$ 2, $CaCl_2$ 2, $NaHCO_3$ 26, NaH_2PO_4 1.25, and glucose 15, pH 7.4, osmolality

Epilepsia, 58(1):27–41, 2017
doi: 10.1111/epi.13602

307 mOsmol, where they stayed at room temperature for an equilibration period of at least 30 min until they were used for recording or preparation of dissociated cells.

For the preparation of dissociated granule cells, one slice at a time was put into trituration solution (in mM): Na methanesulfonate 145, KCl 3, $CaCl_2$ 0.5, $MgCl_2$ 1, 4-(2-hydroxyethyl)-1-piperazineethanesulfonic acid (HEPES) 10, glucose 15, pH 7.4 adjusted with NaOH, osmolality 315 mOsmol, mixed with pronase (protease type XIV, 2 mg/ml; Sigma) under constant supply with oxygen (100%) for 12 min at 36°C. After an equilibration period of 10 min at room temperature, slices were washed in pronase-free solution. Subsequently, the dentate gyrus was dissected and triturated with fire-polished Pasteur pipettes of decreasing aperture in a Nunc Dish (3.5 cm; Thermo Scientific) filled with bath solution (see bath solution described below for isolated cells). Cells were allowed to settle for at least 10 min before start of the patch-clamp experiments.

Whole-cell patch-clamp analysis of neuronal firing behavior

Action potential firing was recorded from rat or human dentate gyrus granule neurons. Cells were visualized using a Zeiss Axioskop upright microscope equipped with infrared difference interference contrast optics and a water-immersion lens (60×, 0.9 NA; Olympus). Somatic whole-cell current-clamp recordings were made with a BVC-700A amplifier (Dagan) run in bridge mode. Data were sampled at 10 kHz (8 s current injection) and 100 kHz (3 msec and 8 s current injections) with a Digidata 1322A or 1440A interface controlled by pClamp software (Molecular Devices). Patch pipettes were pulled from borosilicate glass capillaries (0.86 mm inner diameter, 1.5 mm outer diameter, with filament; Science Products) with a micropipette puller (PP-830; Narishige). Electrode resistance in the bath ranged from 3 to 7 MΩ. The internal solution contained the following (in mM): K-gluconate 127, KCl 20, HEPES 10, ethylene glycol-bis (2-aminoethylether)-*N*,*N*,*N*′,*N*′-tetraacetic acid (EGTA) 0.16, Mg-ATP 4, Na_2-ATP 2, D-glucose 10 (pH adjusted to 7.25 with KOH, 295 mOsmol). The extracellular ACSF was identical to that used for slice storage (31°C). Membrane potential was corrected offline for a liquid junction potential of 14.0 mV.

Data analysis, current clamp experiments

The voltage traces recorded in current clamp mode were analyzed with custom routines in Igor Pro (Wavemetrics). Action potentials were described quantitatively by determining their peak amplitude, the maximal rate of rise of the voltage trace, the action potential threshold, and the width at the voltage level halfway between threshold and peak. The action potential threshold was determined as the voltage at which the slope of the voltage trace (dV/dt) exceeded 15 mV/msec. Repetitive firing was examined using prolonged current injections (8 s). Input–output relations were obtained with an automatic action potential detection routine programmed in Igor Pro. For analysis of use dependence, only traces with action potential firing throughout the entire duration of depolarization (8 s) were used. The traces were then divided into eight bins of 1 s each, and the maximal dV/dt for all action potentials within the same time bin was averaged. To examine the effect of LCM, traces were selected to exhibit approximately the same number of action potentials during baseline, LCM application, and washout.

Patch-clamp analysis of Na^+ currents in isolated neurons

For recording transient Na^+ currents (I_{NaT}), the trituration solution was exchanged with bath solution (in mM): Na-methanesulfonate 40, tetraethylammonium-Cl 90, $CaCl_2$ 1.6, $MgCl_2$ 2, HEPES 10, $CdCl_2$ 0.2, 4-aminopyridine 5, glucose 15, pH 7.4 adjusted with HCl; osmolality 310 mOsmol, adjusted with glucose. The Nunc dish was then mounted on an inverted microscope (Axiovert 100; Zeiss) and constantly superfused with bath solution. Patch pipettes were pulled from borosilicate glass capillaries as stated above with a micropipette puller (Model P-97; Sutter Instruments & Co) and filled with intracellular solution (in mM): CsF 110, HEPES-Na 10, EGTA 11, $MgCl_2$ 2, TEA-Cl 20, Na_2-GTP 0.5, ATP-Na_2 5, pH 7.25 adjusted with CsOH; osmolality 300 mOsmol. Only pipettes with a resistance of 4.5–6.5 MΩ were used for the experiments. Tight-seal whole-cell recordings were obtained with a seal-resistance of >1 GΩ using a patch-clamp amplifier (Axopatch 200B; Molecular Devices). Series resistance was 6.4 ± 0.3 MΩ for rat recordings and 6.6 ± 0.7 for human recordings, and could be compensated between 70 and 90%. Maximal residual voltage error was 5.3 ± 0.4 mV for rat recordings and 5.0 ± 0.6 for human recordings. Currents were filtered at 10 kHz, sampled at 50 kHz with a Digidata 1440A and recorded by a personal computer using the Clampex 10.2 acquisition software (Molecular Devices). In addition, all command and measured voltages were corrected for the liquid junction potential (10.0 mV).

Data analysis, voltage-clamp experiments

The conductance G(V) was calculated according to:

$$G(V) = I(V)/(V - V_{Na}),$$

where V_{Na} is the Na^+ reversal potential, V the command potential, and I(V) is the peak current amplitude. In addition, G(V) was then fitted with the following Boltzmann equation:

$$G(V) = A_1 + (A_1 - A_2)/(1 + e^{(V-V_{50})/k}).$$

A_1 and A_2 are sodium conductances, V_{50} is the voltage where G(V) reaches its half-maximal value, and k indicates

the slope of the relation between channel activation or inactivation and membrane voltage.

Double-pulse experiments to examine recovery from fast inactivation were analyzed in the following way. First the current amplitudes obtained during the test-pulse were normalized to the amplitudes obtained during the conditioning pulse. The curve resulting from a plot of the maximal amplitude against the corresponding time interval was best described by a bi-exponential equation:

$$I(t) = A_0 + A_{fast1} * e^{-t/\tau fast1} + A_{fast2} * e^{-t/\tau fast2},$$

where I(t) is the normalized current amplitude at the timepoint t after onset of the voltage command, A_{fast1} and A_{fast2} are the relative amplitude contributions of the two recovery time constants τ_{fast1} and τ_{fast2}, respectively, and A_0 is a constant offset. Recovery from slow inactivation was fitted with an equivalent equation, with the time constants of slow recovery denoted τ_{slow1} and τ_{slow2}. Fitting was done using a Levenberg-Marquardt algorithm. Data for recovery from slow inactivation were fitted with equivalent methods.

Pharmacology, compounds, and stock solutions

LCM and CBZ were prepared as stock in ethanol and added to the bath 1:1,000. Control ACSF included equal concentrations of ethanol. In general baseline and wash values were averaged for all protocols, termed "ACSF" and compared to a single "LCM" value. For estimating the LCM-induced reduction of I_{NaT}, control values were generated by averaging the current amplitudes immediately before washin and immediately after washout as a control current amplitude. These were related to the average of the current amplitude immediately after saturation of the LCM effect and the current amplitude immediately before starting washout.

Statistical analysis

For statistical comparison the Student's *t*-test at a significance level α of 0.05 was used, if appropriate a paired *t*-test was applied. In some instances, analysis of variance (ANOVA) was used with an appropriate posttest mentioned in each individual experiment. If assumptions for an ANOVA were not met, appropriate nonparametric methods were used which are also indicated for each individual statistical comparison. Results are always presented as mean ± standard error of the mean (SEM).

RESULTS

LCM reduces voltage-gated Na^+ current amplitude in experimental and human epilepsy

We systematically compared the effects of LCM on granule cells isolated from brain slices of control animals to those of animals who experienced status epilepticus (SE) following intraperitoneal administration of pilocarpine and who subsequently showed spontaneous seizures (see Materials and Methods). We used an initial test concentration of 100 μM LCM. We first applied LCM while delivering brief depolarizations from a holding potential of −90 mV (to −30 mV, 15 msec). To assess the magnitude of LCM effects, data points obtained under control conditions and after washout of LCM were averaged to generate a single control value for each cell, to which the current magnitude after saturation of the LCM effect was compared. This analysis revealed a consistent reduction of peak I_{NaT} by 41.1 ± 3.0% and 41.5 ± 4.7% in sham-control and pilocarpine-treated animals, respectively (Fig. 1A,C, n = 6 and 7). A rundown of peak I_{NaT} was apparent in these recordings. We therefore performed experiments exactly as described, but omitted LCM from the perfusate (ACSF control application). Calculating the magnitude of effects of the ACSF control application as for LCM effects (LCM shown in Fig. 1C) yielded a

Figure 1.

Robust reduction of peak transient Na^+ current (I_{NaT}) significant shifts in inactivation gating in dentate gyrus granule cells by LCM. (**A**) I_{NaT} was elicited with brief depolarizations from a holding potential of −90 mV (left). Currents were obtained in control solution, after application of 100 μM LCM just before washout, and after stabilization of washout (black, orange, and blue traces, respectively). Representative examples shown for sham-control and epileptic (post-SE) animals. (**B**) Representative examples of LCM effects (also 100 μM) on a human isolated granule cells. Line colors as in panel **A**. (**C**) Average reduction of peak sodium currents in sham-control and pilocarpine-treated animals, as well as human granule cells (n = 6, 7 and 6). (**D**) Transient Na^+ current (I_{NaT}) was elicited by depolarizing pulses from a −90 mV holding potential to various test potentials (a), followed after 500 msec by a brief step to −30 mV (b). Example traces of I_{NaT} recorded at the indicated time points in the protocol (left panel) to assess channel activation (a) and inactivation (b). Example from a sham-control animal. (**E**) I_{NaT} was converted to conductance and normalized to the cell's maximal conductance. Plots summarize LCM effects (100 μM) in sham-control and pilocarpine-treated (post-SE) rats (n = 6 each). (**F**) Effects of LCM on voltage-dependence of I_{NaT} in dentate gyrus granule cells isolated from human brain tissue (n = 9). (**G**, **H**) Summary of LCM effects on the potential of half-maximal I_{NaT} activation (**G**) and inactivation (**H**). Asterisks in panel **E** indicate $p < 0.001$, 0.006, and 0.006 for sham-control, post-SE and human groups, respectively, paired *t*-test). (**I**) Summary of the shift in V_{50} of activation and inactivation seen in sham-control and epileptic animals, as well as granule cells obtained from patients with TLE.

Epilepsia, 58(1):27–41, 2017
doi: 10.1111/epi.13602

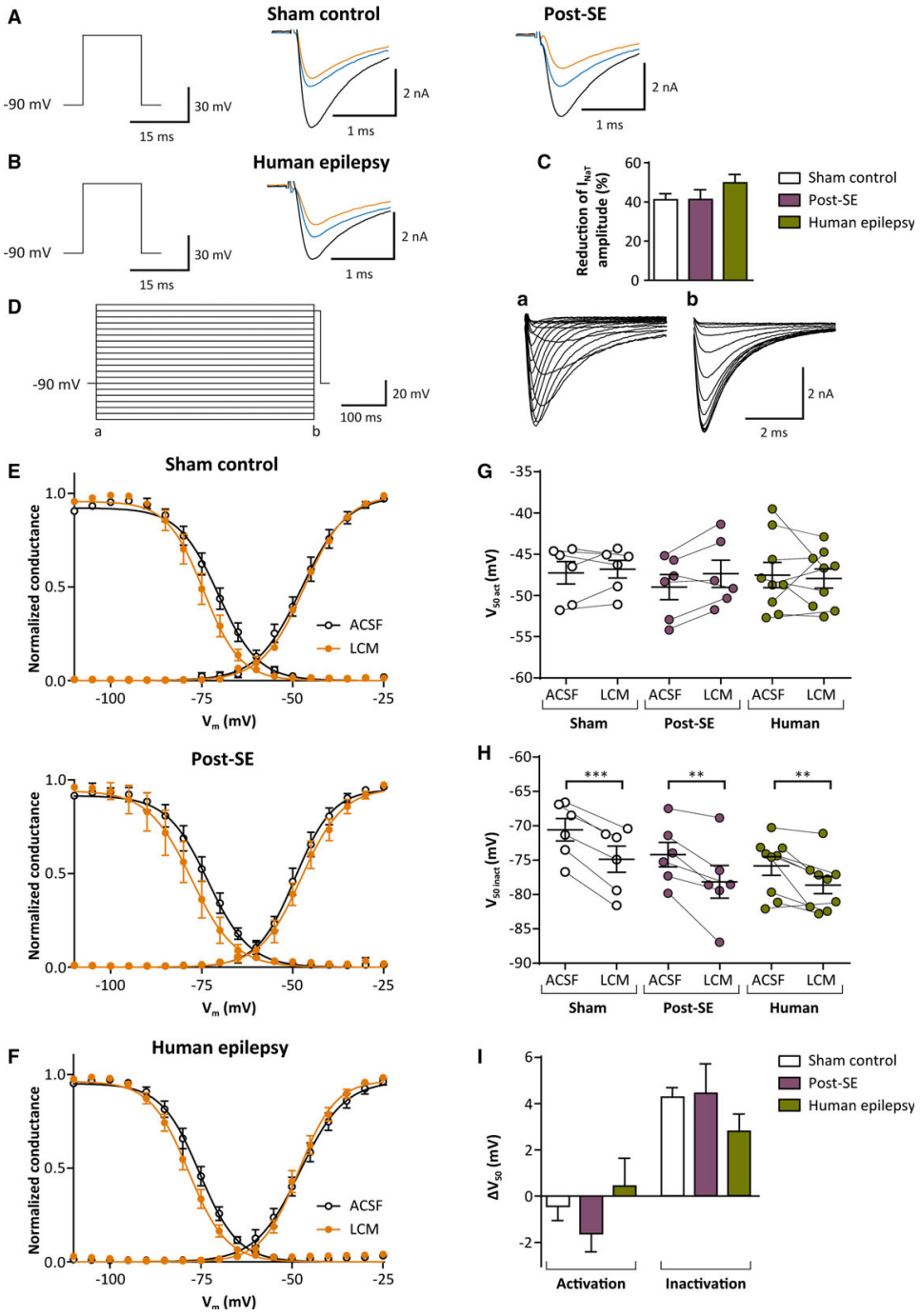

negligible effect of sham ACSF application (0.6 ± 1.4% and −1.4 ± 1.5% for control and pilocarpine-treated rats, respectively, n = 7 and 3).

We next examined effects of 100 μM LCM on the properties of I_{NaT} in human isolated granule cells from epileptic patients (Fig. 1B) using the same stimulation protocol.

Epilepsia, 58(1):27–41, 2017
doi: 10.1111/epi.13602

These recordings also revealed a robust reduction of peak Na^+ currents by 49.8 ± 4.3% (Fig. 1C, n = 6). The magnitude of the blocking effects was not significantly different between any of these three groups (Kruskal-Wallis test, n.s.).

LCM effects on steady state voltage-dependence

We then examined the voltage-dependence of I_{NaT} under control conditions, after washin of LCM, and after washout using standard protocols. Voltage steps ranging from −120 to −25 mV were applied, followed by a constant voltage step to −30 mV (Fig. 1D). The first of the two steps causes activation of I_{NaT}, allowing analysis of the voltage-dependence of activation. The steady-state inactivation was examined by evaluating the peak Na^+ current during the second voltage step to −30 mV, and determining how much of this current is inactivated due to the first voltage step (Fig. 1D, traces labeled with lowercase b). As in Figure 1C, data points obtained under control conditions and after washout of LCM were averaged to generate a single control dataset for each cell. Fitting with a modified Boltzmann equation to describe the voltage dependence of the conductance revealed no effects of 100 μM LCM on the voltage-dependence of activation (Fig. 1E,G). We observed small but significant effects on the voltage-dependence of inactivation, manifesting in a small hyperpolarizing shift of the voltage of half-maximal inactivation (Fig. 1E,H, shift of 4.3 ± 0.4 and 4.4 ± 1.3 mV in sham-control and pilocarpine-treated animals, respectively, n = 6 for both groups, ***p < 0.001, **p = 0.006, paired *t*-test).

Similar results were obtained for human epileptic granule cells. One hundred micromolar LCM had no effects on the voltage-dependence of activation, but had a small hyperpolarizing effect of the voltage of half-maximal inactivation (Fig. 1F–I, shift of 2.8 ± 0.8 mV, **p = 0.006, paired *t*-test). The magnitude of the LCM effects was not different between any group (Fig. 1I, Kruskal-Wallis test, n.s.). Thus, small effects on inactivation voltage-dependence exist in both experimental and human epilepsy. However, these shifts do not explain the large reduction in peak Na^+ currents observed in Figure 1A–C.

LCM effects on recovery from fast inactivation

In the pilocarpine model of temporal lobe epilepsy, a distinctive loss of CBZ effects on the recovery behavior was observed, both in the pilocarpine model of epilepsy and in patients with therapy-refractory epilepsy. This raises the question if LCM shows reduced or maintained effects in chronic experimental epilepsy. We examined the recovery from fast inactivation using standard protocols, both in control and pilocarpine-treated animals (Fig. 2A). Two brief depolarizations of 15 msec (−30 mV) were applied with a varying interpulse interval of 1–8,192 msec, and a holding potential of −90 mV. Plotting the magnitude of the normalized current during the second of the two depolarizations versus the interpulse interval allows evaluation of the recovery from fast inactivation. The time course of recovery did not reveal large effects of 100 μM LCM (n = 6 and 7, Fig. 2B). However, fitting the time course did show a small significant effect of LCM in control rats (30.1% increase of the time constant of fast recovery, ***p < 0.001, paired *t*-test, Fig. 2D). In human dentate granule cells, there was no effect of 100 μM LCM on fast recovery (n = 9, Fig. 2C, D). There were, however, no significant differences between control and epileptic rats as well as human specimens regarding the effects of LCM (Fig. 2E, Kruskal-Wallis test, n.s.).

Effects of LCM on Na^+ channel slow inactivation in experimental and human epilepsy

The experiments so far show a robust reduction of Na^+ channel conductance (see Fig. 1A–C), which is not easily explained by effects of LCM on voltage-dependence or recovery from fast inactivation. We therefore next examined the effects of LCM on slow inactivation of Na^+ channels in rat and human dentate gyrus granule cells. In these experiments, entry of Na^+ channels into slow inactivation was induced by holding neurons for 1, 10, or 30 s at a depolarizing membrane potential (−30 mV). The membrane potential was then returned to −90 mV for 1-s to allow complete recovery from fast inactivation (Fig. 3A). This allows determination of the magnitude of the remaining slow inactivation. The fraction of channels entering slow inactivation can be quantified by comparison of the peak Na^+ channel amplitude during the test pulse to the amplitude obtained with the conditioning pulse (black vs. red lines in Fig. 3B, examples shown for sham-control and pilocarpine-treated rats and epilepsy patients as indicated). This allowed us to assess the effects of LCM on the time course of entry into slow inactivation.

As expected, prolonging the conditioning pulse from 1 to 30 s resulted in a marked increase in channels undergoing slow inactivation, both in sham-control animals and in pilocarpine-treated animals (Fig. 3B, compare black vs. red lines, n = 7 and 6). Small but statistically significant increases in the fraction of channels entering slow inactivation during the depolarizing prepulse were observed after application of 100 μM LCM (Fig. 3C, two-way ANOVA, sham control: $F_{1,15} = 20.3$, $p < 0.001$, pilocarpine-treated: $F_{1,15} = 4.9$, $p = 0.04$, followed by Bonferroni posttest for LCM efficacy with **p < 0.01). In human dentate granule cells, the results were very similar, with an also small but significant enhancement of entry into slow inactivation by 100 μM LCM (Fig. 3C, lower panel, n = 9, two-way ANOVA, $F_{1,24} = 19.3$, $p < 0.001$, followed by Bonferroni posttest for LCM efficacy with **p < 0.01). There were no significant differences between control and epileptic rats as well as human specimens regarding the effects of LCM (Fig. 3D, Kruskal-Wallis test, n.s.).

Epilepsia, 58(1):27–41, 2017
doi: 10.1111/epi.13602

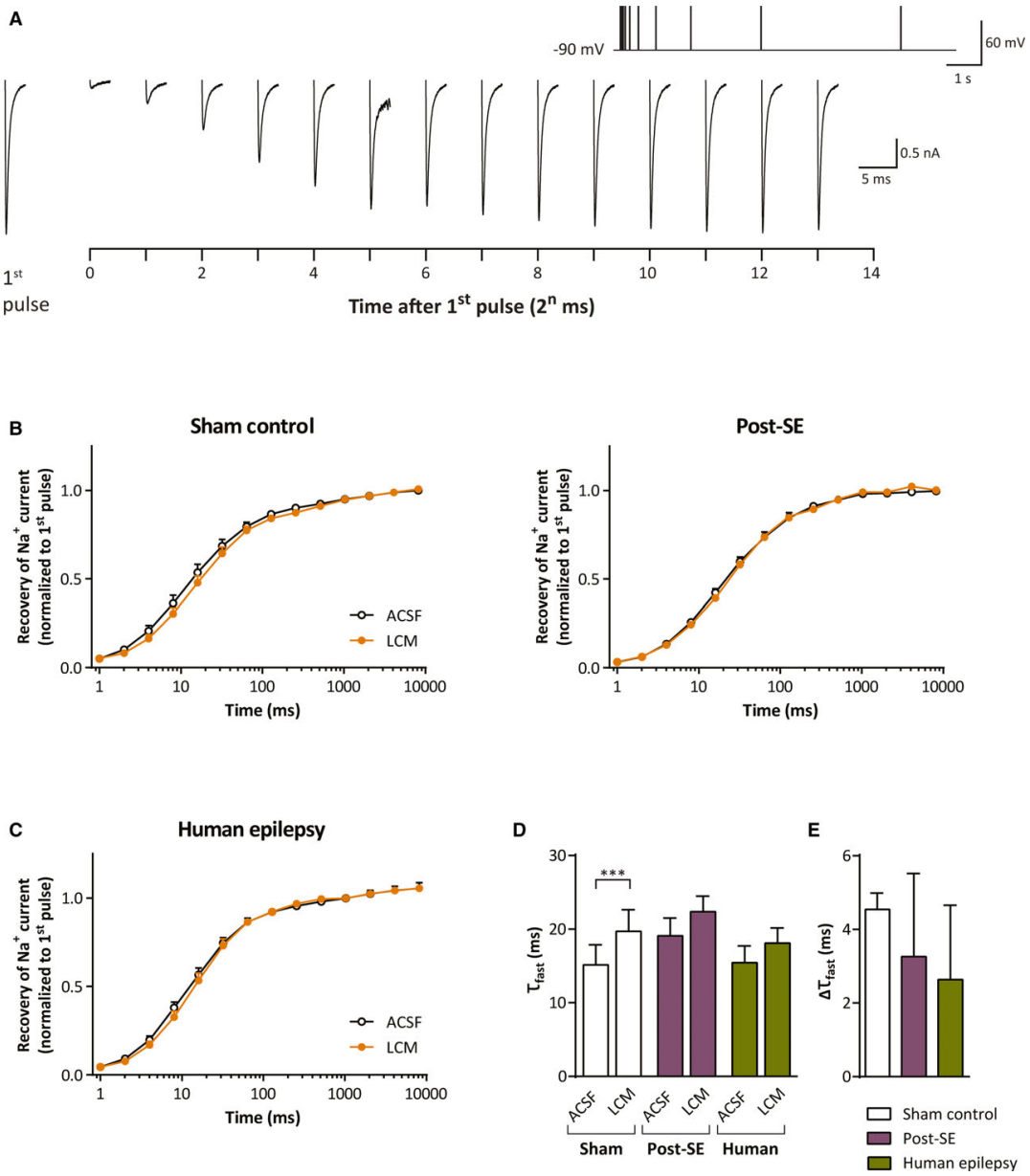

Figure 2.
Effects of LCM on recovery from fast inactivation of Na^+ channels in dentate gyrus granule cells. (**A**) Sample traces illustrating recovery from fast inactivation elicited by the voltage step protocol displayed in the inset. I_{NaT} was elicited by pairs of brief 15 msec depolarizing pulses from −90 mV holding to −30 mV test potential. The interval between the two pulses was varied from 1 msec up to 8,192 msec in increments of 2^n. This stimulation protocol was applied three times to every neuron tested: under baseline condition, after application of 100 μM LCM, and after a washout period. Baseline and washout data were averaged for comparison to 100 μM LCM. (**B**) Summary of experiments in sham-control and pilocarpine-treated (post-SE) rats (n = 6 and 7, respectively). (**C**) Summary of experiments in granule cells from TLE patients (n = 9). (**D**) Quantification of the kinetics of recovery from fast inactivation. The time constant of fast recovery (τ_{fast}) was obtained by fitting the individual recovery time courses. A small but significant increase of τ_{fast} was found only for control rats (asterisks indicate $p < 0.001$, paired *t*-test). (**E**) Quantification of the magnitude of LCM effects on τ_{fast}.

Epilepsia, 58(1):27–41, 2017
doi: 10.1111/epi.13602

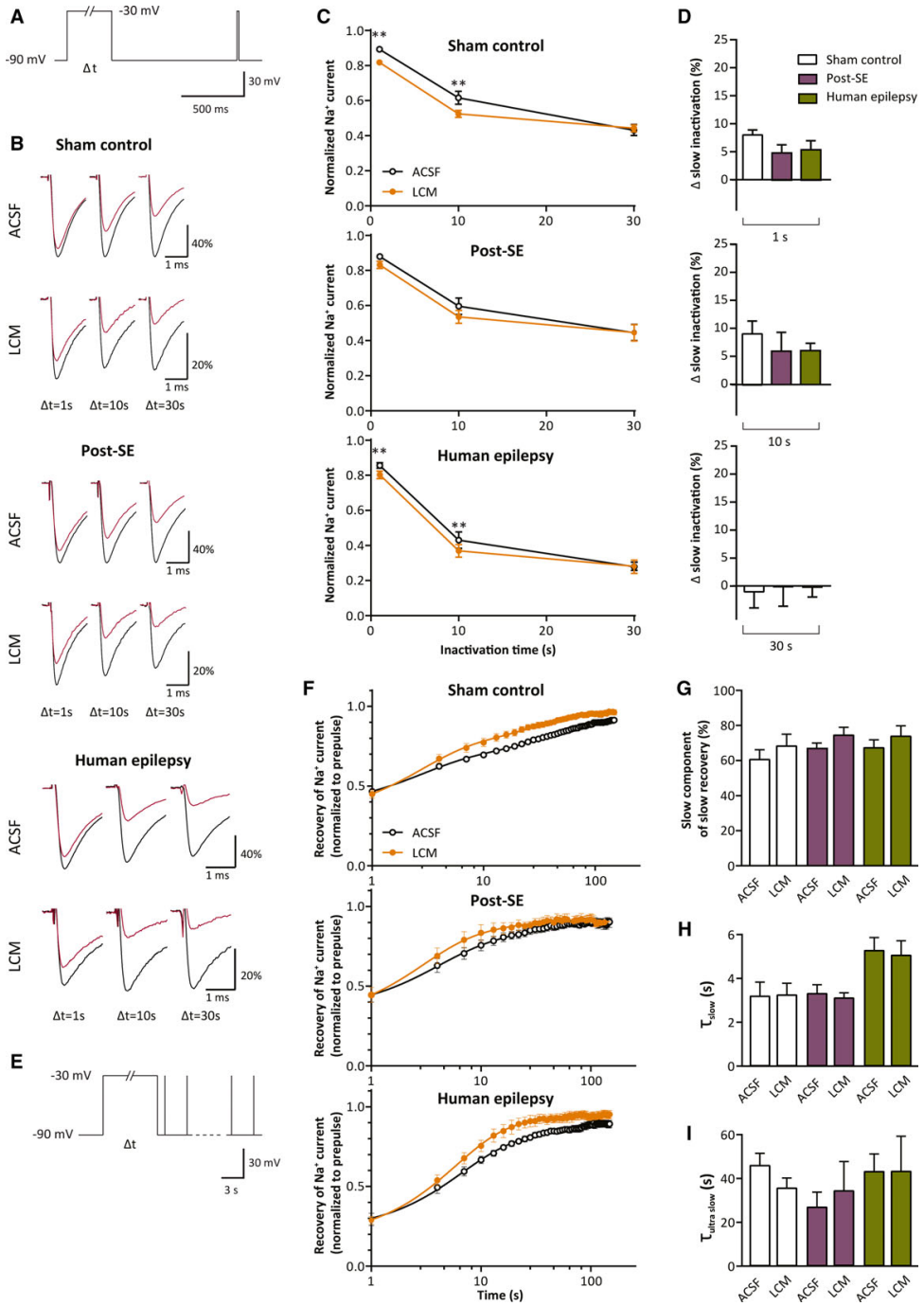

We then examined the time course of recovery from slow inactivation, which was monitored starting 1 s after returning the holding potential to −90 mV with brief (15 msec) test pulses to −30 mV every 3 s (Fig. 3E, examples shown in Fig. S1B for sham control and epileptic animals, n = 7 and 6, respectively, left panels). The average time course of

Figure 3.
LCM effects on entry into and recovery from slow inactivation of Na^+ channels in rat and human dentate gyrus granule cells. (**A**) Voltage step protocol used to analyze entry of Na^+ channels into slow inactivation. The membrane was depolarized from −90 to −30 mV for variable durations and then returned to −90 mV for 1 s to allow complete recovery from fast inactivation before recording a brief (15 msec) test pulse. (**B**) Representative examples for currents elicited by 1, 10, and 30 s conditioning pulses (black lines) and respective test pulses (red lines) for granule cells from sham-control and pilocarpine-treated rats as well as TLE patients. Traces are depicted under baseline conditions (top row) and after application of 100 μM LCM (bottom row). (**C**) Summary of test pulse amplitudes normalized to conditioning pulse amplitudes in sham-control and pilocarpine-treated rats (n = 7 and 6) as well as TLE patients (n = 9). Values during application of 100 μM LCM and the averages of baseline and washout conditions are shown. Asterisks indicate significant differences of Bonferroni posttest indicated with **p < 0.01. (**D**) Summary of the relative magnitude of effects on entry into slow inactivation. (**E**) Voltage step protocol used to analyze recovery of Na^+ channels from slow inactivation. Starting 1 s after the conditioning pulse, test pulses (15 msec) at 3 s intervals were used for determining the time course of recovery from slow inactivation. (**F**) Time course of test pulse amplitudes normalized to the amplitude of the conditioning pulse for granule cells isolated from sham control and pilocarpine-treated rats or TLE patients. LCM indicates data points corresponding to washin of 100 μM LCM (orange); ACSF indicates data points from an average of baseline and washout data (white). (**G**–**I**) Quantification of the time course of recovery from slow inactivation. Panels **H** and **I** denote the slow and ultra-slow time constants of recovery. Panel **G** depicts the fraction of current recovering with the slow time constant τ_{slow}.

recovery with prepulse durations of 30 s is depicted in Figure 3F. The time course of recovery from slow inactivation was fit with a biexponential equation. No significant effects of 100 μM LCM were observed (Fig. 3G, Wilcoxon matched-pairs test, Fig. 3H,I, paired *t*-test). In human dentate granule cells, LCM also had no significant effects on the dynamics of slow recovery from inactivation (Fig. 3F, lower panel, example in Fig. S1C). There were no significant differences between control and epileptic rats as well as human specimens regarding the effects of LCM (Fig. 3G–I, Kruskal-Wallis test, n.s.).

For conditioning prepulses shorter than 30 s, it proved difficult to obtain consistent fitting of the second, ultra-slow component of slow recovery, as these components become very small and are contaminated by run-down over the time course of long-duration pharmacologic experiments. We therefore focused on the recovery from robust inactivation induced by 30 s prepulses, and refrained from further analyzing recovery from inactivation induced by shorter prepulses.

Potent effects of LCM on the voltage-dependence of slow inactivation in experimental and human epilepsy

Our results so far show only small effects of LCM on the biophysical properties of Na^+ channels related to fast-inactivation processes. They also revealed small effects of LCM on the kinetics of slow inactivation. This raises the question of why we observe a robust decrease of Na^+ currents elicited with holding potentials of −90 mV (see Fig. 1). These findings would be consistent with a hyperpolarizing shift of the voltage dependence of slow inactivation, as observed in previous studies.[10,11] We, therefore, assessed entry into slow inactivation with different prepulse potentials. We used 10 s prepulses to voltages of −110 to −50 mV as conditioning prepulses to induce entry into slow inactivation. Values for −30 mV were derived from the previous recordings of slow inactivation (Fig. 4A). These results show a voltage-dependence of slow inactivation, with increasing fractions of the Na^+ channels inactivated at increasingly depolarized prepulse potentials (Fig. 4B, n = 7 and n = 6 for sham-control and pilocarpine-treated animals, respectively). One hundred micromolar LCM caused a strong reduction of Na^+ current amplitudes that was voltage-dependent (Fig. 4B, two-way ANOVA, sham control: $F_{1,30} = 558.1$, $p < 0.001$, pilocarpine-treated: $F_{1,27} = 96.96$, $p < 0.001$, followed by Bonferroni posttest for LCM efficacy with **p < 0.01 and ***p < 0.001). These effects of LCM were not different when comparing sham-control and epileptic animals (Fig. 4D, Kruskal-Wallis test, n.s.). The voltage-dependent effects were not contaminated by run-down problems, as became clear when recordings were performed exactly as described in Figure 4, but omitting LCM from the perfusion solution (see Fig. S2). We next performed identical experiments in human dentate granule cells (n = 6). Also here, 100 μM LCM had potent effects on the voltage-dependence of slow inactivation (Fig. 4C, two-way ANOVA, $F_{1,28} = 238.7$, $p < 0.001$, followed by Bonferroni posttest for LCM efficacy with **p < 0.01 and ***p < 0.001) similar to those seen in sham-control or epileptic animals (Fig. 4D, Kruskal-Wallis test, n.s.).

In contrast to the dominant effects of many Na^+ channel–acting anticonvulsants on voltage-dependence and recovery from fast in activation, the major effects of LCM are on the voltage-dependence of slow recovery from inactivation. This effect causes a robust reduction of Na^+ currents elicited from holding potentials between −110 and −50 mV. It is important to note that these effects of LCM are completely unchanged in chronic epilepsy, and are also present to a quantitatively similar extent in cells from human epileptic patients.

Effects of LCM on repetitive firing in experimental and human epilepsy

Based on the pronounced effects of LCM on slow inactivation we speculated that the effects of LCM on neuronal firing should also be maintained in chronic epilepsy, in

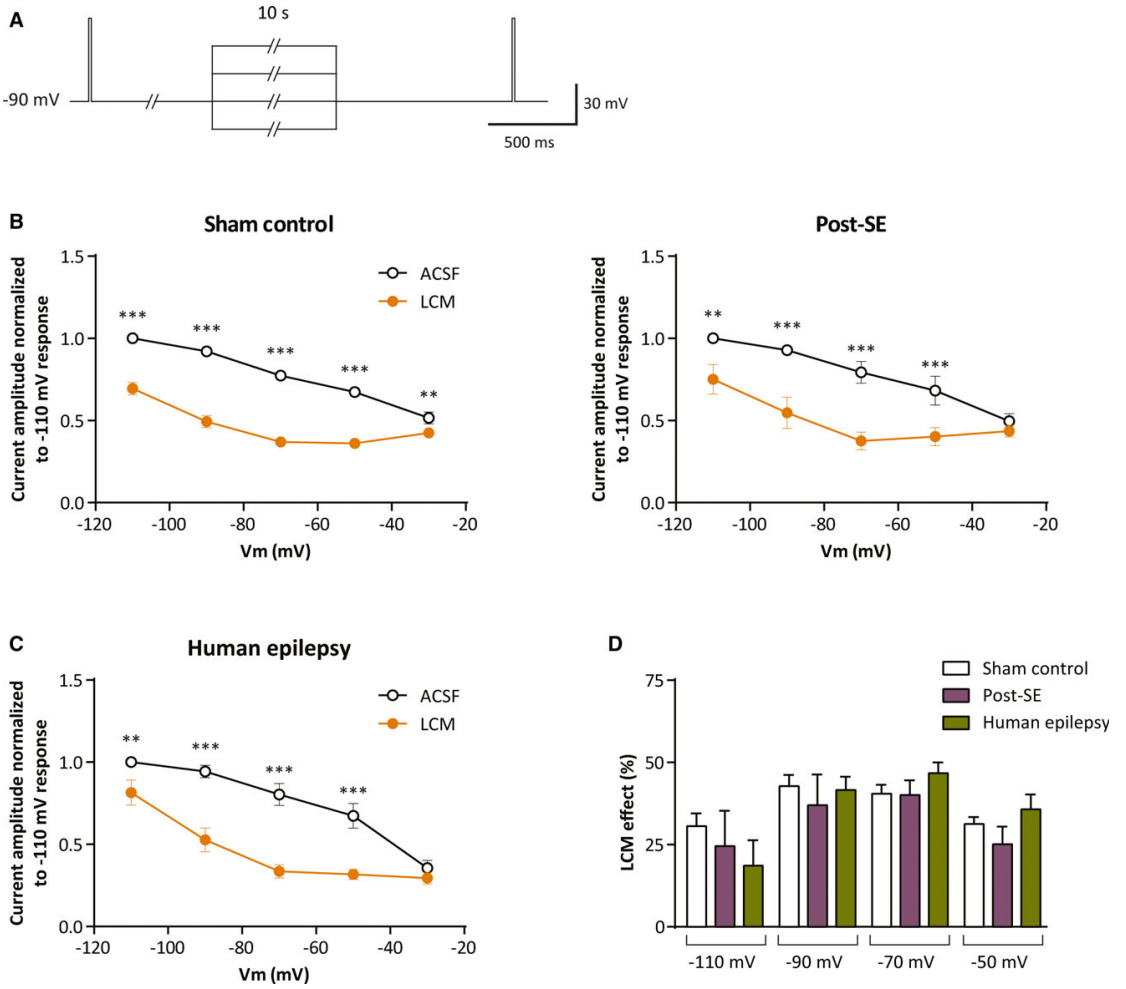

Figure 4.

LCM effects on voltage-dependence of slow inactivation of Na^+ channels in dentate gyrus granule cells. (**A**) Voltage step protocol used to analyze voltage-dependence of slow inactivation. A brief test pulse (15 msec to −30 mV) was followed by conditioning pulses to potentials ranging from −110 to −50 mV (10 s). Another test pulse (15 msec) was applied after recovery from fast inactivation 1 s after the end of the conditioning pulse. (**B**, **C**) Summary of test pulse amplitudes normalized to the test pulse of the corresponding −110 mV recording. Amplitudes for −30 mV were derived from the previous recordings of slow inactivation. A comparison of averaged baseline and washout amplitudes (white symbols) to those of 100 μM LCM (orange symbols) shows a significant and very pronounced reduction of sodium currents both in rat (B) and human (C) granule cells. (n = 7, 6 and 6 for sham-control and pilocarpine-treated animals, and human granule cells, respectively. For Bonferroni posttests, ** and *** indicate significance levels of $p < 0.01$ and $p < 0.001$, respectively). (**D**) Summary of the effects of LCM at different conditioning pulse potentials.

contrast to, for example, CBZ.[1,9] We therefore next examined effects of LCM on action potential firing in rat and human dentate granule cells. We first obtained patch-clamp recordings from hippocampal dentate granule cells in the slice preparation in sham-control and pilocarpine-treated rats (see Materials and Methods), and elicited neuronal firing with current injections of different magnitude (Fig. 5A). In these recordings, the membrane potential was not clamped, but was uniformly at −86.9 ± 0.9 mV in sham-control and −84.4 ± 0.9 mV in pilocarpine animals (n = 11 for both groups, n.s.). The maximal firing frequencies obtained without LCM in sham versus pilocarpine-treated animals were not different (26.2 ± 2.5 vs. 25.7 ± 1.9 Hz). There were also no clear differences in

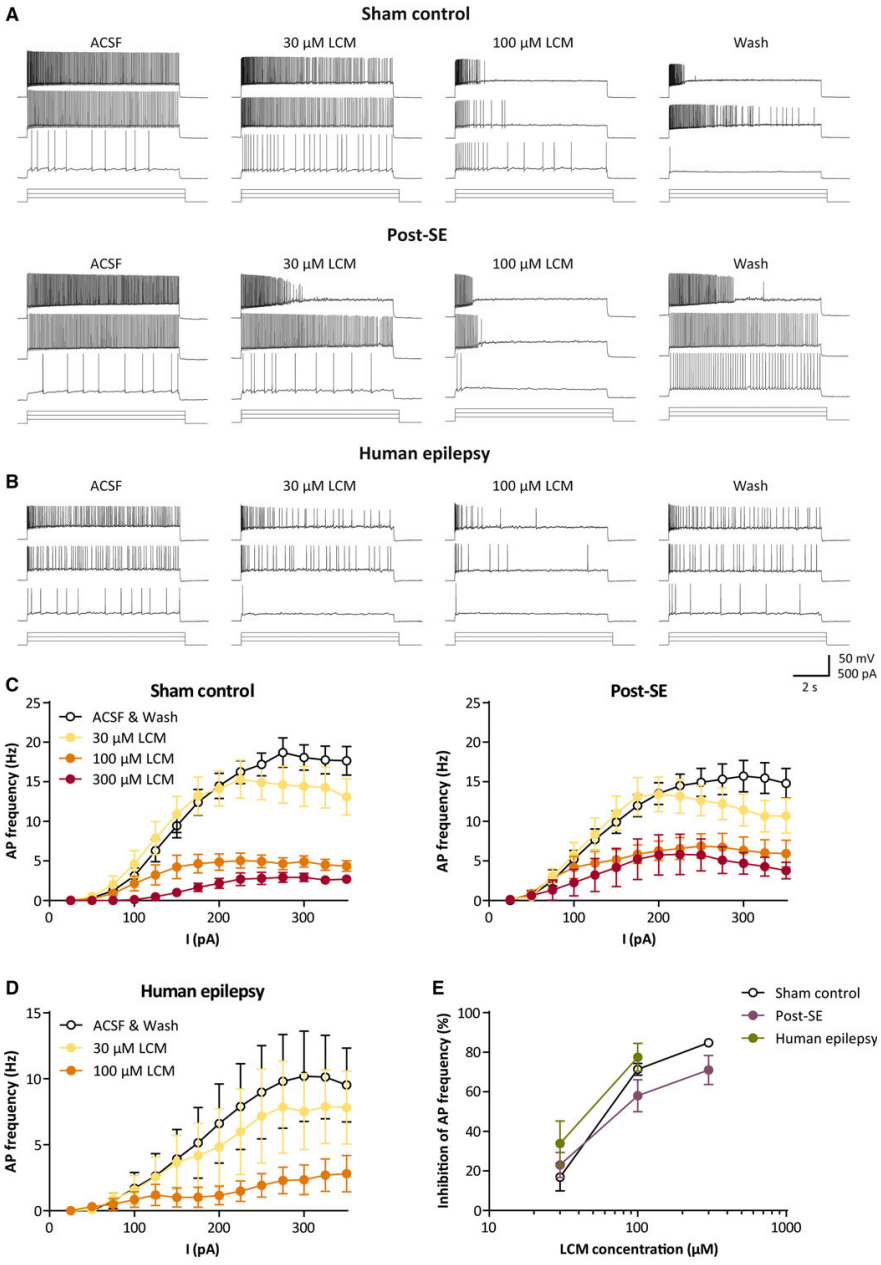

Figure 5.
Effects of LCM on repetitive action potential firing of rat and human dentate gyrus cells. (**A**, **B**) Representative voltage traces elicited by current injections at threshold for eliciting firing, as well as 2× and 3× threshold current injection. Data are shown for sham-control rats and pilocarpine-treated rats (**A**) and patients with TLE (**B**). Current injection steps are depicted in the bottom row. (**C**, **D**) Input–output diagrams illustrate the action potential frequency plotted against injected current for sham control and pilocarpine-treated (**C**, n = 11 for both groups) and human granule cells (**D**, n = 9). Average firing frequency was assessed during the consecutive application of 30 µM (yellow symbols) and 100 µM LCM (orange symbols) and compared to the average values of preapplication (ACSF) and postapplication (wash) period (white symbols). (**E**) Inhibitory effects of different concentrations of LCM on repetitive firing. A significant reduction of action potential frequency was found in all three experimental groups for concentrations ≥100 µM (asterisks omitted for clarity, Dunnett multiple comparison test, $p < 0.01$).

Epilepsia, 58(1):27–41, 2017
doi: 10.1111/epi.13602

input-output relationships between these groups (c.f. Fig. 5C, left vs. right panel).

LCM application induced a reversible, dose-dependent inhibition of firing in both sham-control animals and pilocarpine-treated animals, as revealed in the input–output curves of firing frequency versus current injection magnitude (Fig. 5A,C). The effects on the firing rate observed at 300 pA current injections were significant for concentrations of LCM >100 μM (one-way ANOVA, sham control: $F_{3,47} = 18.41$, $p < 0.001$, pilocarpine-treated: $F_{3,42} = 5.77$, $p = 0.002$, followed by Dunnett posttest for LCM efficacy). Thus, these results show that while CBZ exhibits reduced effects on repetitive firing,[9] LCM effects are maintained in chronic experimental epilepsy.

We next examined if LCM is capable of efficiently modulating neuronal excitability and firing behavior in human epilepsy. We obtained whole-cell patch-clamp recordings from human dentate granule cells in the slice preparation, and examined their firing behavior during prolonged (8 s) current injections. Again, the effects on the firing rate observed at 300 pA current injections were significant for 100 μM LCM (one-way ANOVA, $F_{2,16} = 5.91$, $p = 0.012$, followed by Dunnett posttest for LCM efficacy). The effects of LCM on human dentate granule cells was indistinguishable from control or epileptic rat dentate granule cells (Fig. 5B,D,E, Kruskal-Wallis test, n.s., for 100 μM LCM).

Effects of LCM on action potential properties in experimental epilepsy

We next examined the use-dependent effects of 100 μM LCM on action potential generation of dentate gyrus neurons in more detail. We selected traces under baseline conditions, 100 μM LCM and after wash that had approximately the same numbers of action potentials (Fig. 6A, uppermost traces, example from a control animal). This strongly underestimates the effects of LCM on neuronal firing, but allows examination of how action potential parameters change systematically with and without LCM during prolonged firing.

Plotting the rate of the membrane potential change (dV/dt) versus membrane potential (V_m; shown for the traces in the upper row, Fig. 6A) for representative action potentials at the onset of firing, in the middle of the current injection, and at the end of the current injection revealed systematic changes in the action potential waveform. No large changes of action potential waveform were observed for the first action potential (black curves). Successively larger effects of 100 μM LCM were found for the middle and last action potentials in the train (orange and blue curves, respectively), consistent with a slowly evolving block of Na^+ channels during prolonged firing (Fig. 6A, lower panels). A detailed summary of action potential properties as well as passive properties can be found in Table S2 (for statistics see Tables S3 and S4).

Plots of the first derivation of V_m binned in 1 s time bins over the time course of the current injection confirmed this impression in sham-control and epileptic rats (Fig. 6B, n = 11 and 17, respectively) and human granule cells (Fig. 6C, n = 5, limited to those cells in which sweeps with persistent firing under LCM could be identified). LCM application led to a significantly stronger decrease in maximal dV/dt during the current injection compared to control conditions in all groups (Fig. 6D, ***$p = 0.001$ for both rat groups and *$p = 0.03$ for human cells, respectively, paired *t*-test). The magnitude of this use-dependent effect was not different between the groups (n.s., Kruskal-Wallis test).

Discussion

The main result of this study is that LCM acts mainly via effects on the voltage-dependence of slow inactivation in native human and rat neurons. Moreover, the efficacy of LCM is maintained in chronic human and experimental epilepsy, unlike the conventional use-dependent blocker CBZ.

Our results in native human and rat neurons are in line with the previous studies in primary neocortical cultures,[10,11] also showing a potent shift of the voltage-dependence of slow inactivation in a hyperpolarizing direction by LCM. The effects on the time course of entry or recovery from slow inactivation were, in contrast, small or nonsignificant.[10] In this previous study, no effects on fast inactivation properties were seen. This is dissimilar to our results, in which we did observe small but significant effects of LCM

Figure 6.
Use-dependent effects of 100 μM LCM on action potential generation of dentate gyrus neurons. (**A**) Upper panel: Examples of representative traces selected for this analysis under baseline conditions, 100 μM LCM and after wash (control animal) with approximately the same numbers of action potentials. Middle panel: Representative action potentials at the onset of firing (black), in the middle of the current injection (orange), at the end of the current injection (blue), and the respective first derivations of the voltage trace (small traces). Lower panels: Plots of the rate of the membrane potential change (dV/dt) versus membrane potential (V_m) for the traces in the middle panels. (**B**, **C**) Plots of the first derivation of V_m binned in 1 s time bins over the time course of the current injection in sham-control and epileptic rats (**B**) and human granule cells (**C**). All data are normalized to the dV/dt values obtained in the first time bin. (**D**) Change in dV/dt over the duration of the current injection under control conditions and after LCM application. For paired *t*-tests of dV/dt differences between first and last time bins, * and *** indicate significance levels of $p < 0.05$ and $p < 0.001$, respectively. Values are illustrated as % reduction of the initial dV/dt.

Epilepsia, 58(1):27–41, 2017
doi: 10.1111/epi.13602

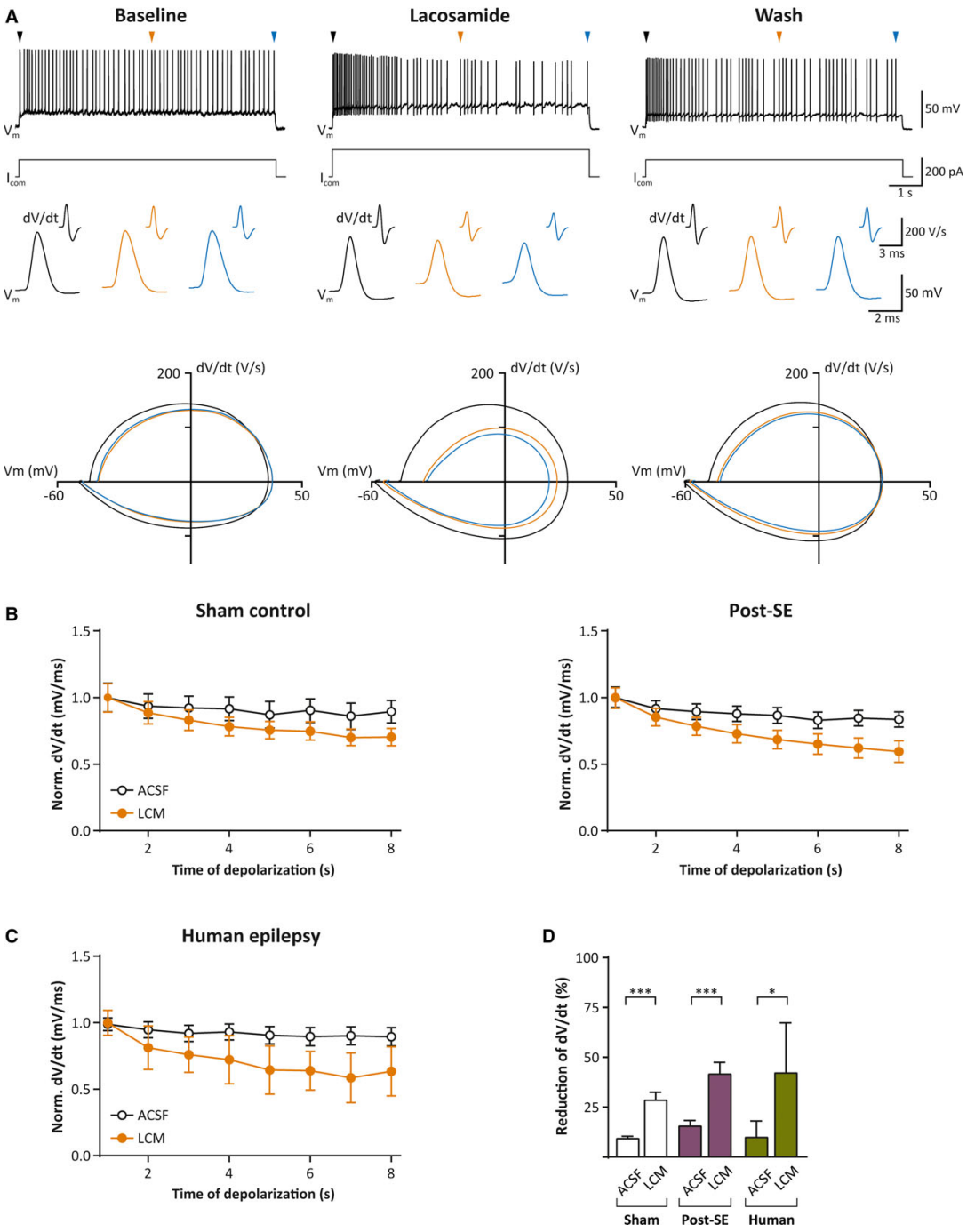

on inactivation voltage dependence. This may be ascribed to the fact that these are native neurons from adult animals, with very different Na^+ channel properties. In addition, it is possible that the prepulses used to invoke inactivation (0.5 s) cause a small amount of slow inactivation that might contribute to this effect. Nonetheless, the effects that these shifts in half-maximal fast inactivation have on the availability of Na^+ channels were—in contrast to the large effects

Epilepsia, 58(1):27–41, 2017
doi: 10.1111/epi.13602

on slow inactivation voltage-dependence—negligible. The effects on neuronal firing that we observed were also largely consistent with data obtained in cultured neurons.[10,18] These studies already show effects of LCM on repetitive firing that were most pronounced with long (10 s) current injections.[10] In our hands, this was similar, with large effects on firing being observed with prolonged current injections. We also observed effects already at low (30 μM) concentrations of LCM, which were markedly increased at higher concentration (100 and 300 μM), likewise consistent with Errington et al.[10]

The voltage-gated Na^+ channel seems to be the major target for LCM, as binding studies have excluded binding of LCM to different types of γ-aminobutyric acid (GABA) and glutamate receptors, as well as a variety of other neurotransmitter receptors, and voltage-gated potassium or calcium channels.[18] Likewise, there was no physiologic effect of LCM on GABA and glutamate receptors, neurotransmitter transporters, or GABA metabolism.[18,19] These results confirm in native adult neurons that the mechanism of action of LCM on Na^+ channels is very different from classical use-dependent Na^+ channel blockers, such as carbamazepine or phenytoin.

This raises the question if the effects of LCM are also lost in chronic epilepsy, which has been shown for use-dependent effects of CBZ in the same model in granule cells.[1] Similarly, an impairment of sodium current modulation by CBZ but not valproic acid has been reported in patients with TLE as well as in the kindling model.[20,21] The answer, at least for LCM in dentate granule cells, is an unequivocal no. We observed quantitatively maintained effects of LCM on slow inactivation in experimental epilepsy. Moreover, we found that Na^+ channels in granule cells obtained from epilepsy surgical specimens were strongly inhibited by LCM, with quantitatively similar, selective effects on the slow inactivation voltage-dependence. These maintained effects of LCM translated into potent inhibition of repetitive firing induced by long current injections in both experimental and human epilepsy. It would be interesting to examine if effects on slow inactivation are maintained in this and perhaps other brain regions that show decreases in anticonvulsant actions on parameters of fast sodium channel inactivation. Taken together, these results suggest that LCM effects are conserved in chronic epilepsy.

What does this finding mean for the key goal of overcoming pharmacoresistance? A previous study has shown that the active metabolite of the anticonvulsant eslicarbazepine has potent use-dependent effects in experimental and human epilepsy, and in fact has add-on effects to CBZ.[9] The molecular mechanism for this effect is unknown, but this article suggested that one way to overcome pharmacoresistance is to design drugs that exhibit maintained use-dependent block on Na^+ channels in chronically epileptic tissue.[9] The present study suggests a viable alternative—to use compounds that do not exert their effects via use-dependent block, but rather act on slow inactivation. These results also may impact thinking about combining classical use-dependent Na^+ channel blockers with compounds such as LCM. Although targeting the same ion channel protein, the compounds have very different mechanisms of action, and add-on treatment with LCM in the presence of conventional Na^+ channel blockers should not be discounted due to mechanistic considerations alone.

In addition to changes in the pharmacology of Na^+ channels in chronic epilepsy, a further candidate mechanism that may underlie pharmacoresistance is an altered expression of multidrug transporters in chronic epilepsy. An upregulation of drug transporters occurs in different types of chronic experimental and human epilepsies, and affects anticonvulsant drug concentrations present in the central nervous system (CNS) parenchyma. The capability of different members of the multidrug transporter family to transport anticonvulsants has been addressed in several publications. These have revealed that multidrug transporters effectively transport many, but not all, anticonvulsant drugs. It has been shown that LCM is a substrate for transport by human P-glycoprotein, which is one of the most consistently upregulated drug transporters in chronic epilepsy.[22] However, this work also revealed that passive diffusion appears to be a major component of LCM distribution. Thus, the role of active transport in the disposition of LCM in vivo is unclear. However, should LCM prove to be subject to active transport, it might be advantageous to design LCM variants acting on slow inactivation that are not transported, thus overcoming both candidate mechanisms of pharmacoresistance.

Taken together, these results show that LCM exhibits maintained efficacy in chronic epilepsy, in contrast to conventional use-dependent Na^+ channel blockers such as CBZ. They also establish that development of compounds targeting slow inactivation may be a promising strategy to overcome target mechanisms of pharmacoresistance.

Acknowledgments

This work was supported by the Deutsche Forschungsgemeinschaft (SFB 1089, to HB) and UCB Pharma. CW and IN are employees of UCB Pharma. HB has served as a paid consultant for UCB Pharma.

Disclosure

The remaining authors have no conflicts of interest. We confirm that we have read the Journal's position on issues involved in ethical publication and affirm that this report is consistent with those guidelines.

References

1. Remy S, Gabriel S, Urban BW, et al. A novel mechanism underlying drug-resistance in chronic epilepsy. *Ann Neurol* 2003;53:469–479.
2. Remy S, Beck H. Molecular and cellular mechanisms of pharmacoresistance in epilepsy. *Brain* 2006;129:18–35.

3. Ragsdale DS, Avoli M. Sodium channels as molecular targets for antiepileptic drugs. *Brain Res Brain Res Rev* 1998;26:16–28.
4. Catterall WA. Molecular properties of brain sodium channels: an important target for anticonvulsant drugs. *Adv Neurol* 1999;79:441–456.
5. Köhling R. Voltage-gated sodium channels in epilepsy. *Epilepsia* 2002;43:1278–1295.
6. Catterall WA, Swanson TM. Structural basis for pharmacology of voltage-gated sodium and calcium channels. *Mol Pharmacol* 2015;88:141–150.
7. Payandeh J, Scheuer T, Zheng N, et al. The crystal structure of a voltage-gated sodium channel. *Nature* 2011;475:353–358.
8. Boiteux C, Vorobyov I, French RJ, et al. Local anesthetic and antiepileptic drug access and binding to a bacterial voltage-gated sodium channel. *Proc Natl Acad Sci U S A* 2014;111:13057–13062.
9. Doeser A, Dickhof G, Reitze M, et al. Targeting pharmacoresistant epilepsy and epileptogenesis with a dual-purpose antiepileptic drug. *Brain* 2015;138:371–387.
10. Errington AC, Stöhr T, Heers C, et al. The investigational anticonvulsant lacosamide selectively enhances slow inactivation of voltage-gated sodium channels. *Mol Pharmacol* 2008;73:157–169.
11. Niespodziany I, Leclere N, Vandenplas C, et al. Comparative study of lacosamide and classical sodium channel blocking antiepileptic drugs on sodium channel slow inactivation. *J Neurosci Res* 2013;91:436–443.
12. Uebachs M, Albus C, Opitz T, et al. Loss of beta1 accessory Na^+ channel subunits causes failure of carbamazepine, but not of lacosamide, in blocking high-frequency firing via differential effects on persistent Na^+ currents. *Epilepsia* 2012;53:1959–1967.
13. Sanabria ERG, Su H, Yaari Y. Initiation of network bursts by Ca^{2+}-dependent intrinsic bursting in the rat pilocarpine model of temporal lobe epilepsy. *J Physiol* 2001;532:205–216.
14. Su H, Sochivko D, Becker A, et al. Upregulation of a T-Type Ca^{2+} channel causes a long-lasting modification of neuronal firing mode after status epilepticus. *J Neurosci* 2002;22:3645–3655.
15. Becker AJ, Pitsch J, Sochivko D, et al. Transcriptional upregulation of Cav3.2 mediates epileptogenesis in the pilocarpine model of epilepsy. *J Neurosci* 2008;28:13341–13343.
16. Klatte K, Kirschstein T, Otte D, et al. Impaired D-serine-mediated cotransmission mediates cognitive dysfunction in epilepsy. *J Neurosci* 2013;33:13066–13080.
17. Pothmann L, Müller C, Averkin RG, et al. Function of inhibitory micronetworks is spared by Na^+ channel-acting anticonvulsant drugs. *J Neurosci* 2014;34:9720–9735.
18. Errington AC, Coyne L, Stöhr T, et al. Seeking a mechanism of action for the novel anticonvulsant lacosamide. *Neuropharmacology* 2006;50:1016–1029.
19. Rogawski MA, Tofighy A, White HS, et al. Current understanding of the mechanism of action of the antiepileptic drug lacosamide. *Epilepsy Res* 2015;110:189–205.
20. Vreugdenhil M, van Veelen CWM, van Rijen PC, et al. Effect of valproic acid on sodium currents in cortical neurons from patients with pharmaco-resistant temporal lobe epilepsy. *Epilepsy Res* 1998;32:309–320.
21. Vreugdenhil M, Wadman WJ. Modulation of sodium currents in rat CA1 neurons by carbamazepine and valproate after kindling epileptogenesis. *Epilepsia* 1999;40:1512–1522.
22. Zhang C, Chanteux H, Zuo Z, et al. Potential role for human P-glycoprotein in the transport of lacosamide. *Epilepsia* 2013;54:1154–1160.

Supporting Information

Additional Supporting Information may be found in the online version of this article:

Figure S1. LCM effects on recovery from slow inactivation of Na^+ channels in human dentate gyrus granule cells.

Figure S2. Evaluation of the stability of Na^+ current slow inactivation voltage dependence under control conditions.

Table S1. Patients with refractory TLE.

Table S2. Passive membrane and action potential properties of dentate gyrus granule neurons in control and epileptic animals, as well as epilepsy patients, in the absence and presence of 100 μM LCM.

Table S3. Statistics for Table S2. Two-way ANOVA (Sham vs. Post-SE vs. Human and Base&Wash vs. LCM).

Table S4. Statistics for Table S2. Two-tailed paired *t*-tests (Base&Wash vs. LCM).

Epilepsia, 58(1):27–41, 2017
doi: 10.1111/epi.13602

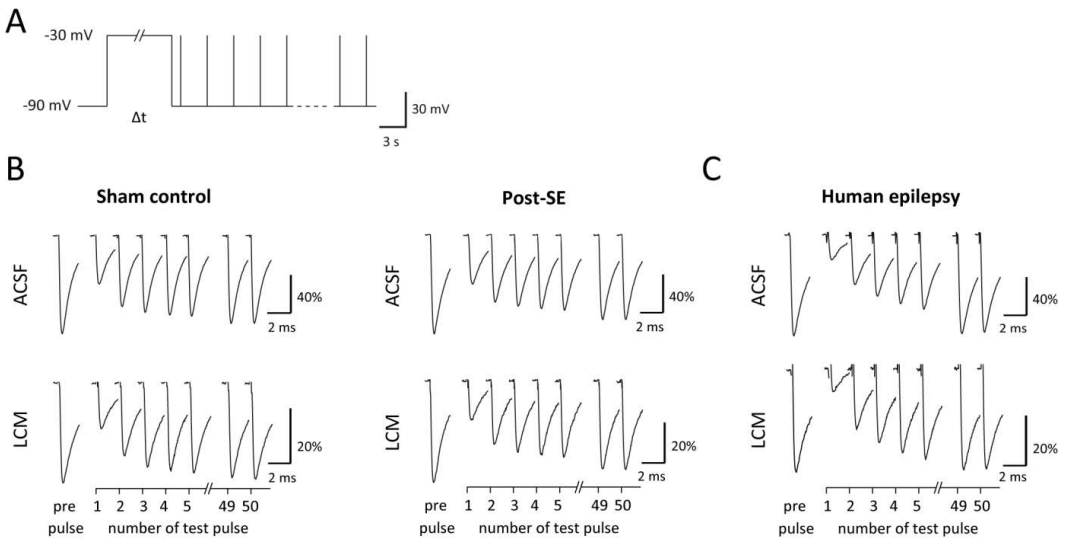

Supplementary Fig. 1: LCM effects on recovery from slow inactivation of Na^+ channels in human dentate gyrus granule cells. **A.** Voltage step protocol used to analyse recovery of Na^+ channels from slow inactivation. Starting 1 second after the conditioning pulse, test pulses (15 ms) at 3 second intervals were used for determining the time course of recovery from slow inactivation. **B.** Representative examples for recovery from slow inactivation in control and pilocarpine-treated rats after 30 second conditioning pulses **C.** Equivalent example traces from a human granule cell.

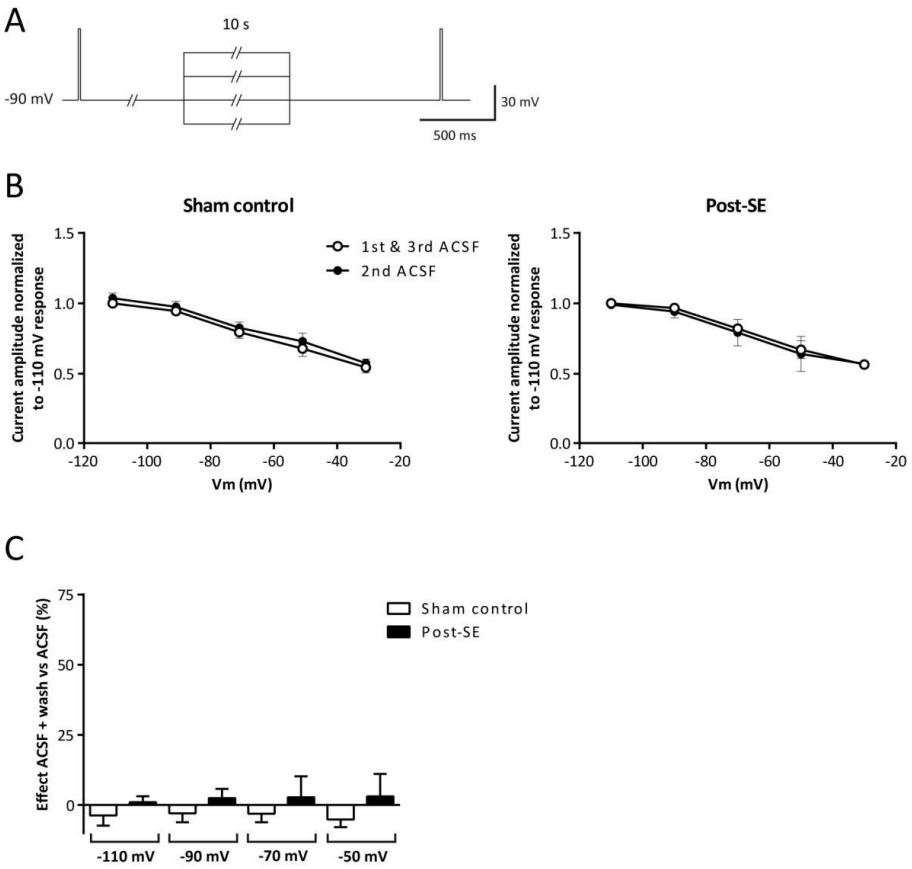

Supplementary Fig. 2: Evaluation of the stability of Na^+ current slow inactivation voltage-dependence under control conditions. **A.** Voltage protocol used (identical to Fig. 4). **B.** Slow inactivation. All recording parameters were identical to the recordings with LCM. ACSF was used for 'control', 'washin' and 'washout' conditions (1st, 2nd and 3rd ACSF). These time-matched control recordings were performed in sham-control (n=7 for -110 to -50 mV; n=6 for -30 mV) and pilocarpine-treated (post-SE) animals (n=3 and 1, respectively). **C.** Analysis of the effect of applying ACSF without LCM. ACSF application had no significant effects.

Age at surgery	Gender	No cells	Type of recording	Part of Figure	Type of surgery	Pathology	Treated with LCM	Current medication	Past medication
39	m	3	CC	5, 6	sel. AH left	AHS left	no	VPA, LEV	CBZ, PB/PRM, LTG
8	f	1	CC	5	sel. AH left	AHS left	no	LTG, LEV	same
55	f	1	CC	5, 6	sel. AH right	AHS right	no	LEV, ESL	OXC, TPM
33	f	2	CC	5, 6	sel. AH left	AHS left	yes	LEV, LCM	CBZ, OXC, LTG, TPM, ZON
24	m	1	CC	5, 6	sel. AH right	Moderate astrogliosis	yes	LEV, LCM	CBZ
29	m	1	CC	5, 6	Lesionectomy & sel. AH left	Developmental malformation left	no	LEV, OXC	CBZ
47	m	1	VC	1-3	Lesionectomy & sel. AH right	Cavernoma right	no	LEV, PGB	same
36	m	1	VC	1-3	sel. AH left	AHS left	no	LTG, LEV, BZO	CBZ
27	m	1	VC	1-3	sel. AH right	unclear	yes	ESL, LEV	LTG, LCM
43	f	4	VC	1-3	sel. AH left	AHS left	yes	LCM, TPM	CBZ, VPA, LTG
17	f	1	VC	1-3	temp. pole resection & AH right	temp. pole loss of grey-white matter differentiation & AHS r	yes	LTG, ZON	OXC, LEV, LCM
22	f	1	VC	1-3, S1	sel. AH left	AHS left	yes	LEV, OXC	LCM
37	f	1	VC	1, 4	sel. AH right	AHS right	no	OXC	LTG, LEV
64	m	2	VC	1, 4	sel. AH left	AHS left	yes	TPM, LEV	CBZ, OXC, VPA, LTG, ZON, LCM
47	f	2	VC	1, 4	sel. AH left	AHS left	no	CBZ, LEV, ZON	same
45	f	1	VC	1, 4	sel. AH left	AHS left	no	LTG, CLB, LEV	same

Supplementary Table 1: Patients with refractory TLE Sel. AH, selective amygdalohippocampectomy; AHS, Ammon's horn sclerosis; VPA, valproic acid; LEV, levetiracetam; CBZ, carbamazepine; PB, phenobarbital; PRM, primidone; LTG, lamotrigine; ESL, eslicarbazepine; LCM, lacosamide; OXC, oxcarbazepine; TPM, topiramate; ZNS, zonisamide; PGB, pregabalin; BZO, oxazepine; CLB, clobazam;

	Sham control (n=17)	Post-SE (n=19)	Human epilepsy (n=9)
ACSF (mean of baseline and wash)			
RMP (mV)	-70.5 ± 1.2	-68.6 ± 0.8	-66.8 ± 1.4
R_m (MΩ)	211.6 ± 16.9	175.3 ± 9.5	109.3 ± 13.9
V_{Peak} [mV]	21.6 ± 2.9	21.4 ± 1.9	25.4 ± 2.5
V_{Thr} [mV]	-57.1 ± 1.4	-51.6 ± 2.1	-52.4 ± 1.7
Width [ms]	0.88 ± 0.02	0.86 ± 0.03	0.94 ± 0.04
Max. slope [V/s]	274 ± 17	251 ± 13	240 ± 10
100 µM lacosamide			
RMP (mV)	-70.0 ± 1.3	-68.3 ± 0.8	-67.0 ± 1.4
R_m (MΩ)	221.7 ± 22.6	190.3 ± 11.8	117.8 ± 20.5
V_{Peak} [mV]	19.6 ± 3.6	20.6 ± 2.6	23.0 ± 2.7
V_{Thr} [mV]	-58.6 ± 1.4	-51.9 ± 1.8	-52.5 ± 1.3
Width [ms]	0.87 ± 0.03	0.85 ± 0.03	0.92 ± 0.05
Max. slope [V/s]	263 ± 18	246 ± 15	234 ± 18

Supplementary Table 2: Passive membrane and action potential properties of dentate gyrus granule neurons in control and epileptic animals, as well as epilepsy patients, in the absence and presence of 100 µM LCM. RMP: resting membrane potential, R_m: membrane resistance, V_{Peak} : peak of action potentials, V_{Thr}: action potential threshold, Width: action potential width halfway between threshold and peak potential.

	Group	**LCM**	**Interaction**
RMP (mV)	F(2,41)=1.847 p=0.1707	F(2,41)=0.337 p=0.5649	F(1,41)=3.328 p=0.7223
R_m (MΩ)	F(2,41)=8.559 p=0.0008*	F(2,41)=1.829 p=0.1837	F(1,41)=0.064 p=0.9383
VPeak [mV]	F(2,42)=0.326 p=0.7235	F(2,42)=0.374 p=0.6901	F(1,42)=3.910 p=0.0546
VThreshold [mV]	F(2,42)=0.796 p=0.4577	F(2,42)=4.068 p=0.0243	F(1,42)=1.577 p=0.2161
Width [ms]	F(2,42)=0.030 p=0.9707	F(2,42)=1.264 p=0.2930	F(1,42)=0.648 p=0.4255
Max. slope [V/s]	F(2,42)=0.108 p=0.8977	F(2,42)=0.9593 p=0.3914	F(1,42)=1.160 p=0.2876

Supplementary Table 3: Statistics for supplementary table 2. Two-way ANOVA (Sham vs Post-SE vs Human and Base&Wash vs LCM). * Tukey's multiple comparisons test yielded for sham control vs. post-SE: p=0.2010, for sham control vs. human epilepsy: p=0.0005, and for post-SE vs. human epilepsy: p=0.0194.

	Sham control	**Post-SE**	**Human epilepsy**
RMP (mV)	t=1.7199, df=16 p=0.4820	t=0.9292, df=18 p=0.3651	t=0.5242, df=7 p=0.6163
R_m (MΩ)	t=0.8412, df=16 p=0.4126	t=1.111, df=18 p=0.2812	t=0.884, df=7 p=0.4060
VPeak [mV]	t=1.411, df=16 p=0.1773	t=0.7048, df=18 p=0.4899	t=1.182, df=8 p=0.2711
VThreshold [mV]	t=1.463, df=16 p=0.1629	t=0.5591, df=18 p=0.5830	t=0.1324, df=8 p=0.8979
Width [ms]	t=0.569, df=16 p=0.5773	t=0.6346, df=18 p=0.5337	t=0.3075 df=8 p=0.7663
Max. slope [V/s]	t=1.130, df=16 p=0.2752	t=0.4238, df=18 p=0.6767	t=0.4708, df=8 p=0.6503

Supplementary Table 4: Statistics for supplementary table 2. Two-tailed paired t-tests (Base&Wash vs LCM). Bonferroni correction for multiple tests yielded $\alpha = 0.05/18 = 0.0028$.

3.3 Summary

A loss or reduction of use-dependent block by conventional sodium channel-acting AEDs has been suggested as an underlying mechanism of pharmacoresistance both in human and experimental epilepsy (Remy et al., 2003a,b). For the third generation sodium channel blocker LCM selective enhancement of the slow inactivation of VGSCs was demonstrated as a novel and unique mechanism of action (Errington et al., 2008; Sheets et al., 2008). A resulting blockade of action potentials emerging during pathological high-frequency firing was considered advantageous over binding to and stabilizing open or fast inactivated channels during pathologic but also physiologic activity as other sodium channel blockers preferentially do (Beyreuther et al., 2007; Rogawski et al., 2015). Since this mechanism of action was unique to LCM and distinguished it from all other sodium channel blockers available at that time, the purpose of the present publication was to determine whether LCM might overcome aforementioned mechanism of pharmacoresistance.

Therefore, we determined the effects of LCM on the voltage dependence of VGSC activation and fast inactivation, the recovery from fast inactivation, entry, recovery, and voltage dependence of VGSC slow inactivation and on repetitive action potential firing in dentate granule neurons. To check for alterations in LCM efficacy in chronic epilepsy, effect sizes observed in control cells and epileptic cells were compared. Voltage-clamp recordings in isolated DGCs revealed that LCM induces small hyperpolarizing shifts of the voltage dependence of the steady-state fast inactivation without affecting the activation of VGSCs. Likewise, recovery from fast inactivation remained largely unaffected. Similar to previous studies in cultured neuroblastoma cells, much stronger voltage-dependent effects of LCM were observed on the entry of slow inactivation without affecting its recovery. LCM shifted the voltage dependence of slow inactivation to more hyperpolarized potentials, indicated by a reversible reduction of sodium current amplitudes. These effects translated into an inhibition of repetitive action potential firing building up over multiple seconds of depolarization. Further analyses revealed that the blockade of repetitive firing was accompanied by systematic changes in action potential waveform. The magnitude of all observed LCM effects were not significantly different between DGCs of nonepileptic rats, epileptic rats and TLE patiens which implies maintained drug efficacy.

Taken together, LCM exerts strong effects on the voltage dependence of slow inactivation in DGCs as it was previously shown for cultured neuroblastoma cells. These effects manifest as inhibition of action potential firing during prolonged depolarizations and importantly are maintained under chronic epileptic conditions.

4 Conclusion

Voltage-gated sodium channels (VGSCs) are critically involved in the generation of action potentials (APs) and repetitive firing under physiological conditions but also during epileptic seizures. Older and commonly used antiepileptic drugs (AEDs) such as carbamazepine (CBZ) exert their anticonvulsant action by slowing the recovery from fast inactivation of sodium channels. Due to higher affinity for fast-inactivated sodium channels, inhibition of VGSCs by CBZ is more effective during depolarization and repetitive AP firing. In animal models of chronic epilepsy and tissue resected from patients with chronic epilepsy, however, a loss of efficacy of CBZ was reported (Remy et al., 2003a).

Another, yet different, mechanism of sodium channel inactivation is slow inactivation. Lacosamide (LCM) and eslicarbazepine acetate (via its active metabolite eslicarbazepine; S-Lic) are the first anticonvulsants described to modulate sodium channel slow inactivation (Errington et al., 2008; Hebeisen et al., 2015). This raised the question whether these compounds with a mode of action distinct from classical use-dependent blockers maintain efficacy in chronic epileptic dentate granule cells (Doeser et al., 2014a; Holtkamp et al., 2018, 2017). Both substances exert their main effects by shifting the voltage dependence of sodium channel slow inactivation in a hyperpolarizing direction, resulting in reduced sodium current amplitudes and reduced AP firing. Interestingly, maintained efficacy in chronic epileptic tissue was found for both compounds.

One of the important questions that consequently arise is how minimal changes in the molecular structure of a drug (in the example of CBZ and S-Lic) can cause a multitude of critical changes involving its mechanism or kinetics of action, its specificity for certain target isoforms or its implication for pharmaocoresistance. Interestingly, these effects seem to occur in an all-or-nothing fashion and not on a gradual scale. Likewise, it would be interesting to know how the structurally dissimilar compounds S-Lic and LCM exert almost identical effects on slow inactivation processes. A recent modeling study proposed a common pharmacophore for many sodium channel acting drugs, however this study fails to explain potential differences regarding slow and fast inactivation or pharmacoresistance (Tikhonov and Zhorov, 2017). Recent advances in the identification of high-resolution structures of target molecules provide the basis for ongoing studies connecting structure, function and drug-target interactions (Shen et al., 2017). Having highlighted the importance of slow inactivation-targeting drugs, future studies will likely address these open questions.

Not only drug specificity for different target isoforms but also distinct effects on

certain cell types are of paramount interest in translating findings from a single-cell level to a network level or even the whole brain. Previous studies already showed that CBZ effects can not only differ between hippocampal pyramidal neurons and dentate granule cells but also between principal cells and interneurons (Pothmann et al., 2014; Remy et al., 2003a; Schaub et al., 2007). Ongoing and future studies will likely also clarify the role of novel AEDs on interneurons and neuronal networks.

Since both, LCM and S-Lic seem to overcome drug resistance on a cellular level, it may be worthwhile to continue developing and researching novel, optimized compounds that target slow inactivation. Especially in the light of growing possibilities and importance of tailored or personalized medicines it may be most helpful to develop a broad spectrum of drugs that may be selective to single channel isoforms or very narrow voltage ranges only. Finally, due to the different mode of action of classical use-dependent sodium channel blockers and novel slow inactivation-targeting anticonvulsants, it may prove useful in clinical use to combine these types of drugs despite acting on the same molecular target.

References

Acsády, L., Kamondi, A., Sík, A., Freund, T., and Buzsáki, G. (1998). GABAergic cells are the major postsynaptic targets of mossy fibers in the rat hippocampus. *J Neurosci* 18, 3386–3403.

Almeida, L., Potgieter, J. H., Maia, J., Potgieter, M. A., Mota, F., and Soares-da-Silva, P. (2008). Pharmacokinetics of eslicarbazepine acetate in patients with moderate hepatic impairment. *Eur J Clin Pharmacol* 64, 267–273.

Altman, J. and Das, G. D. (1965). Autoradiographic and histological evidence of postnatal hippocampal neurogenesis in rats. *J Comp Neurol* 124, 319–335.

Alves, G., Figueiredo, I., Falcão, A., Castel-Branco, M., Caramona, M., and Soares-da-Silva, P. (2008). Stereoselective disposition of S-and R-licarbazepine in mice. *Chirality* 20, 796–804.

Alzheimer, C., Schwindt, P. C., and Crill, W. E. (1993). Modal gating of Na^+ channels as a mechanism of persistent Na^+ current in pyramidal neurons from rat and cat sensorimotor cortex. *J Neurosci* 13, 660–673.

Amaral, D. and Lavenex, P. (2007). Hippocampal neuroanatomy. In: Andersen, P., Morris, R., Amaral, D., Bliss, T., and O'Keefe, J. (Eds.), *The hippocampus book*. New York: Oxford University Press, 37–117.

Amaral, D. G. (1978). A Golgi study of cell types in the hilar region of the hippocampus in the rat. *J Comp Neurol* 182, 851–914.

Amaral, D. G., Scharfman, H. E., and Lavenex, P. (2007). The dentate gyrus: fundamental neuroanatomical organization (dentate gyrus for dummies). *Prog Brain Res* 163, 3–22.

Ambrogini, P., Lattanzi, D., Ciuffoli, S., Agostini, D., Bertini, L., Stocchi, V., Santi, S., and Cuppini, R. (2004). Morpho-functional characterization of neuronal cells at different stages of maturation in granule cell layer of adult rat dentate gyrus. *Brain Res* 1017, 21–31.

Androsova, G., Krause, R., Borghei, M., Wassenaar, M., Auce, P., Avbersek, A., Becker, F., Berghuis, B., Campbell, E., Coppola, A., Francis, B., Wolking, S., Cavalleri, G. L., Craig, J., Delanty, N., Koeleman, B. P. C., Kunz, W. S., Lerche, H., Marson, A. G., Sander, J. W., Sills, G. J., Striano, P., Zara, F., Sisodiya, S. M., and Depondt, C. (2017). Comparative effectiveness of antiepileptic drugs in patients with mesial temporal lobe epilepsy with hippocampal sclerosis. *Epilepsia* 58, 1734–1741.

Annegers, J. F., Hauser, W. A., and Elveback, L. R. (1979). Remission of seizures and relapse in patients with epilepsy. *Epilepsia* 20, 729–737.

Araújo, I. M., Ambrósio, A. F., Leal, E. C., Verdasca, M. J., Malva, J. O., Soares-da-Silva, P., Carvalho, A. P., and Carvalho, C. M. (2004). Neurotoxicity induced by antiepileptic drugs in cultured hippocampal neurons: a comparative study between carbamazepine, oxcarbazepine, and two new putative antiepileptic drugs, BIA 2-024 and BIA 2-093. *Epilepsia* 45, 1498–1505.

Baltes, S., Gastens, A. M., Fedrowitz, M., Potschka, H., Kaever, V., and Löscher, W. (2007). Differences in the transport of the antiepileptic drugs phenytoin, levetiracetam and carbamazepine by human and mouse P-glycoprotein. *Neuropharmacology* 52, 333–346.

Bayer, S. A. (1982). Changes in the total number of dentate granule cells in juvenile and adult rats: a correlated volumetric and 3H-thymidine autoradiographic study. *Exp Brain Res* 46, 315–323.

Beck, H., Clusmann, H., Kral, T., Schramm, J., Heinemann, U., and Elger, C. E. (1997a). Potassium currents in acutely isolated human hippocampal dentate granule cells. *J Physiol* 498, 73–85.

Beck, H., Ficker, E., and Heinemann, U. (1992). Properties of two voltage-activated potassium currents in acutely isolated juvenile rat dentate gyrus granule cells. *J Neurophysiol* 68, 2086–2099.

Beck, H., Steffens, R., Heinemann, U., and Elger, C. E. (1997b). Properties of voltage-activated Ca^{2+} currents in acutely isolated human hippocampal granule cells. *J Neurophysiol* 77, 1526–1537.

Behr, J., Lyson, K. J., and Mody, I. (1998). Enhanced propagation of epileptiform activity through the kindled dentate gyrus. *J Neurophysiol* 79, 1726–1732.

Benes, J., Parada, A., Figueiredo, A. A., Alves, P. C., Freitas, A. P., Learmonth, D. A., Cunha, R. A., Garrett, J., and Soares-da-Silva, P. (1999). Anticonvulsant and sodium channel-blocking properties of novel 10, 11-dihydro-5 H-dibenz [b, f] azepine-5-carboxamide derivatives. *J Med Chem* 42, 2582–2587.

Berg, A. T., Vickrey, B. G., Testa, F. M., Levy, S. R., Shinnar, S., DiMario, F., and Smith, S. (2006). How long does it take for epilepsy to become intractable? A prospective investigation. *Ann Neurol* 60, 73–79.

Bergmann, O., Liebl, J., Bernard, S., Alkass, K., Yeung, M. S. Y., Steier, P., Kutschera, W., Johnson, L., Landén, M., Druid, H., Spalding, K. L., and Frisén, J. (2012). The age of olfactory bulb neurons in humans. *Neuron* 74, 634–639.

Beyreuther, B. K., Freitag, J., Heers, C., Krebsfänger, N., Scharfenecker, U., and Stöhr, T. (2007). Lacosamide: a review of preclinical properties. *CNS Drug Rev* 13, 21–42.

Bialer, M., Johannessen, S. I., Levy, R. H., Perucca, E., Tomson, T., and White, H. S. (2017). Progress report on new antiepileptic drugs: a summary of the Thirteenth Eilat Conference on New Antiepileptic Drugs and Devices (EILAT XIII). *Epilepsia* 58, 181–221.

Blümcke, I., Thom, M., Aronica, E., Armstrong, D. D., Bartolomei, F., Bernasconi, A., Bernasconi, N., Bien, C. G., Cendes, F., Coras, R., Cross, J. H., Jacques, T. S., Kahane, P., Mathern, G. W., Miyata, H., Moshé, S. L., Oz, B., Özkara, Ç., Perucca, E., Sisodiya, S., Wiebe, S., and Spreafico, R. (2013). International consensus classification of hippocampal sclerosis in temporal lobe epilepsy: a task force report from the ILAE commission on diagnostic methods. *Epilepsia* 54, 1315–1329.

Boiteux, C., French, C., and Allen, T. W. (2016). Modulation of a bacterial voltage-gated sodium channel by the anti-epileptic drug lacosamide. *Biophys J* 110, 111a.

Boiteux, C., Vorobyov, I., and Allen, T. W. (2014a). Ion conduction and conformational flexibility of a bacterial voltage-gated sodium channel. *Proc Natl Acad Sci U S A* 111, 3454–3459.

Boiteux, C., Vorobyov, I., French, R. J., French, C., Yarov-Yarovoy, V., and Allen, T. W. (2014b). Local anesthetic and antiepileptic drug access and binding to a bacterial voltage-gated sodium channel. *Proc Natl Acad Sci U S A* 111, 13057–13062.

Booker, S. A., Pires, N., Cobb, S., Soares-da-Silva, P., and Vida, I. (2015). Carbamazepine and oxcarbazepine, but not eslicarbazepine, enhance excitatory synaptic transmission onto hippocampal CA1 pyramidal cells through an antagonist action at adenosine A1 receptors. *Neuropharmacology* 93, 103–115.

Brandt, M. D., Jessberger, S., Steiner, B., Kronenberg, G., Reuter, K., Bick-Sander, A., von der Behrens, W., and Kempermann, G. (2003). Transient calretinin expression defines early postmitotic step of neuronal differentiation in adult hippocampal neurogenesis of mice. *Mol Cell Neurosci* 24, 603–613.

Brodie, M. J. (2017). Sodium channel blockers in the treatment of epilepsy. *CNS Drugs* 31, 527–534.

Brooks-Kayal, A. R., Shumate, M. D., Jin, H., Lin, D. D., Rikhter, T. Y., Holloway, K. L., and Coulter, D. A. (1999). Human neuronal γ-aminobutyric acid

A receptors: coordinated subunit mRNA expression and functional correlates in individual dentate granule cells. *J Neurosci* 19, 8312–8318.

Brooks-Kayal, A. R., Shumate, M. D., Jin, H., Rikhter, T. Y., and Coulter, D. A. (1998). Selective changes in single cell $GABA_A$ receptor subunit expression and function in temporal lobe epilepsy. *Nat Med* 4, 1166–1172.

Brown, J. P., Couillard-Després, S., Cooper-Kuhn, C. M., Winkler, J., Aigner, L., and Kuhn, H. G. (2003). Transient expression of doublecortin during adult neurogenesis. *J Comp Neurol* 467, 1–10.

Cabezas, C., Irinopoulou, T., Cauli, B., and Poncer, J. C. (2013). Molecular and functional characterization of GAD67-expressing, newborn granule cells in mouse dentate gyrus. *Front Neural Circuits* 7:60, 1–16.

Caccamo, D., Pisani, L. R., Mazzocchetti, P., Ientile, R., Calabresi, P., Pisani, F., and Costa, C. (2016). Neuroprotection as a potential therapeutic perspective in neurodegenerative diseases: focus on antiepileptic drugs. *Neurochem Res* 41, 340–352.

Cameron, H. A. and Mckay, R. D. G. (2001). Adult neurogenesis produces a large pool of new granule cells in the dentate gyrus. *J Comp Neurol* 435, 406–417.

Catterall, W. A. (2017). Forty years of sodium channels: structure, function, pharmacology, and epilepsy. *Neurochem Res* 42, 2495–2504.

Catterall, W. A., Perez-Reyes, E., Snutch, T. P., and Striessnig, J. (2005). International Union of Pharmacology. XLVIII. Nomenclature and structure-function relationships of voltage-gated calcium channels. *Pharmacol Rev* 57, 411–425.

Catterall, W. A. and Swanson, T. M. (2015). Structural basis for pharmacology of voltage-gated sodium and calcium channels. *Mol Pharmacol* 88, 141–150.

Cavalheiro, E. A., Leite, J. P., Bortolotto, Z. A., Turski, W. A., Ikonomidou, C., and Turski, L. (1991). Long-term effects of pilocarpine in rats: structural damage of the brain triggers kindling and spontaneous Recurrent Seizures. *Epilepsia* 32, 778–782.

Chavkin, C., Bakhit, C., Weber, E., and Bloom, F. E. (1983). Relative contents and concomitant release of prodynorphin/neoendorphin-derived peptides in rat hippocampus. *Proc Natl Acad Sci U S A* 80, 7669–7673.

Chevaleyre, V. and Siegelbaum, S. A. (2010). Strong CA2 pyramidal neuron synapses define a powerful disynaptic cortico-hippocampal loop. *Neuron* 66, 560–572.

Choi, D., Stables, J. P., and Kohn, H. (1996). Synthesis and anticonvulsant activities of N-benzyl-2-acetamidopropionamide derivatives. *J Med Chem* 39, 1907–1916.

Claiborne, B. J., Amaral, D. G., and Cowan, W. M. (1990). Quantitative, three-dimensional analysis of granule cell dendrites in the rat dentate gyrus. *J Comp Neurol* 302, 206–219.

Clifford, D. B., Olney, J. W., Maniotis, A., Collins, R. C., and Zorumski, C. F. (1987). The functional anatomy and pathology of lithium-pilocarpine and high-dose pilocarpine seizures. *Neuroscience* 23, 953–968.

Collins, R. C., Tearse, R. G., and Lothman, E. W. (1983). Functional anatomy of limbic seizures: focal discharges from medial entorhinal cortex in rat. *Brain Res* 280, 25–40.

Cook, M. J., Fish, D. R., Shorvon, S. D., Straughan, K., and Stevens, J. M. (1992). Hippocampal volumetric and morphometric studies in frontal and temporal lobe epilepsy. *Brain* 115, 1001–1015.

Covolan, L. and Mello, L. E. A. M. (2000). Temporal profile of neuronal injury following pilocarpine or kainic acid-induced status epilepticus. *Epilepsy Res* 39, 133–152.

Crespel, A., Rigau, V., Coubes, P., Rousset, M. C., de Bock, F., Okano, H., Baldy-Moulinier, M., Bockaert, J., and Lerner-Natoli, M. (2005). Increased number of neural progenitors in human temporal lobe epilepsy. *Neurobiol Dis* 19, 436–450.

Curia, G., Lucchi, C., Vinet, J., Gualtieri, F., Marinelli, C., Torsello, A., Costantino, L., and Biagini, G. (2014). Pathophysiogenesis of mesial temporal lobe epilepsy: is prevention of damage antiepileptogenic? *Curr Med Chem* 21, 663–688.

Curia, G., Longo, D., Biagini, G., Jones, R. S. G., and Avoli, M. (2008). The pilocarpine model of temporal lobe epilepsy. *J Neurosci Methods* 172, 143–157.

Das, S., Gilchrist, J., Bosmans, F., and van Petegem, F. (2016). Binary architecture of the $Na_v1.2$-$\beta2$ signaling complex. *eLife* 5:e10960, 1–21.

de Lanerolle, N. C., Kim, J. H., Robbins, R. J., and Spencer, D. D. (1989). Hippocampal interneuron loss and plasticity in human temporal lobe epilepsy. *Brain Res* 495, 387–395.

de Ruiter, J. P. and Uylings, H. B. M. (1987). Morphometric and dendritic analysis of fascia dentata granule cells in human aging and senile dementia. *Brain Res* 402, 217–229.

Dixit, A. B., Sharma, D., Srivastava, A., Banerjee, J., Tripathi, M., Prakash, D., and Chandra, P. S. (2017). Upregulation of breast cancer resistance protein and major vault protein in drug resistant epilepsy. *Seizure* 47, 9–12.

Doeser, A., Dickhof, G., Reitze, M., Uebachs, M., Schaub, C., Pires, N. M., Bonifácio, M. J., Soares-da-Silva, P., and Beck, H. (2014a). Targeting pharmacoresistant epilepsy and epileptogenesis with a dual-purpose antiepileptic drug. *Brain* 138, 371–387.

Doeser, A., Soares-da-Silva, P., Beck, H., and Uebachs, M. (2014b). The effects of eslicarbazepine on persistent Na^+ current and the role of the Na+ channel β subunits. *Epilepsy Res* 108, 202–211.

Doty, P., Rudd, G. D., Stoehr, T., and Thomas, D. (2007). Lacosamide. *Neurotherapeutics* 4, 145–148.

Dupont, S., Semah, F., Boon, P., Saint-Hilaire, J.-M., Adam, C., Broglin, D., and Baulac, M. (1999). Association of ipsilateral motor automatisms and contralateral dystonic posturing: a clinical feature differentiating medial from neocortical temporal lobe epilepsy. *Arch Neurol* 56, 927–932.

Eijkelkamp, N., Linley, J. E., Baker, M. D., Minett, M. S., Cregg, R., Werdehausen, R., Rugiero, F., and Wood, J. N. (2012). Neurological perspectives on voltage-gated sodium channels. *Brain* 135, 2585–2612.

Elger, C., Halász, P., Maia, J., Almeida, L., and Soares-da-Silva, P. (2009). Efficacy and safety of eslicarbazepine acetate as adjunctive treatment in adults with refractory partial-onset seizures: a randomized, double-blind, placebo-controlled, parallel-group phase III study. *Epilepsia* 50, 454–463.

Ellerkmann, R. K., Remy, S., Chen, J., Sochivko, D., Elger, C. E., Urban, B. W., Becker, A., and Beck, H. (2003). Molecular and functional changes in voltage-dependent Na^+ channels following pilocarpine-induced status epilepticus in rat dentate granule cells. *Neuroscience* 119, 323–333.

Ellerkmann, R. K., Riazanski, V., Elger, C. E., Urban, B. W., and Beck, H. (2001). Slow recovery from inactivation regulates the availability of voltage-dependent Na^+ channels in hippocampal granule cells, hilar neurons and basket cells. *J Physiol* 532, 385–397.

Eriksson, P. S., Perfilieva, E., Björk-Eriksson, T., Alborn, A.-M., Nordborg, C., Peterson, D. A., and Gage, F. H. (1998). Neurogenesis in the adult human hippocampus. *Nat Med* 4, 1313–1317.

Ernst, A., Alkass, K., Bernard, S., Salehpour, M., Perl, S., Tisdale, J., Possnert, G., Druid, H., and Frisén, J. (2014). Neurogenesis in the striatum of the adult human brain. *Cell* 156, 1072–1083.

Errington, A. C., Coyne, L., Stöhr, T., Selve, N., and Lees, G. (2006). Seeking a mechanism of action for the novel anticonvulsant lacosamide. *Neuropharmacology* 50, 1016–1029.

Errington, A. C., Stöhr, T., Heers, C., and Lees, G. (2008). The investigational anticonvulsant lacosamide selectively enhances slow inactivation of voltage-gated sodium channels. *Mol Pharmacol* 73, 157–169.

Espósito, M. S., Piatti, V. C., Laplagne, D. A., Morgenstern, N. A., Ferrari, C. C., Pitossi, F. J., and Schinder, A. F. (2005). Neuronal differentiation in the adult hippocampus recapitulates embryonic development. *J Neurosci* 25, 10074–10086.

Falcão, A., Fuseau, E., Nunes, T., Almeida, L., and Soares-da-Silva, P. (2012). Pharmacokinetics, drug interactions and exposure-response relationship of eslicarbazepine acetate in adult patients with partial-onset seizures. *CNS Drugs* 26, 79–91.

Fanselow, M. S. and Dong, H.-W. (2010). Are the dorsal and ventral hippocampus functionally distinct structures? *Neuron* 65, 7–19.

Fisher, R. S., Acevedo, C., Arzimanoglou, A., Bogacz, A., Cross, J. H., Elger, C. E., Engel, J., Forsgren, L., French, J. A., Glynn, M., Hesdorffer, D. C., Lee, B. I., Mathern, G. W., Moshé, S. L., Perucca, E., Scheffer, I. E., Tomson, T., Watanabe, M., and Wiebe, S. (2014). ILAE official report: a practical clinical definition of epilepsy. *Epilepsia* 55, 475–482.

Fisher, R. S., Cross, J. H., French, J. A., Higurashi, N., Hirsch, E., Jansen, F. E., Lagae, L., Moshé, S. L., Peltola, J., Roulet Perez, E., Scheffer, I. E., and Zuberi, S. M. (2017). Operational classification of seizure types by the International League Against Epilepsy: position paper of the ILAE commission for classification and terminology. *Epilepsia* 58, 522–530.

Fisher, R. S., van Emde Boas, W., Blume, W., Elger, C., Genton, P., Lee, P., and Engel, J. (2005). Epileptic seizures and epilepsy: definitions proposed by the International League Against Epilepsy (ILAE) and the International Bureau for Epilepsy (IBE). *Epilepsia* 46, 470–472.

Flesch, G., Francotte, E., Hell, F., and Degen, P. H. (1992). Determination of the R-(-) and S-(+) enantiomers of the monohydroxylated metabolite of oxcarbazepine in human plasma by enantioselective high-performance liquid chromatography. *J Chromatogr B Biomed Sci Appl* 581, 147–151.

Fortuna, A., Alves, G., Soares-da-Silva, P., and Falcão, A. (2013). Pharmacokinetics, brain distribution and plasma protein binding of carbamazepine and nine

derivatives: new set of data for predictive in silico ADME models. *Epilepsy Res* 107, 37–50.

Gaarskjaer, F. B. and Laurberg, S. (1983). Ectopic granule cells of hilus fasciae dentatae projecting to the ipsilateral regio inferior of the rat hippocampus. *Brain Res* 274, 11–16.

Gáll, Z. and Vancea, S. (2018). Distribution of lacosamide in the rat brain assessed by in vitro slice technique. *Arch Pharm Res* 41, 79–86.

Gasparini, S., Ferlazzo, E., Leonardi, C. G., Cianci, V., Mumoli, L., Sueri, C., Labate, A., Gambardella, A., and Aguglia, U. (2016). The natural history of epilepsy in 163 untreated patients: looking for "oligoepilepsy". *PLoS One* 11:e0161722, 1–8.

Gilchrist, J., Das, S., van Petegem, F., and Bosmans, F. (2013). Crystallographic insights into sodium-channel modulation by the $\beta 4$ subunit. *Proc Natl Acad Sci U S A* 110, E5016–E5024.

Gillham, R. A., Williams, N., Wiedmann, K., Butler, E., Larkin, J. G., and Brodie, M. J. (1988). Concentration-effect relationships with carbamazepine and its epoxide on psychomotor and cognitive function in epileptic patients. *J Neurol Neurosurg Psychiatry* 51, 929–933.

Glien, M., Brandt, C., Potschka, H., and Löscher, W. (2002). Effects of the novel antiepileptic drug levetiracetam on spontaneous recurrent seizures in the rat pilocarpine model of temporal lobe epilepsy. *Epilepsia* 43, 350–357.

Goffin, K., Nissinen, J., van Laere, K., and Pitkänen, A. (2007). Cyclicity of spontaneous recurrent seizures in pilocarpine model of temporal lobe epilepsy in rat. *Exp Neurol* 205, 501–505.

Goldin, A. L. (2001). Resurgence of sodium channel research. *Annu Rev Physiol* 63, 871–894.

Greenaway, C., Ratnaraj, N., Sander, J. W., and Patsalos, P. N. (2011). Saliva and serum lacosamide concentrations in patients with epilepsy. *Epilepsia* 52, 258–263.

Grieco, T. M., Malhotra, J. D., Chen, C., Isom, L. L., and Raman, I. M. (2005). Open-channel block by the cytoplasmic tail of sodium channel $\beta 4$ as a mechanism for resurgent sodium current. *Neuron* 45, 233–244.

Gupta, A., Elgammal, F. S., Proddutur, A., Shah, S., and Santhakumar, V. (2012). Decrease in tonic inhibition contributes to increase in dentate semilunar granule cell excitability after brain injury. *J Neurosci* 32, 2523–2537.

Hainzl, D., Parada, A., and Soares-da-Silva, P. (2001). Metabolism of two new antiepileptic drugs and their principal metabolites S (+)-and R (-)-10, 11-dihydro-10-hydroxy carbamazepine. *Epilepsy Res* 44, 197–206.

Han, Z.-S., Buhl, E. H., Lörinczi, Z., and Somogyi, P. (1993). A high degree of spatial selectivity in the axonal and dendritic domains of physiologically identified local-circuit neurons in the dentate gyrus of the rat hippocampus. *Eur J Neurosci* 5, 395–410.

Hartley, T., Lever, C., Burgess, N., and O'Keefe, J. (2014). Space in the brain: how the hippocampal formation supports spatial cognition. *Philos Trans R Soc Lond B Biol Sci* 369:20120510, 1–18.

Hauser, W. A., Annegers, J. F., and Rocca, W. A. (1996). Descriptive epidemiology of epilepsy: contributions of population-based studies from Rochester, Minnesota. *Mayo Clin Proc* 71, 576–586.

Hauser, W. A. and Kurland, L. T. (1975). The epidemiology of epilepsy in Rochester, Minnesota, 1935 through 1967. *Epilepsia* 16, 1–66.

Hebeisen, S., Pires, N., Loureiro, A. I., Bonifácio, M. J., Palma, N., Whyment, A., Spanswick, D., and Soares-da-Silva, P. (2015). Eslicarbazepine and the enhancement of slow inactivation of voltage-gated sodium channels: a comparison with carbamazepine, oxcarbazepine and lacosamide. *Neuropharmacology* 89, 122–135.

Heinemann, U., Beck, H., Dreier, J. P., Ficker, E., Stabel, J., and Zhang, C. L. (1991). The dentate gyrus as a regulated gate for the propagation of epileptiform activity. *Epilepsy Res Suppl* 7, 273–280.

Hille, B. (1971). The permeability of the sodium channel to organic cations in myelinated nerve. *J Gen Physiol* 58, 599–619.

Hille, B. (1972). The permeability of the sodium channel to metal cations in myelinated nerve. *J Gen Physiol* 59, 637–658.

Hille, B. (1977). Local anesthetics: hydrophilic and hydrophobic pathways for the drug-receptor reaction. *J Gen Physiol* 69, 497–515.

Hirtz, D., Thurman, D. J., Gwinn-Hardy, K., Mohamed, M., Chaudhuri, A. R., and Zalutsky, R. (2007). How common are the "common" neurologic disorders? *Neurology* 68, 326–337.

Hodgkin, A. L. and Huxley, A. F. (1952). The dual effect of membrane potential on sodium conductance in the giant axon of *Loligo*. *J Physiol* 116, 497–506.

Holtkamp, D., Opitz, T., Hebeisen, S., Soares-da-Silva, P., and Beck, H. (2018). Effects of eslicarbazepine on slow inactivation processes of sodium channels in dentate gyrus granule cells. *Epilepsia* 59, 1492–1506.

Holtkamp, D., Opitz, T., Niespodziany, I., Wolff, C., and Beck, H. (2017). Activity of the anticonvulsant lacosamide in experimental and human epilepsy via selective effects on slow Na^+ channel inactivation. *Epilepsia* 58, 27–41.

Houser, C. R., Miyashiro, J. E., Swartz, B. E., Walsh, G. O., Rich, J. R., and Delgado-Escueta, A. V. (1990). Altered patterns of dynorphin immunoreactivity suggest mossy fiber reorganization in human hippocampal epilepsy. *J Neurosci* 10, 267–282.

Houser, C. R. (1990). Granule cell dispersion in the dentate gyrus of humans with temporal lobe epilepsy. *Brain Res* 535, 195–204.

Howell, G. A., Welch, M. G., and Frederickson, C. J. (1984). Stimulation-induced uptake and release of zinc in hippocampal slices. *Nature* 308, 736–738.

Hsu, D. (2007). The dentate gyrus as a filter or gate: a look back and a look ahead. *Prog Brain Res* 163, 601–613.

Huang, L. Y., Moran, N., and Ehrenstein, G. (1982). Batrachotoxin modifies the gating kinetics of sodium channels in internally perfused neuroblastoma cells. *Proc Natl Acad Sci U S A* 79, 2082–2085.

Isokawa, M., Avanzini, G., Finch, D. M., Babb, T. L., and Levesque, M. F. (1991). Physiologic properties of human dentate granule cells in slices prepared from epileptic patients. *Epilepsy Res* 9, 242–250.

Iwano, T., Masuda, A., Kiyonari, H., Enomoto, H., and Matsuzaki, F. (2012). Prox1 postmitotically defines dentate gyrus cells by specifying granule cell identity over CA3 pyramidal cell fate in the hippocampus. *Development* 139, 3051–3062.

Jandová, K., Päsler, D., Antonio, L. L., Raue, C., Ji, S., Njunting, M., Kann, O., Kovács, R., Meencke, H.-J., Cavalheiro, E. A., Heinemann, U., Gabriel, S., and Lehmann, T.-N. (2006). Carbamazepine-resistance in the epileptic dentate gyrus of human hippocampal slices. *Brain* 129, 3290–3306.

Jensen, F. E. (2011). Epilepsy as a spectrum disorder: implications from novel clinical and basic neuroscience. *Epilepsia* 52, 1–6.

Jinde, S., Zsiros, V., and Nakazawa, K. (2013). Hilar mossy cell circuitry controlling dentate granule cell excitability. *Front Neural Circuits* 7:14, 1–10.

Jung, M. W. and McNaughton, B. L. (1993). Spatial selectivity of unit activity in the hippocampal granular layer. *Hippocampus* 3, 165–182.

Kandratavicius, L., Balista, P. A., Lopes-Aguiar, C., Ruggiero, R. N., Umeoka, E. H., Garcia-Cairasco, N., Bueno-Junior, L. S., and Leite, J. P. (2014). Animal models of epilepsy: use and limitations. *Neuropsychiatr Dis Treat* 10, 1693–1705.

Kesner, R. P. (2017). An analysis of dentate gyrus function (an update). *Behav Brain Res* 354, 84–91.

Ketelaars, S. O. M., Gorter, J. A., van Vliet, E. A., da Silva, F. H. L., and Wadman, W. J. (2001). Sodium currents in isolated rat CA1 pyramidal and dentate granule neurones in the post-status epilepticus model of epilepsy. *Neuroscience* 105, 109–120.

King, A. N., Manning, C. F., and Trimmer, J. S. (2014). A unique ion channel clustering domain on the axon initial segment of mammalian neurons. *J Comp Neurol* 522, 2594–2608.

Kobayashi, M. and Buckmaster, P. S. (2003). Reduced inhibition of dentate granule cells in a model of temporal lobe epilepsy. *J Neurosci* 23, 2440–2452.

Kohara, K., Pignatelli, M., Rivest, A. J., Jung, H.-Y., Kitamura, T., Suh, J., Frank, D., Kajikawa, K., Mise, N., Obata, Y., Wickersham, I. R., and Tonegawa, S. (2014). Cell type-specific genetic and optogenetic tools reveal hippocampal CA2 circuits. *Nat Neurosci* 17, 269–279.

Köhr, G. and Mody, I. (1991). Endogenous intracellular calcium buffering and the activation/inactivation of HVA calcium currents in rat dentate gyrus granule cells. *J Gen Physiol* 98, 941–967.

Koo, T.-S., Kim, S.-J., Ha, D.-J., Baek, M., and Moon, H. (2011). Pharmacokinetics, brain distribution, and plasma protein binding of the antiepileptic drug lacosamide in rats. *Arch Pharm Res* 34, 2059–2064.

Kühn, F. J. P. and Greeff, N. G. (1999). Movement of voltage sensor S4 in domain 4 is tightly coupled to sodium channel fast inactivation and gating charge immobilization. *J Gen Physiol* 114, 167–184.

Kuo, C.-C. (1998). A common anticonvulsant binding site for phenytoin, carbamazepine, and lamotrigine in neuronal Na^+ channels. *Mol Pharmacol* 54, 712–721.

Kuo, C.-C., Chen, R.-S., Lu, L., and Chen, R.-C. (1997). Carbamazepine inhibition of neuronal Na^+ currents: quantitative distinction from phenytoin and possible therapeutic implications. *Mol Pharmacol* 51, 1077–1083.

Kuwabara, T., Hasegawa, D., Kobayashi, M., Fujita, M., and Orima, H. (2010). Clinical magnetic resonance volumetry of the hippocampus in 58 epileptic dogs. *Vet Radiol Ultrasound* 51, 485–490.

Kwan, P., Arzimanoglou, A., Berg, A. T., Brodie, M. J., Hauser, W. A., Mathern, G., Moshé, S. L., Perucca, E., Wiebe, S., and French, J. (2010). Definition of drug resistant epilepsy: consensus proposal by the ad hoc Task Force of the ILAE commission on therapeutic strategies. *Epilepsia* 51, 1069–1077.

Kwan, P. and Brodie, M. J. (2000). Early identification of refractory epilepsy. *N Engl J Med* 342, 314–319.

Kwan, P., Schachter, S. C., and Brodie, M. J. (2011). Drug-resistant epilepsy. *N Engl J Med* 365, 919–926.

Landmark, C. J. (2008). Antiepileptic drugs in non-epilepsy disorders. *CNS Drugs* 22, 27–47.

Landmark, C. J., Svendsen, T., Dinarevic, J., Kufaas, R. F., Reimers, A., Brodtkorb, E., Baftiu, A., Burns, M. L., and Johannessen, S. I. (2016). The impact of pharmacokinetic interactions with eslicarbazepine acetate versus oxcarbazepine and carbamazepine in clinical practice. *Ther Drug Monit* 38, 499–505.

Larimer, P. and Strowbridge, B. W. (2010). Representing information in cell assemblies: persistent activity mediated by semilunar granule cells. *Nat Neurosci* 13, 213–222.

Lazarowski, A., Czornyj, L., Lubienieki, F., Girardi, E., Vazquez, S., and D'Giano, C. (2007). ABC transporters during epilepsy and mechanisms underlying multidrug resistance in refractory epilepsy. *Epilepsia* 48, 140–149.

Lenkowski, P. W., Shah, B. S., Dinn, A. E., Lee, K., and Patel, M. K. (2003). Lidocaine block of neonatal $Na_v1.3$ is differentially modulated by co-expression of $\beta 1$ and $\beta 3$ subunits. *Eur J Pharmacol* 467, 23–30.

Lerche, H., Shah, M., Beck, H., Noebels, J., Johnston, D., and Vincent, A. (2013). Ion channels in genetic and acquired forms of epilepsy. *J Physiol* 591, 753–764.

Leutgeb, J. K., Leutgeb, S., Moser, M.-B., and Moser, E. I. (2007). Pattern separation in the dentate gyrus and CA3 of the hippocampus. *Science* 315, 961–966.

Licko, T., Seeger, N., Zellinger, C., Russmann, V., Matagne, A., and Potschka, H. (2013). Lacosamide treatment following status epilepticus attenuates neuronal cell loss and alterations in hippocampal neurogenesis in a rat electrical status epilepticus model. *Epilepsia* 54, 1176–1185.

Lim, C., Blume, H. W., Madsen, J. R., and Saper, C. B. (1997). Connections of the hippocampal formation in humans: I. The mossy fiber pathway. *J Comp Neurol* 385, 325–351.

Lipkind, G. M. and Fozzard, H. A. (2010). Molecular model of anticonvulsant drug binding to the voltage-gated sodium channel inner pore. *Mol Pharmacol* 78, 631–638.

Liu, M., Pleasure, S. J., Collins, A. E., Noebels, J. L., Naya, F. J., Tsai, M.-J., and Lowenstein, D. H. (2000). Loss of BETA2/NeuroD leads to malformation of the dentate gyrus and epilepsy. *Proc Natl Acad Sci U S A* 97, 865–870.

Liu, Y.-B., Lio, P. A., Pasternak, J. F., and Trommer, B. L. (1996). Developmental changes in membrane properties and postsynaptic currents of granule cells in rat dentate gyrus. *J Neurophysiol* 76, 1074–1088.

Löscher, W. and Rundfeldt, C. (1991). Kindling as a model of drug-resistant partial epilepsy: selection of phenytoin-resistant and nonresistant rats. *J Pharmacol Exp Ther* 258, 483–489.

Löscher, W. (2011). Critical review of current animal models of seizures and epilepsy used in the discovery and development of new antiepileptic drugs. *Seizure* 20, 359–368.

Löscher, W. and Schmidt, D. (2006). Experimental and clinical evidence for loss of effect (tolerance) during prolonged treatment with antiepileptic drugs. *Epilepsia* 47, 1253–1284.

Maglóczky, Z., Wittner, L., Borhegyi, Z., Halasz, P., Vajda, J., Czirjak, S., and Freund, T. F. (2000). Changes in the distribution and connectivity of interneurons in the epileptic human dentate gyrus. *Neuroscience* 96, 7–25.

Mantegazza, M., Curia, G., Biagini, G., Ragsdale, D. S., and Avoli, M. (2010). Voltage-gated sodium channels as therapeutic targets in epilepsy and other neurological disorders. *Lancet Neurol* 9, 413–424.

Margerison, J. H. and Corsellis, J. A. N. (1966). Epilepsy and the temporal lobes. A clinical, electroencephalographic and neuropathological study of the brain in epilepsy, with particular reference to the temporal lobes. *Brain* 89, 499–530.

Marsh, L., Morrell, M. J., Shear, P. K., Sullivan, E. V., Freeman, H., Marie, A., Lim, K. O., and Pfefferbaum, A. (1997). Cortical and hippocampal volume deficits in temporal lobe epilepsy. *Epilepsia* 38, 576–587.

Martin, L. J. and Corry, B. (2014). Locating the route of entry and binding sites of benzocaine and phenytoin in a bacterial voltage gated sodium channel. *PLoS Comput Biol* 10:e1003688, 1–12.

Mathern, G. W., Adelson, P. D., Cahan, L. D., and Leite, J. P. (2002a). Hippocampal neuron damage in human epilepsy: Meyer's hypothesis revisited. *Prog Brain Res* 135, 237–251.

Mathern, G. W., Leiphart, J. L., de Vera, A., Adelson, P. D., Seki, T., Neder, L., and Leite, J. P. (2002b). Seizures decrease postnatal neurogenesis and granule cell development in the human fascia dentata. *Epilepsia* 43, 68–73.

Mathern, G. W., Pretorius, J. K., Kornblum, H. I., Mendoza, D., Lozada, A., Leite, J. P., Chimelli, L. M., Fried, I., Sakamoto, A. C., Assirati, J. A., Levesque, M. F., Adelson, P. D., and Peacock, W. J. (1997). Human hippocampal AMPA and NMDA mRNA levels in temporal lobe epilepsy patients. *Brain* 120, 1937–1959.

Mathern, G. W., Pretorius, J. K., Leite, J. P., Kornblum, H. I., Mendoza, D., Lozada, A., and Bertram III, E. H. (1998). Hippocampal AMPA and NMDA mRNA levels and subunit immunoreactivity in human temporal lobe epilepsy patients and a rodent model of chronic mesial limbic epilepsy. *Epilepsy Res* 32, 154–171.

May, T. W., Brandt, C., Helmer, R., Bien, C. G., and Cawello, W. (2015). Comparison of lacosamide concentrations in cerebrospinal fluid and serum in patients with epilepsy. *Epilepsia* 56, 1134–1140.

Mazzuferi, M., Kumar, G., Rospo, C., and Kaminski, R. M. (2012). Rapid epileptogenesis in the mouse pilocarpine model: video-EEG, pharmacokinetic and histopathological characterization. *Exp Neurol* 238, 156–167.

McLean, M. J., Schmutz, M., Wamil, A. W., Olpe, H.-R., Portet, C., and Feldmann, K. F. (1994). Oxcarbazepine: mechanisms of action. *Epilepsia* 35, S5–S9.

Mody, I., Salter, M. W., and MacDonald, J. F. (1989). Whole-cell voltage-clamp recordings in granule cells acutely isolated from hippocampal slices of adult or aged rats. *Neurosci Lett* 96, 70–75.

Morris, R. (2007). Theories of hippocampal function. In: Andersen, P., Morris, R., Amaral, D., Bliss, T., and O'Keefe, J. (Eds.), *The hippocampus book*. New York: Oxford University Press, 581–714.

Morrisett, R. A., Jope, R. S., and Snead, O. C. (1987). Status epilepticus is produced by administration of cholinergic agonists to lithium-treated rats: comparison with kainic acid. *Exp Neurol* 98, 594–605.

Morselli, P. L. and Frigerio, A. (1975). Metabolism and pharmacokinetics of carbamazepine. *Drug Metab Rev* 4, 97–113.

Morte, M. I., Carreira, B. P., Falcão, M. J., Ambrósio, A. F., Soares-da-Silva, P., Araújo, I. M., and Carvalho, C. M. (2013). Evaluation of neurotoxic and neuroprotective pathways affected by antiepileptic drugs in cultured hippocampal neurons. *Toxicol In Vitro* 27, 2193–2202.

Ngugi, A. K., Bottomley, C., Kleinschmidt, I., Sander, J. W., and Newton, C. R. (2010). Estimation of the burden of active and life-time epilepsy: a meta-analytic approach. *Epilepsia* 51, 883–890.

Ngugi, A. K., Kariuki, S. M., Bottomley, C., Kleinschmidt, I., Sander, J. W., and Newton, C. R. (2011). Incidence of epilepsy: a systematic review and meta-analysis. *Neurology* 77, 1005–1012.

Niespodziany, I., Leclère, N., Vandenplas, C., Foerch, P., and Wolff, C. (2013). Comparative study of lacosamide and classical sodium channel blocking antiepileptic drugs on sodium channel slow inactivation. *J Neurosci Res* 91, 436–443.

Notenboom, R. G. E., Hampson, D. R., Jansen, G. H., van Rijen, P. C., van Veelen, C. W. M., van Nieuwenhuizen, O., and de Graan, P. N. E. (2005). Up-regulation of hippocampal metabotropic glutamate receptor 5 in temporal lobe epilepsy patients. *Brain* 129, 96–107.

Novy, J., Patsalos, P. N., Sander, J. W., and Sisodiya, S. M. (2011). Lacosamide neurotoxicity associated with concomitant use of sodium channel-blocking antiepileptic drugs: a pharmacodynamic interaction? *Epilepsy Behav* 20, 20–23.

O'Keefe, J. and Dostrovsky, J. (1971). The hippocampus as a spatial map. Preliminary evidence from unit activity in the freely-moving rat. *Brain Res* 34, 171–175.

Overstreet, L. S., Hentges, S. T., Bumaschny, V. F., de Souza, F. S. J., Smart, J. L., Santangelo, A. M., Low, M. J., Westbrook, G. L., and Rubinstein, M. (2004). A transgenic marker for newly born granule cells in dentate gyrus. *J Neurosci* 24, 3251–3259.

Palmer, T. D., Takahashi, J., and Gage, F. H. (1997). The adult rat hippocampus contains primordial neural stem cells. *Mol Cell Neurosci* 8, 389–404.

Parent, J. M., Tada, E., Fike, J. R., and Lowenstein, D. H. (1999). Inhibition of dentate granule cell neurogenesis with brain irradiation does not prevent seizure-induced mossy fiber synaptic reorganization in the rat. *J Neurosci* 19, 4508–4519.

Parent, J. M., Timothy, W. Y., Leibowitz, R. T., Geschwind, D. H., Sloviter, R. S., and Lowenstein, D. H. (1997). Dentate granule cell neurogenesis is increased by seizures and contributes to aberrant network reorganization in the adult rat hippocampus. *J Neurosci* 17, 3727–3738.

Patlak, J. B. and Ortiz, M. (1986). Two modes of gating during late Na^+ channel currents in frog sartorius muscle. *J Gen Physiol* 87, 305–326.

Patsalos, P. N., Berry, D. J., Bourgeois, B. F., Cloyd, J. C., Glauser, T. A., Johannessen, S. I., Leppik, I. E., Tomson, T., and Perucca, E. (2008). Antiepileptic drugs — best practice guidelines for therapeutic drug monitoring: a position paper by the subcommission on therapeutic drug monitoring, ILAE Commission on Therapeutic Strategies. *Epilepsia* 49, 1239–1276.

Paxinos, G. and Watson, C. (2009). The rat brain in stereotaxic coordinates. Sixth edition. San Diego: Academic Press.

Pedroni, A., Minh, D. D., Mallamaci, A., and Cherubini, E. (2014). Electrophysiological characterization of granule cells in the dentate gyrus immediately after birth. *Front Cell Neurosci* 8:44, 1–9.

Penttonen, M., Kamondi, A., Sík, A., Acsády, L., and Buzsáki, G. (1997). Feed-forward and feed-back activation of the dentate gyrus in vivo during dentate spikes and sharp wave bursts. *Hippocampus* 7, 437–450.

Perez, M. M., Trimble, M. R., Murray, N. M., and Reider, I. (1985). Epileptic psychosis: an evaluation of PSE profiles. *Br J Psychiatry* 146, 155–163.

Persinger, M. A., Peredery, O., Desjardins, D., and Eastman, A. (1998). Ventricular dilatation over several weeks following induction of excitotoxic (systemic lithium/pilocarpine) lesions: potential role of damage to the substantia nigra reticulata. *Int J Neurosci* 94, 63–74.

Perucca, E., Elger, C., Halasz, P., Falcao, A., Almeida, L., and Soares-da-Silva, P. (2011). Pharmacokinetics of eslicarbazepine acetate at steady-state in adults with partial-onset seizures. *Epilepsy Res* 96, 132–139.

Pitkänen, A. and Lukasiuk, K. (2011). Mechanisms of epileptogenesis and potential treatment targets. *Lancet Neurol* 10, 173–186.

Pitsch, J., Becker, A. J., Schoch, S., Müller, J. A., Curtis, M., and Gnatkovsky, V. (2017). Circadian clustering of spontaneous epileptic seizures emerges after pilocarpine-induced status epilepticus. *Epilepsia* 58, 1159–1171.

Polli, R. S., Malheiros, J. M., Santos, R. dos, Hamani, C., Longo, B. M., Tannús, A., Mello, L. E., and Covolan, L. (2014). Changes in hippocampal volume are

correlated with cell loss but not with seizure frequency in two chronic models of temporal lobe epilepsy. *Front Neurol* 5:111, 1–11.

Pothmann, L., Müller, C., Averkin, R. G., Bellistri, E., Miklitz, C., Uebachs, M., Remy, S., de la Prida, L. M., and Beck, H. (2014). Function of inhibitory microcircuits is spared by Na^+ channel-acting anticonvulsant drugs. *Journal of Neuroscience* 34, 9720–9735.

Priel, M. R. and Albuquerque, E. X. (2002). Short-term effects of pilocarpine on rat hippocampal neurons in culture. *Epilepsia* 43, 40–46.

Racine, R. J. (1972). Modification of seizure activity by electrical stimulation: II. Motor seizure. *Electroencephalogr Clin Neurophysiol* 32, 281–294.

Ragsdale, D. S. and Avoli, M. (1998). Sodium channels as molecular targets for antiepileptic drugs. *Brain Res Rev* 26, 16–28.

Rakhade, S. N. and Jensen, F. E. (2009). Epileptogenesis in the immature brain: emerging mechanisms. *Nat Rev Neurol* 5, 380–391.

Raman, I. M. and Bean, B. P. (1997). Resurgent sodium current and action potential formation in dissociated cerebellar Purkinje neurons. *J Neurosci* 17, 4517–4526.

Reckziegel, G., Beck, H., Schramm, J., Elger, C. E., and Urban, B. W. (1998). Electrophysiological characterization of Na^+ currents in acutely isolated human hippocampal dentate granule cells. *J Physiol* 509, 139–150.

Reckziegel, G., Beck, H., Schramm, J., Urban, B. W., and Elger, C. E. (1999). Carbamazepine effects on Na^+ currents in human dentate granule cells from epileptogenic tissue. *Epilepsia* 40, 401–407.

Remy, S. and Beck, H. (2006). Molecular and cellular mechanisms of pharmacoresistance in epilepsy. *Brain* 129, 18–35.

Remy, S., Gabriel, S., Urban, B. W., Dietrich, D., Lehmann, T. N., Elger, C. E., Heinemann, U., and Beck, H. (2003a). A novel mechanism underlying drug resistance in chronic epilepsy. *Ann Neurol* 53, 469–479.

Remy, S., Urban, B. W., Elger, C. E., and Beck, H. (2003b). Anticonvulsant pharmacology of voltage-gated Na^+ channels in hippocampal neurons of control and chronically epileptic rats. *Eur J Neurosci* 17, 2648–2658.

Ribak, C. E., Tran, P. H., Spigelman, I., Okazaki, M. M., and Nadler, J. V. (2000). Status epilepticus-induced hilar basal dendrites on rodent granule cells contribute to recurrent excitatory circuitry. *J Comp Neurol* 428, 240–253.

Rizzi, M., Caccia, S., Guiso, G., Richichi, C., Gorter, J. A., Aronica, E., Aliprandi, M., Bagnati, R., Fanelli, R., D'Incalci, M., Samanin, R., and Vezzani, A. (2002).

Limbic seizures induce P-glycoprotein in rodent brain: functional implications for pharmacoresistance. *J Neurosci* 22, 5833–5839.

Rogawski, M. A., Loescher, W., and Rho, J. M. (2016). Mechanisms of action of antiseizure drugs and the ketogenic diet. *Cold Spring Harb Perspect Med* a022780, 1–28.

Rogawski, M. A., Tofighy, A., White, H. S., Matagne, A., and Wolff, C. (2015). Current understanding of the mechanism of action of the antiepileptic drug lacosamide. *Epilepsy Res* 110, 189–205.

Roger, J., Dreifuss, F. E., Martinez-Lage, M., Munari, C., Porter, R. J., Seino, M., and Wolf, P. (1989). Proposal for revised classification of epilepsies and epileptic syndromes. Commission on classification and terminology of the International League Against Epilepsy. *Epilepsia* 30, 389–399.

Ruff, R. L. (1996). Single-channel basis of slow inactivation of Na^+ channels in rat skeletal muscle. *Am J Physiol Cell Physiol* 271, C971–C981.

Sanabria, E. R. G., da Silva, A. V., Spreafico, R., and Cavalheiro, E. A. (2002). Damage, reorganization, and abnormal neocortical hyperexcitability in the pilocarpine model of temporal lobe epilepsy. *Epilepsia* 43, 96–106.

Sancho-Bielsa, F. J., Navarro-López, J. D., Alonso-Llosa, G., Molowny, A., Ponsoda, X., Yajeya, J., and López-García, C. (2012). Neurons of the dentate molecular layer in the rabbit hippocampus. *PLoS One* 7:e48470, 1–16.

Sato, C., Ueno, Y., Asai, K., Takahashi, K., Sato, M., Engel, A., and Fujiyoshi, Y. (2001). The voltage-sensitive sodium channel is a bell-shaped molecule with several cavities. *Nature* 409, 1047–1051.

Sattler, A., Schaefer, M., May, T. W., Rambeck, B., and Brandt, C. (2011). Fluctuation of lacosamide serum concentrations during the day and occurrence of adverse drug reactions–first clinical experience. *Epilepsy Res* 95, 207–212.

Scharfman, H. E., Sollas, A. E., Berger, R. E., Goodman, J. H., and Pierce, J. P. (2003). Perforant path activation of ectopic granule cells that are born after pilocarpine-induced seizures. *Neuroscience* 121, 1017–1029.

Scharfman, H. E. (2016). The enigmatic mossy cell of the dentate gyrus. *Nat Rev Neurosci* 17, 562–575.

Scharfman, H. E., Goodman, J. H., and Sollas, A. L. (2000). Granule-like neurons at the hilar/CA3 border after status epilepticus and their synchrony with area CA3 pyramidal cells: functional implications of seizure-induced neurogenesis. *J Neurosci* 20, 6144–6158.

Schaub, C., Uebachs, M., and Beck, H. (2007). Diminished response of CA1 neurons to antiepileptic drugs in chronic epilepsy. *Epilepsia* 48, 1339–1350.

Scheffer, I. E., Berkovic, S., Capovilla, G., Connolly, M. B., French, J., Guilhoto, L., Hirsch, E., Jain, S., Mathern, G. W., Moshé, S. L., Nordli, D. R., Perucca, E., Tomson, T., Wiebe, S., Zhang, Y.-H., and Zuberi, S. M. (2017). ILAE classification of the epilepsies: position paper of the ILAE commission for classification and terminology. *Epilepsia* 58, 512–521.

Scheibel, M. E., Crandall, P. H., and Scheibel, A. B. (1974). The hippocampal-dentate complex in temporal lobe epilepsy. *Epilepsia* 15, 55–80.

Schmidt-Hieber, C. and Bischofberger, J. (2010). Fast sodium channel gating supports localized and efficient axonal action potential initiation. *J Neurosci* 30, 10233–10242.

Schmied, O., Scharf, G., Hilbe, M., Michal, U., Tomsa, K., and Steffen, F. (2008). Magnetic resonance imaging of feline hippocampal necrosis. *Vet Radiol Ultrasound* 49, 343–349.

Schuele, S. U. and Lüders, H. O. (2008). Intractable epilepsy: management and therapeutic alternatives. *Lancet Neurol* 7, 514–524.

Semah, F., Picot, M.-C., Adam, C., Broglin, D., Arzimanoglou, A., Bazin, B., Cavalcanti, D., and Baulac, M. (1998). Is the underlying cause of epilepsy a major prognostic factor for recurrence? *Neurology* 51, 1256–1262.

Seress, L. and Frotscher, M. (1990). Morphological variability is a characteristic feature of granule cells in the primate fascia dentata: a combined Golgi/electron microscope study. *J Comp Neurol* 293, 253–267.

Seress, L. and Mrzljak, L. (1987). Basal dendrites of granule cells are normal features of the fetal and adult dentate gyrus of both monkey and human hippocampal formations. *Brain Res* 405, 169–174.

Sheets, P. L., Heers, C., Stoehr, T., and Cummins, T. R. (2008). Differential block of sensory neuronal voltage-gated sodium channels by lacosamide [(2R)-2-(acetylamino)-N-benzyl-3-methoxypropanamide], lidocaine, and carbamazepine. *J Pharmacol Exp Ther* 326, 89–99.

Shen, H., Zhou, Q., Pan, X., Li, Z., Wu, J., and Yan, N. (2017). Structure of a eukaryotic voltage-gated sodium channel at near-atomic resolution. *Science* 355:eaal4326, 1–14.

Shirley, M. and Dhillon, S. (2016). Eslicarbazepine acetate monotherapy: a review in partial-onset seizures. *Drugs* 76, 707–717.

Sillanpää, M., Jalava, M., Kaleva, O., and Shinnar, S. (1998). Long-term prognosis of seizures with onset in childhood. *N Engl J Med* 338, 1715–1722.

Sloviter, R. S., Zappone, C. A., Harvey, B. D., Bumanglag, A. V., Bender, R. A., and Frotscher, M. (2003). "Dormant basket cell" hypothesis revisited: relative vulnerabilities of dentate gyrus mossy cells and inhibitory interneurons after hippocampal status epilepticus in the rat. *J Comp Neurol* 459, 44–76.

So, E. L., Ruggles, K. H., Cascino, G. D., Ahmann, P. A., and Weatherford, K. W. (1994). Seizure exacerbation and status epileptics related to carbamazepine-10, 11-epoxide. *Ann Neurol* 35, 743–746.

Soares-da-Silva, P., Pires, N., Bonifácio, M. J., Loureiro, A. I., Palma, N., and Wright, L. C. (2015). Eslicarbazepine acetate for the treatment of focal epilepsy: an update on its proposed mechanisms of action. *Pharmacol Res Perspect* 3:e00124, 1–21.

Soriano, E. and Frotscher, M. (1989). A GABAergic axo-axonic cell in the fascia dentata controls the main excitatory hippocampal pathway. *Brain Res* 503, 170–174.

Spalding, K. L., Bergmann, O., Alkass, K., Bernard, S., Salehpour, M., Huttner, H. B., Boström, E., Westerlund, I., Vial, C., Buchholz, B. A., Possnert, G., Mash, D. C., Druid, H., and Frisén, J. (2013). Dynamics of hippocampal neurogenesis in adult humans. *Cell* 153, 1219–1227.

Spampanato, J. and Dudek, F. E. (2017). Targeted interneuron ablation in the mouse hippocampus can cause spontaneous recurrent seizures. *eNeuro* 4:e0130, 1–17.

Spruston, N. and Johnston, D. (1992). Perforated patch-clamp analysis of the passive membrane properties of three classes of hippocampal neurons. *J Neurophysiol* 67, 508–529.

Squire, L. R. (1992). Memory and the hippocampus: a synthesis from findings with rats, monkeys, and humans. *Psychol Rev* 99, 195.

Squire, L. R., Stark, C. E. L., and Clark, R. E. (2004). The medial temporal lobe. *Annu Rev Neurosci* 27, 279–306.

Stafstrom, C. E. (2007). Persistent sodium current and its role in epilepsy. *Epilepsy Curr* 7, 15–22.

Staley, K. J., Otis, T. S., and Mody, I. (1992). Membrane properties of dentate gyrus granule cells: comparison of sharp microelectrode and whole-cell recordings. *J Neurophysiol* 67, 1346–1358.

Stephen, L. J., Kelly, K., Parker, P., and Brodie, M. J. (2014). Adjunctive lacosamide—5 years' clinical experience. *Epilepsy Res* 108, 1385–1391.

Stevens, M., Peigneur, S., and Tytgat, J. (2011). Neurotoxins and their binding areas on voltage-gated sodium channels. *Front Pharmacol* 2:71, 1–13.

Stringer, J. L. and Lothman, E. W. (1992). Reverberatory seizure discharges in hippocampal-parahippocampal circuits. *Exp Neurol* 116, 198–203.

Surges, R. and Elger, C. E. (2013). Reoperation after failed resective epilepsy surgery. *Seizure* 22, 493–501.

Sutula, T. P., Cavazos, J. E., and Woodard, A. R. (1994). Long-term structural and functional alterations induced in the hippocampus by kindling: implications for memory dysfunction and the development of epilepsy. *Hippocampus* 4, 254–258.

Tang, F., Hartz, A., and Bauer, B. (2017). Drug-resistant epilepsy: multiple hypotheses, few answers. *Front Neurol* 8:301, 1–19.

Tauck, D. L. and Nadler, J. V. (1985). Evidence of functional mossy fiber sprouting in hippocampal formation of kainic acid-treated rats. *J Neurosci* 5, 1016–1022.

Taverna, S., Mantegazza, M., Franceschetti, S., and Avanzini, G. (1998). Valproate selectively reduces the persistent fraction of Na^+ current in neocortical neurons. *Epilepsy Res* 32, 304–308.

Terrian, D. M., Hernandez, P. G., Rea, M. A., and Peters, R. I. (1989). ATP release, adenosine formation, and modulation of dynorphin and glutamic acid release by adenosine analogues in rat hippocampal mossy fiber synaptosomes. *J Neurochem* 53, 1390–1399.

Terrian, D. M., Johnston, D., Claiborne, B. J., Ansah-Yiadom, R., Strittmatter, W. J., and Rea, M. A. (1988). Glutamate and dynorphin release from a subcellular fraction enriched in hippocampal mossy fiber synaptosomes. *Brain Res Bull* 21, 343–351.

Tikhonov, D. B. and Zhorov, B. S. (2005). Sodium channel activators: model of binding inside the pore and a possible mechanism of action. *FEBS Lett* 579, 4207–4212.

Tikhonov, D. B. and Zhorov, B. S. (2007). Sodium channels: ionic model of slow inactivation and state-dependent drug binding. *Biophys J* 93, 1557–1570.

Tikhonov, D. B. and Zhorov, B. S. (2017). Mechanism of sodium channel block by local anesthetics, antiarrhythmics, and anticonvulsants. *Journal Gen Physiol* 149, 465–481.

Tsang, S. Y., Tsushima, R. G., Tomaselli, G. F., Li, R. A., and Backx, P. H. (2005). A multifunctional aromatic residue in the external pore vestibule of Na^+ channels contributes to the local anesthetic receptor. *Mol Pharmacol* 67, 424–434.

Turski, W. A., Cavalheiro, E. A., Schwarz, M., Czuczwar, S. J., Kleinrok, Z., and Turski, L. (1983). Limbic seizures produced by pilocarpine in rats: behavioural, electroencephalographic and neuropathological study. *Behav Brain Res* 9, 315–335.

Uebachs, M., Albus, C., Opitz, T., Isom, L., Niespodziany, I., Wolff, C., and Beck, H. (2012). Loss of $\beta 1$ accessory Na^+ channel subunits causes failure of carbamazepine, but not of lacosamide, in blocking high-frequency firing via differential effects on persistent Na^+ currents. *Epilepsia* 53, 1959–1967.

Uebachs, M., Opitz, T., Royeck, M., Dickhof, G., Horstmann, M.-T., Isom, L. L., and Beck, H. (2010). Efficacy loss of the anticonvulsant carbamazepine in mice lacking sodium channel β subunits via paradoxical effects on persistent sodium currents. *J Neurosci* 30, 8489–8501.

Vacher, H., Mohapatra, D. P., and Trimmer, J. S. (2008). Localization and targeting of voltage-dependent ion channels in mammalian central neurons. *Physiol Rev* 88, 1407–1447.

van Strien, N. M., Cappaert, N. L. M., and Witter, M. P. (2009). The anatomy of memory: an interactive overview of the parahippocampal-hippocampal network. *Nat Rev Neurosci* 10, 272–282.

van Vliet, E. A., da Costa Araujo, S., Redeker, S., van Schaik, R., Aronica, E., and Gorter, J. A. (2006). Blood–brain barrier leakage may lead to progression of temporal lobe epilepsy. *Brain* 130, 521–534.

van Vliet, E. A., Zibell, G., Pekcec, A., Schlichtiger, J., Edelbroek, P. M., Holtman, L., Aronica, E., Gorter, J. A., and Potschka, H. (2010). COX-2 inhibition controls P-glycoprotein expression and promotes brain delivery of phenytoin in chronic epileptic rats. *Neuropharmacology* 58, 404–412.

Vassilev, P. M., Scheuer, T., and Catterall, W. A. (1988). Identification of an intracellular peptide segment involved in sodium channel inactivation. *Science* 241, 1658–1661.

Vilin, Y. Y. and Ruben, P. C. (2001). Slow inactivation in voltage-gated sodium channels. *Cell Biochem Biophys* 35, 171–190.

Villanueva, V., Giráldez, B. G., Toledo, M., de Haan, G. J., Cumbo, E., Gambardella, A., de Backer, M., Joeres, L., Brunnert, M., Dedeken, P., and Serratosa, J. (2018).

Lacosamide monotherapy in clinical practice: a retrospective chart review. *Acta Neurol Scand* 00, 1–9.

Volk, H. A. and Löscher, W. (2005). Multidrug resistance in epilepsy: rats with drug-resistant seizures exhibit enhanced brain expression of P-glycoprotein compared with rats with drug-responsive seizures. *Brain* 128, 1358–1368.

von Campe, G., Spencer, D. D., and de Lanerolle, N. C. (1997). Morphology of dentate granule cells in the human epileptogenic hippocampus. *Hippocampus* 7, 472–488.

Vreugdenhil, M., Faas, G. C., and Wadman, W. J. (1998). Sodium currents in isolated rat CA1 neurons after kindling epileptogenesis. *Neuroscience* 86, 99–107.

Vreugdenhil, M. and Wadman, W. J. (1999). Modulation of sodium currents in rat CA1 neurons by carbamazepine and valproate after kindling epileptogenesis. *Epilepsia* 40, 1512–1522.

Wagner, E., Rosati, M., Molin, J., Foitzik, U., Wahle, A. M., Fischer, A., Matiasek, L. A., Reese, S., Flegel, T., and Matiasek, K. (2014). Hippocampal sclerosis in feline epilepsy. *Brain Pathol* 24, 607–619.

Walker, M. C., Ruiz, A., and Kullmann, D. M. (2002). Do mossy fibers release GABA? *Epilepsia* 43, 196–202.

Wang, S.-Y. and Wang, G. K. (2003). Voltage-gated sodium channels as primary targets of diverse lipid-soluble neurotoxins. *Cell Signal* 15, 151–159.

Waszkielewicz, A. M., Gunia, A., Szkaradek, N., Sloczynska, K., Krupinska, S., and Marona, H. (2013). Ion channels as drug targets in central nervous system disorders. *Curr Med Chem* 20, 1241–1285.

Wehner, T. and Lüders, H. (2008). Role of neuroimaging in the presurgical evaluation of epilepsy. *J Clin Neurol* 4, 1–16.

West, M. J., Slomianka, L. H. J. G., and Gundersen, H. J. G. (1991). Unbiased stereological estimation of the total number of neurons in the subdivisions of the rat hippocampus using the optical fractionator. *Anat Rec* 231, 482–497.

West, M. J. and Gundersen, H. J. G. (1990). Unbiased stereological estimation of the number of neurons in the human hippocampus. *J Comp Neurol* 296, 1–22.

Williams, P. A., Larimer, P., Gao, Y., and Strowbridge, B. W. (2007). Semilunar granule cells: glutamatergic neurons in the rat dentate gyrus with axon collaterals in the inner molecular layer. *J Neurosci* 27, 13756–13761.

Williamson, A., Spencer, D. D., and Shepherd, G. M. (1993). Comparison between the membrane and synaptic properties of human and rodent dentate granule cells. *Brain Res* 622, 194–202.

Witter, M. P., Doan, T. P., Jacobsen, B., Nilssen, E. S., and Ohara, S. (2017). Architecture of the entorhinal cortex a review of entorhinal anatomy in rodents with some comparative notes. *Front Syst Neurosci* 11:46, 1–12.

World Health Organization (2017). Fact sheet 999: epilepsy. URL: `http://www.who.int/mediacentre/factsheets/fs999/en/`.

Xiong, W., Farukhi, Y. Z., Tian, Y., DiSilvestre, D., Li, R. A., and Tomaselli, G. F. (2006). A conserved ring of charge in mammalian Na^+ channels: a molecular regulator of the outer pore conformation during slow inactivation. *J Physiol* 576, 739–754.

Yang, Y.-C., Huang, C.-S., and Kuo, C.-C. (2010). Lidocaine, carbamazepine, and imipramine have partially overlapping binding sites and additive inhibitory effect on neuronal Na^+ channels. *Anesthesiology* 113, 160–174.

Zhang, C., Chanteux, H., Zuo, Z., Kwan, P., and Baum, L. (2013a). Potential role for human P-glycoprotein in the transport of lacosamide. *Epilepsia* 54, 1154–1160.

Zhang, C., Kwan, P., Zuo, Z., and Baum, L. (2012). The transport of antiepileptic drugs by P-glycoprotein. *Adv Drug Deliv Rev* 64, 930–942.

Zhang, M.-M., Wilson, M. J., Azam, L., Gajewiak, J., Rivier, J. E., Bulaj, G., Olivera, B. M., and Yoshikami, D. (2013b). Co-expression of $Na_v\beta$ subunits alters the kinetics of inhibition of voltage-gated sodium channels by pore-blocking μ-conotoxins. *Br J Pharmacol* 168, 1597–1610.

Zhang, X., Cui, S.-S., Wallace, A. E., Hannesson, D. K., Schmued, L. C., Saucier, D. M., Honer, W. G., and Corcoran, M. E. (2002). Relations between brain pathology and temporal lobe epilepsy. *J Neurosci* 22, 6052–6061.

Zipp, F., Nitsch, R., Soriano, E., and Frotscher, M. (1989). Entorhinal fibers form synaptic contacts on parvalbumin-immunoreactive neurons in the rat fascia dentata. *Brain Res* 495, 161–166.